Title

FISSION AND SPALLATION COMPETITION FROM THE INTERMEDIATE NUCLEI AMERICIUM-241 AND NEPTUNIUM-235

Author

Gibson, Walter Maxwell.

Publication Date

1956-11-01

UCRL 3493

UNIVERSITY OF CALIFORNIA

Radiation Laboratory

FISSION AND SPALLATION COMPETITION FROM THE INTERMEDIATE NUCLEI AMERICIUM-241 AND NEPTUNIUM-235

DISCLAIMER

UCRL-3493

UNIVERSITY OF CALIFORNIA

Radiation Laboratory
Berkeley, California

Contract No. W-7405-eng-48

FISSION AND SPALLATION COMPETITION FROM THE INTERMEDIATE NUCLEI AMERICIUM-241 AND NEPTUNIUM-235

Walter Maxwell Gibson

(Thesis)

November, 1956

Printed for the U. S. Atomic Energy Commission

2. Pu^{239} plus deuterons..... 53
3. Np^{237} plus helium ions..... 53
4. U^{233} plus deuterons..... 54
IV. DISCUSSION..... 81
A. Fission Yields..... 81
1. Charge distribution in fission..... 81
2. Fission asymmetry..... 84
3. Total fission cross sections..... 92
B. Spallation Yields..... 96
1. Test of the predictions of Bohr's Compound Nucleus Theory..... 97
2. General features of the spallation excitation Functions..... 102
C. Summary..... 104
V. ACKNOWLEDGMENTS..... 105
VI. APPENDIX..... 106
VII. REFERENCES..... 114

FISSION AND SPALLATION COMPETITION FROM THE INTERMEDIATE NUCLEI AMERICIUM-241 AND NEPTUNIUM-235

Walter Maxwell Gibson

Radiation Laboratory
and
Department of Chemistry and Chemical Engineering
University of California, Berkeley, California

ABSTRACT

The yields of fission and spallation products of 9-24 Mev deuteron bombardments of Pu^{239} and U^{233} and of 18-46 Mev helium ion bombardments of Np^{237} have been measured. Radiochemical methods were used to prepare the target materials and to separate and purify the products of the reactions studied. Determinations of primary fission yields indicate that the charge distribution in fission at these energies is intermediate to the equal charge displacement noted at lower energies and the constant charge to mass ratio suggested at very high energies but appears to be closer to the latter case. Fission yield curves have been determined which show the familiar transition from asymmetric to symmetric fission as the excitation energy is increased. An increase in the number of neutrons emitted before or during the fission process as the excitation energy is increased is noted by a gradual shift to lower mass of the center of symmetry of the fission yield curves. The results of the fission studies are interpreted qualitatively in terms of a statistical fission mechanism. No Z^2/A dependence of the relative fissionability of the target nuclides is noted. No apparent Z dependence is seen but a strong A dependence (fissionability increasing as A decreases) is suggested. The (d,2n) and (d,3n) excitation functions of Pu^{239} and the (α,2n) and (α,3n) excitation functions of Np^{237} have been compared to test the predictions of the compound nucleus model that σ (d,2n) : σ(d,3n) = σ (α,2n) : σ (α,3n) and σ (d,2n) : σ (α,2n) = σ_c (d) : σ_c (α) = σ(d,3n) : σ (α,3n). The predictions of the compound nucleus theory of Bohr are verified at all except the very lowest energies, indicating that these reactions are taking place predominantly by a compound nucleus mechanism. The (d,2n) and (α,2n) cross sections are radically affected by the

magnitude of the fission reaction, hence the excitation functions for these reactions are very sensitive indicators of the relative fissionability of heavy nuclides at these excitation energies. The general features of the other spallation excitation functions (d,n), (d,dp), (d,αn), (α,n), (α,αn) are discussed. Direct intercation, or non-compound nucleus processes are used to explain most of the spallation excitation functions except for the (d,xn) and (α,xn) reactions where $X > 2$. The total reaction cross sections (fission plus spallation) correspond in each case to a nuclear radius of $R = 1.5 \times 10^{-13} A^{1/3}$ cm.

A discussion of the determination of nucleometer (windowless methane flow proportional counter) counting efficiencies for the electron capture isotopes Am^{239}, Am^{240}, Np^{234} is appended. Counting efficiencies for other electron-capture isotopes are also discussed and summarized.

LIST OF TABLES

I. Tracers used to determine spallation product yields.....23
II. Nucleometer counting efficiencies used in the present study...36
III. Plutonium (239) plus deuterons; spallation cross sections.....43
IV. Neptunium (237) plus helium ions; spallation cross sections...45
V. Uranium (233) plus deuterons; spallation cross sections.....45
VI. Primary fission product cross sections and fractions of total chain yield.....50
VII. Plutonium (239) plus deuterons; fission cross sections.....55
VIII. Neptunium (237) plus helium ions; fission cross sections.....65
IX. Uranium (233) plus deuterons; fission cross sections.....76
X. Summary of nucleometer counting efficiencies for electron capture isotopes.....112

LIST OF ILLUSTRATIONS

1. The chemical separation scheme used in the plutonium and neptunium bombardments..... 25
2. The chemical separation scheme used in the uranium bombardments..... 29
3. Growth and decay of U^{230} in a Pa^{230} sample..... 34
4. Spallation excitation functions for deuteron-induced reactions of Pu^{239}..... 44
5. Spallation excitation functions for helium ion-induced reactions of Np^{237}..... 46
6. Spallation excitation functions for deuteron-induced reactions of U^{233}..... 47
7. Fractions of total chain yield vs the chain positions predicted by the equal charge displacement hypothesis..... 51
8. Fractions of total chain yield vs the chain positions predicted by assuming the same neutron to proton ratio for the most probable primary fission product as for the apparent fissioning nucleus..... 52
9. Fission yield curves for 9.2- and 12.3-Mev deuteron-induced fission of Pu^{239}..... 57
10. Fission yield curve for 15.0 Mev deuteron-induced fission of Pu^{239}..... 58
11. Fission yield curve for 16.1-Mev deuteron-induced fission of Pu^{239}..... 59
12. Fission yield curve for 17.9-Mev deuteron-induced fission of Pu^{239}..... 60
13. Fission yield curve for 20.4-Mev deuteron-induced fission of Pu^{239}..... 61
14. Fission yield curve for 23.4-Mev dueteron-induced fission of Pu^{239}..... 62
15. Variation of fission yield curves with energy for deuteron-induced fission of Pu^{239}..... 63
16. Comparison of total fission excitation function with spallation excitation functions for deuteron-induced reactions of Pu^{239}..... 64

17. Fission yield curves for 19.8- and 22.7-Mev helium ion-induced fission of Np^{237} 67
18. Fission yield curves for 24.2- and 28.1-Mev helium ion-induced fission of Np^{237} 68
19. Fission yield curve for 31.5-Mev helium ion-induced fission of Np^{237} 69
20. Fission yield curve for 35.0-Mev helium ion-induced fission of Np^{237} 70
21. Fission yield curve for 38.1-Mev helium ion-induced fission of Np^{237} 71
22. Fission yield curve for 44.9-Mev helium ion-induced fission of Np^{237} 72
23. Fission yield curve for 45.7-Mev helium ion-induced fission of Np^{237} 73
24. Variation of fission yield curves with energy for helium ion-induced fission of Np^{237} 74
25. Comparison of total fission excitation function with spallation excitation functions for helium ion-induced reactions of Np^{237} 75
26. Fission yield curves for deuteron-induced fission of U^{233} 77
27. Fission yield curves for deuteron-induced fission of U^{233} 78
28. Variation of fission yield curves with energy for deuteron-induced fission of U^{233} 79
29. Comparison of total fission excitation function with spallation excitation functions for deuteron-induced reactions of U^{233} 80
30. Fission asymmetry vs excitation energy for deuteron bombardments of U^{233} and Pu^{239} and for helium ion bombardments of Np^{237} 86
31. Fission asymmetry vs $(E_x-5)^{-1/2}$ for the fission of various heavy element nuclides excited by charged particles, neutrons and photons 91

32. Total fission yields and theoretical compound nucleus formation cross sections for deuteron bombardments of Pu^{239} 93

33. Total fission yields and theoretical compound nucleus formation cross sections for helium ion bombardments of Np^{237} 94

34. Total fission yields and theoretical compound nucleus formation cross sections for deuteron bombardments of U^{233} 95

35. Comparison of the excitation functions for $Np^{237} + \alpha$ and $Pu^{239} + d$ 99

36. Cross section ratios for $Np^{237} + \alpha$ and $Pu^{239} + d$ 101

I. INTRODUCTION

A highly excited heavy nucleus ($Z > \sim 80$) can de-excite by one or both of two quite different mechanisms. It can break up into two more or less equal parts (fission) or it can emit various numbers of nucleons or simple nuclei (i.e. deuterons, tritons, or alpha particles). The latter class of reactions have been called "spallation reactions". The name was suggested by G. T. Seaborg and comes from the verb "to spall" meaning to break up by chipping off small fragments. The number and complexity of the emitted particles depends on the excitation energy. A reduction of 16 charge units and 37 mass units has been observed in the bombardment of arsenic with 400 Mev helium ions.[1] If the nucleus is still highly excited after some spallation has taken place fission can result.[2]

The conceptual framework for the interpretation of nuclear reactions in the medium energy region ($E < 50$ Mev) was laid by Bohr with the compound nucleus model.[3] As pointed out by Serber,[4] at energies above 50 Mev the nucleus becomes somewhat "transparent" to the bombarding particles. Effects such as direct nucleon-nucleon collisions or knock-on reactions then become prominent. A detailed model of the knock-on process in high energy reactions has been developed by Goldberger[5] which is in qualitative agreement with experiment.[6,7]

The statistical theory is an elaboration of Bohr's compound nucleus concept. The special assumptions of the statistical model have been listed by Weisskopf.[8,9] Various features of nuclear reactions have been successfully explained in terms of this theory.[10-15] However the charged particle emission probability is, in many cases, much greater than predicted,[16,17,18] and angular distributions of reaction products have been found to be strongly peaked forward[19-21] instead of symmetric about 90° in the center-of-mass system as predicted by the statistical model. Also the expected level density formula[8] has failed to be verified by experimental measurements.[22-24] An explanation of these phenomena has been offered in terms of direct interaction processes which take place in addition to the compound nucleus process.[25-27] The breakdown of some of the fundamental assumptions behind the statistical theory

has also been suggested.[28] These and other serious disagreements with the statistical model indicate that considerable caution should be exercised in applying it to any specific problem. However, this model still appears to be valid in many cases and, because of its simplicity and utility, may still yield considerable valuable information.[29,30]

According to the compound nucleus concept of Bohr,[3] the decay of a compound nucleus is independent of the method in which it is formed. The cross section can therefore be expressed as;

$$\sigma(a,b) = \sigma_c(a)\, G_c(b)$$

Where $\sigma_c(a)$ is the cross section for formation of the compound nucleus c with the incident particle a. $G_c(b)$ is the probability that the compound nucleus will de-excite by the emission of b, where b designates one or more small particles. $G_c(b)$ depends only on the energy of c and not on the method of formation. Let us then consider the cross section for the emission of b' from the same compound nucleus as above and the emission of b and b' from the same compound nucleus formed by a different projectile a'. If the compound nucleus has the same excitation energy in each case the following expression can be derived.

$$\frac{\sigma(a,b)}{\sigma(a,b')} = \frac{G_c(b)}{G_c(b')} = \frac{\sigma(a',b)}{\sigma(a',b')}$$

Ghoshal[10] bombarded Ni^{60} with helium ions and Cu^{63} with protons to produce the compound nucleus Zn^{64}. The relation $\sigma(p,n)/\sigma(p,2n)/\sigma(p,pn) = \sigma(\alpha,n)/\sigma(\alpha,2n)/\sigma(\alpha,pn)$ was observed to hold for each excitation energy of the compound nucleus. For the purpose of imparting excitation energy, protons were as effective as helium ions with 7 Mev greater energy. John[11] has applied a similar test for the compound nucleus Po^{210} by comparing the (α,xn) cross sections from helium ion bombardments of Pb^{206} to the (p,xn) cross section from proton bombardments of Bi^{209} by Kelley.[31] A similar result to that of Ghoshal's was obtained. The prediction of Bohr's assumption was thus verified.

An alternative representation can be obtained in the same fashion as the above expression by considering slightly different ratios.

$$\frac{\sigma(a,b)}{\sigma(a',b)} = \frac{\sigma_c(a)}{\sigma_c(a')} = \frac{\sigma(a,b')}{\sigma(a',b')}$$

The observed cross section ratios can then be compared to the ratio of the theoretical compound nucleus cross sections which have been developed by Weisskopf[9] and Shapiro.[32]

The fission process has been described by Bohr and Wheeler[33] on the basis of the liquid drop model of the nucleus proposed by Bohr.[3] This simplified model has been successful in describing many features of low energy fission.[34-37] By this treatment the fission process is pictured as a competition between the electrostatic energy of the nucleus (Coulombic effect) and the deficit of binding of particles at the surface (surface tension). The stabilizing effect of the surface tension overbalances the potentially disruptive influence of the electrostatic repulsion even for heavy nuclei in their normal approximately spherical configurations. Small distrubances lead to oscillations about the equilibrium shape. However as the distortion increases, the effect of the surface tension decreases relative to the Coulombic effect so for sufficiently large distortion the repulsion predominates and the nucleus breaks into two or more parts. On the basis of liquid drop considerations a semi-empirical mass equation has been developed[33,38,39] which can be used to calculate the energy release and hence the relative probability for any particular mode of fission (i.e., a particular distribution of neutrons and protons between the two fragments). This calculation indicated[33,36,39] that the total energy release is largest for symmetric fission. It was also predicted that as the excitation energy of the nucleus is increased, asymmetric fission would become more probable. These predictions are at complete variance with the experimental evidence.[40,41] The very extensive evidence to date can be summarized by the observations that (1) at low excitation energies, fission is predominantly asymmetric and (2) as the excitation energy is increased the probability for symmetric fission increases until at high energies asymmetric fission is the favored mode.

Many proposals have been made to explain the phenomena of asymmetric fission.[42] The shell model[43] of the nucleus, which has been particularly successful in explaining low lying excited states of nuclei and accounting for the increased beta stability of certain "magic number" nuclides, has been a popular basis for many of these proposals.[44-48] A "closed shell"(region of increased beta stability) is associated with 50

or 82 neutrons, consequently it is proposed that the nucleus divides in such a way that the small fragment contains at least 50 neutrons while the large fragment contains at least 82 neutrons with the remaining neutrons being distributed between the two fragments. The proton distribution would ostensibly be affected in the same manner but to a lesser degree since the number of protons does not come so close to being the sum of two closed shell configurations.

An alternative mechanism for the effect of shell structure has been proposed by Hill.[49] In this approach the shell structure of the fissioning nucleus is considered. It is suggested that low energy excitation of the nucleus is not statistical. Only the nucleons outside a given closed shell are excited. The excited nucleons then divide statistically with the unexcited "core" accompanying one of the two groups of dividing nucleons. As the excitation energy is increased, the probability for symmetric fission increases since more of the nucleons in the core are excited.

Other suggestions include a barrier leakage mechanism by Frenkel[50] which predicts an energy dependence for low energy fission quite different from that observed,[51] and a proposal by Present and Knipp[52] that the critical form of unstable equilibrium is asymmetric thus leading to a preference for asymmetric fission. Frankel and Metropolos have investigated the fission barrier by means of ENIAC calculations[36] and find no indications of the asymmetry assumed in the latter proposal. Hill and Wheeler have examined the fission process in terms of a collective model.[51] The fission asymmetry is explained by a shape dependent viscosity and an inviscid hydrodynamic instability of the incompressible nuclear fluid. It is proposed that minute asymmetries at the critical deformation can lead to large asymmetries if there exists a hydrodynamic instability tending to magnify the amplitude of the disturbance.

The desire to retain the basic concepts of the Bohr and Wheeler statistically excited liquid drop has prompted many workers to examine possible effects tending to make asymmetric fission entergetically more favored and hence statistically more probable than symmetric fission. Swiatecki[53] has noted that nuclear polarization and compressibility will

change slightly the simple liquid drop dependence of energy on the deformation and has suggested that this effect will work in such a direction as to split the symmetric saddle point into two asymmetric ones. Maris[54] has discussed the effect of non-uniform charge distribution in the nucleus and Fong[55] has investigated the effects of deformation of the fission fragments during the fission process. The magnitude of these effects is difficult to estimate. It is probable that all of these considerations may produce an increased probability for asymmetric fission.

The most significant factor behind the renewed interest in the statistical model of fission has been the accurate determination of nuclear masses in the fission product region[56,57] and in the heavy element region[58,59] and improved beta decay systematics.[60] These measurements indicate clearly that the mass equation used by the earlier workers[33,36,39] was seriously in error. The most notable deviation is in the region of the 50 neutron and the 82 neutron closed shells where the experimentally determined masses are significantly smaller than predicted by the mass equation. Fong[61] and Maris[62] have pointed out that on the basis of these revised masses asymmetric fission is energetically favored, (that is, produces more kinetic and excitation energy) over symmetric modes of fission. Fong[55] has extended this treatment and has also considered possible Coulomb barrier effects and fission fragment distortion effects in an effort to calculate relative fission probabilities. The calculated fission yields for U^{235} fission with thermal neutrons agree remarkably well with the experimental results.[55] Perring and Story[63] have attempted to apply the calculations of Fong to the slow neutron fission of Pu^{239} and have noted large deviations.

Other, more indirect evidence concerning fission asymmetry supports the notion of energetically favored asymmetric fission. Fowler, Jones, and Phaehler[64] have observed a relationship between the valley to peak ratio (fission asymmetry) of the fission yield curves of several nuclides and the quantity $(E_x-5)^{-1/2}$. Where E_x is the bombarding particle energy plus its binding energy in Mev. It was found that if the logarithm of valley to peak ratio was plotted against the above energy expression a straight line could be drawn through the experimental points.

$(E_x-5)^{-1/2}$ is proportional to the reciprocal nuclear temperature. The 5 Mev which is subtracted from the excitation energy is interpreted as the effect of cooling of the nucleus as it is distorted and is chosen because of the measured photofission threshold of about 5 Mev. The proportionality constant between the nuclear temperature and the square root of (E_x-5) can be evaluated on the basis of energy level densities as estimated by Weisskopf.[65,9] When this is done the straight line through the experimental points corresponds to the expression Ymin/Ymax = 2.8 exp [-2.9/T]. Since the relative probability of two states differing in energy by an amount ΔE is exp [$-\Delta E/T$], it is thus inferred that 2.9 Mev is the additional energy required to produce symmetric in preference to asymmetric fission.

Along with the study of fission asymmetry, which has perhaps received a large bulk of the effort because of its striking and obvious contridiction of commonly accepted ideas, there are several other very interesting and important aspects of the fission process. The charge distribution in low energy fission has been investigated by Glendenin, Coryell and Edwards.[66] It was found that the experimentally determined independent fission yields could be best explained if it was assumed that the most probable primary fission product in every mass chain was displaced the same number of charge units from the beta stability line. By applying corrections for closed shell effects to the beta stability line assumed by Glendenin, Pappas[67] was able to obtain a better correlation. Very recent mass spectrographically determined primary fission yields[68] indicate a discrepancy in the postulate of equal charge displacement. This discrepancy can be explained if the effect of the 50 proton closed shell is taken into account in evaluating the most probable nuclear charge Zp for a given mass chain. It is suggested that the most probable charge distribution is that which will yield the greatest energy release in the fission process.

Another tool in determining the fission mechanism is the measurement of the distribution of the fission energy between the kinetic and excitation energies of the fission fragments.[69] Also of interest is the variation of the kinetic energy with fission fragment mass[70] and with the excitation energy of the fissioning nucleus.[71,72] The consistency of the kinetic energy of the fission fragments with the excitation

energy of the fissioning nucleus and the variation of the kinetic energy with mass strongly suggest that the kinetic energy is derived almost entirely from the Coulomb repulsion of the two fission fragments. An interpretation of this kind is consistent with the predictions of both a statistical fission model and the collective model of Hill and Wheeler.

The isotropic distribution of fission fragments from low energy fission and the anisotropic distribution for higher energies predicted by the collective[51] and by the statistical models[73,74] have been experimentally verified.[75,76] Measurements of the relative anisotropy of fragments which correspong to symmetric and asymmetric fission modes indicate a preference for the statistical fission mechanism as opposed to the collective model.[77,78] It was observed that the anisotropy is greater for the products of asymmetric fission. This is explained in terms of the statistical model by noting that there is more energy available in asymmetric fission than in symmetric fission hence the anisotropy, which has a marked energy dependence in the region studied, is greater for asymmetric fission.

Various measurements of the prompt neutrons emitted in the fission process give "model-sensitive" tests of the fission mechanism. The multiplicity of prompt neutrons from low energy fission[79,80] has been explained by Leachman[81] in terms of a statistical mechanism. It might also be noted that if more energy is released in asymmetric modes of fission than in symmetric modes one would expect the prompt neutron emission probability to be higher for asymmetric fission. This is found to be the case.[82] The observed energy spectrum of prompt neutrons from fission[83,84] have been fitted by the calculations of Watt[83] and Leachman[81] which are based on liquid drop model (statistical model) considerations. The angular distribution of fission neutrons has been shown by Fraser[85] to be isotropic in the frame of reference of the moving fission fragments as predicted by the statistical model. The collective model of Hill and Wheeler[51] predicts preferred neutron emission parallel to the axis of fission.

It is of special interest to consider the details of charged particle induced reactions of fissionable nuclides. The observed spallation products are the survivors of the preponderant fission reaction.

Therefore the variation of specific spallation yields with the fissionability of the nucleus is very instructive in investigating the fission process and in determining the relative effect of various possible reaction mechanisms. A systematic study of the variation of individual spallation reactions as the charge, mass and nuclear type of the target material and the charge, mass and energy of the bombarding particle is changed, should also yield valuable information about the mechanism of nuclear reactions. The present study is part of such a series of investigations on heavy mass nuclides.[86,87,88] The results of helium ion bombardments of plutonium isotopes[86] and U^{238} [87] are summarized below.

1. High cross sections for charged particle emission, particularly the $(\alpha,p2n)$ cross section which is higher than the $(\alpha,3n)$ cross section in some cases.
2. Low (1-3mb) and flat (α,n) excitation functions.
3. Prominent "tails" on the $(\alpha,2n)$ excitation functions.
4. A striking mass dependence of the magnitude of the $(\alpha,2n)$ cross section for Pu^{238} and Pu^{242} in which the cross section for the latter is about seven times higher than for the former.[86]
5. A high (up to 100 mb) $(\alpha,\alpha n)$ cross section in the U^{238} bombardments.[87]
6. A total reaction cross section conforming to a nuclear radius of about $R = 1.5 \times 10^{-13} A^{1/3}$ cm.

The present study is an extension of these previous investigations. The effect of deuterons as a projectile and direct testing of the compound nucleus assumption were of particular interest in this program as well as the detailed investigation of the fission reaction.

II. EXPERIMENTAL PROCEDURES

A. Target Preparation

The total cross section for a particular nuclear reaction is dependent on a number of factors. Each of these must be either controlled or measured in the course of an experiment designed to measure the cross section. The expression for the cross section is of the following form for the case of a thin target (beam not attenuated) bombarded with a non-uniform beam:

$$\sigma = \frac{N}{n/cm^2\ (It)}.$$

σ is expressed as cm^2 per atom, N is the number of product atoms formed, n/cm^2 is the number of target atoms per square centimeter and (It) is the total number of projectile particles (product of current and time) which strick the target. The target material must be of uniform thickness and all of the measured beam must hit the target.

Various techniques are available for preparing thin, uniform films of target materials.[89-91] The method employed throughout this study was electrodeposition. This method has afforded maximum target uniformity with a minimum expenditure of time, equipment and valuable target material compared with other commonly employed methods of evaporation or sublimation. A new method based on painting thin films of materials suspended in a cellulose nitrate lacquer has been described recently.[92]

It was necessary that the material on which the targets were to be plated be readily dissolvable in order to recover the fission recoils. In addition, the material could not become intensely radioactive and remain so for a long period after the bombardment. Aluminum met both of these requirements satisfactorily. The fission recoils are stopped completely by less than 1 mil (6.86 mg/cm^2) of aluminum foil[72,93] Ten-mil 2S aluminum shaped in the form of a shallow "hat" was used as the backing material.

1. Plutonium

The "low GT" Pu^{239} used in the plutonium bombardments contained only 0.02 atom percent of Pu^{240} and was essentially free of Pu^{241}.[94]

The method described by Hufford and Scott[89] as modified by Glass[94] for plutonium was used.

About one mg of plutonium in acid solution was oxidized to Pu (VI) by evaporating to dryness with 1 M sodium bromate. Three to four drops of concentrated nitric acid were added to the residue and this was again boiled to dryness to destroy excess bromate. The residue was then dissolved in 1 to 2 ml of 0.4M ammonium oxalate. This solution was transferred to a plating cell consisting of a platinum anode with the aluminum "hat" as the cathode. The potential drop across the cell was maintained at 4 to 5 volts and the spacing of the electrodes was adjusted to keep the plating current at 100 to 200 ma (over the 1.23 cm^2 area of the aluminum hat). It was found that 0.2 to 0.4 mg/cm^2 of plutonium could be plated in a 30-min period.

2. Neptunium

The plutonium procedure was employed except that it was found benificial to adjust the acidity of the plating solution to the methyl red endpoint with nitric acid and ammonium hydroxide. With neptunium, considerable difficulty was encountered in obtaining acceptable target plates. Frequently, targets containing only 0.06 to 0.1 mg/cm^2 of neptunium were used although on occasion up to 0.4 mg/cm^2 could be plated successfully.

3. Uranium

The U^{233} used was determined to contain about 5 percent U^{238} by mass spectroscopic measurements.[95] The plating method described by Hufford and Scott[89] was used. This is essentially the same as used for plutonium except for omission of the pre-oxidation by sodium bromate. It was found that up to 1.5 mg/cm^2 of uranium could be plated uniformly although the targets used were limited to 0.4 to 0.6 mg/cm^2.

In the earlier bombardments the area of the target was defined by the diameter of the plating cell used. Frequently, however, otherwise acceptable target plates were rejected because of small non-uniformities at the edge of the plated area due to bubble formation at the junction of the aluminum cathode and the glass plating cell. This was circumvented on later bombardments by using a cell larger than the area desired and masking the aluminum hat to the desired area by carefully painting it with a thin coat of 4A (Inter-Chemical Corporation,

San Francisco, Calif.) lacquer. This was baked on under a heat lamp and removed after the plating by soaking in acetone and peeling the 4A off with a sharp tool.

In all cases the area of the target was determined by carefully measuring several diameters and computing the area from the average.

The plates were determined to be uniform within 1 to 2 percent by scanning with a narrow slit low-geometry alpha counter[96] and by making radioautographa of several of the target plates selected at random.

In most cases three checks were made on the amount of target material bombarded. The targets were counted in a low-geometry alpha counter for which the geometry and counting efficiency had been determined to better than 1 percent,[97] the plating solution was assayed before and after plating, and finally, the dissolved target solution was assayed after the bombardment. The first two methods checked consistently; hence the average of these numbers was used in the cross-section calculations. The value obtained from radiometric assays of the dissolved target solution was 5 to 10 percent lower than that obtained from direct counting of the target plate. This effect has been noted by others.[94,98] The specific activities used for conversion of alpha counting rates to number of atoms, given in disintegrations per minute per milligram, were; Pu^{239}, 1.365×10^{8};[99] Np^{237}, 1.53×10^{6};[100] U^{233}, 2.10×10^{7}.[101]

B. Target Assembly

The requirements of an adequate target assembly in the measurement of cross sections include provision for controlling the angle and area of the incident beam (collimation), monitoring the number of particles hitting the target, and controlling the energy of the incident particles. Other considerations of a practical nature are cooling of the target and degrading foils and convenience and safety in loading and unloading the radioactive target plates. The target assembly used in the plutonium bombardments was identical to that described by Glass.[94] A modified "microtarget" assembly having somewhat improved cooling properties was used in the neptunium and uranium bombardments. This assembly has been described and pictured by Ritsema.[87]

The external 48-Mev helium ion beam and the 24-Mev deuteron beam of the Crocker Laboratory 60-inch cyclotron were degraded to the desired energy by weighed aluminum and platinum foils. The range-energy curves of Aron, Hoffman, and Williams[102] were used to calculate the final deuteron and helium ion energies. These curves were interpolated for platinum by B. M. Foreman, Jr.[103] The foils were placed in an air-cooled block in front of the target assembly. It was found that the aluminum foils were affected less than the platinum by the heating effect of the beam, so aluminum was used wherever possible. The foil immediately in front of the target was 1-mil aluminum in all cases. This foil was dissolved with the target in order to recover the trapped fission recoils. The uncertainty in the initial energy of the beam, before degredation, was about ±0.5 Mev, but may run as high as ± 1 Mev.[104] This uncertainty is mainly due to changes in the ion source and changes in the deflector magnet setting.

The beam was collimated to a cross-sectional area of about 0.9 cm^2. Beam patterns were taken before each bombardment by irradiating "Scotch tape" placed in the target position. This precaution was necessary to insure that all of the beam passing through the collimator would hit the target.

The beam was completely stopped in the target assembly which was electrically insulated from the rest of the system. Hence the build-up of positive charge in the Faraday cup formed by the target-backing material and holder was directly related to the number of particles hitting the target (since secondary electrons could not escape from the enclosed system). The beam current was measured and recorded as a function of time on a Speedomax recorder. The current was also integrated automatically over the period of the bombardment so that the total current could be obtained directly. The integrating capacitor of the cyclotron can be calibrated to a precision of greater than 0.1 percent with an accuracy of about 3 percent.[105]

C. Chemical Separations

Due to the large number of possible nuclear reactions induced in the target nuclei and in the aluminum backing plate, extensive chemical procedures were necessary to purify the products for which yields were to be determined. In many cases the total activity of some of the products was less than 1000 counts/min, making it impossible to separate the target into separate aliquots for each of the products. The desired products first had to be separated from each other and from the target and backing material. They were then radiochemically purified. The amount of induced activity was limited by the amount of material bombarded which was in turn drastically limited by the necessity of using thin targets and by the availability of valuable target material. Other limiting factors were the amount of beam the foils and target could tolerate before overheating (< 7 ua) and the length of the bombardment (1/2 to 4 hr) which was determined by available cyclotron time and by the half lives of the product nuclei.

Another problem was introduced by the presence of large amounts of aluminum. The aluminum target hat and the 1-mil aluminum front foil were dissolved with the target to recover fission recoils, making a total of about 130 mg of aluminum. Because of the intense alpha radioactivity of the target materials, the initial chemical procedures were carried out in an enclosed "glove box."[106]

1. Determination of chemical yields

The chemical yields of the various products were determined by the addition of standardized weights of carriers for each of the fission products and known disintegration rates of alpha-emitting tracers for the spallation products. The carriers and tracers were present in the beaker in which the target plate and cover foil were dissolved. Care was taken to avoid spattering or other losses until equilibrium between the induced activities and the carrier and tracer solution was reached.

Table I shows the isotopes used as tracers to give the yields of the respective spallation products.

Table I. Tracers Used to Determine Spallation Product Yields

Element	Tracer		Energy of principle alpha groups (Mev)[a]
Americium	Am^{243}	88%	5.267, 5.226
	Am^{241}	12%	5,476, 5,433
Plutonium	Pu^{239}	b	5.150, 5.137, 5.099
	Pu^{242}	18.5%[c]	4.88
	Pu^{238}	76.9%	5.492, 5.450
	Pu^{239}	4.6%	5.150, 5.137, 5.099
Neptunium	Np^{237}		4.77
Protactinium	Pa^{231}		5.042, 5.002, 4.938, 4.720

a. From Hollander, Perlman and Seaborg, Rev. of Mod. Phys. 25, 469 (1953).

b. Used to give yield of first plutonium fraction from neptunium bombardments.

c. For second plutonium fraction from neptunium bombardments (plutonium milking).

Neptunium-237 and uranium-233 have very nearly the same alpha-particle energy (4.77 Mev and 4.82 Mev respectively) and could not be distinguished separately on the alpha pulse analyzer (see section on counting instruments). Therefore, in the series of deuteron bombardments on U^{233}, any uranium from the target material which should stay with the neptunium fraction through the purification, would cause the apparent neptunium yield to be too high. There are no prominent gamma-rays associated with the decay of either the U^{233} or the Np^{237} which could be used to distinguish between the two isotopes. In an attempt to decrease the effect or to determine the magnitude of small amounts of uranium contamination, the following precautions were taken: a fairly large amount of neptunium tracer (about 800 c/m) was added initially so that a few counts of U^{233} would not make a large error in the neptunium yield. Also, on two of the low-energy bombardments (12.1 and 14.0 Mev), about half of the neptunium fraction was taken through a second TTA extraction cycle (see Sec. 4). The ratio of nucleometer counts to alpha

counts for this sample was compared to the same ratio for the sample which had only the regular chemical purification, the two ratios (extrapolated to a common time) agreed within the counting statistics in both cases. This same treatment could not be applied to the higher-energy bombardments because the bombardment time was reduced from 2 hr to 1/2 hr so a more favorable Np^{232}/Np^{233} ratio could be obtained. This reduced the amount of the longer-lived Np^{234} (4.4d) to such a low level that it was deemed unwise to divide the sample. It is believed that any errors which might be introduced by uranium contamination are small, both for the above reasons and because of the flat (d,n) excitation function obtained. It is expected from other cases[107-109] that the (d,n) excitation function will be constant from about 14 to above 24 Mev.

2. Target dissolution

The plutonium, neptunium, and uranium were plated as the hydrated oxides or as hydroxides. In the course of the bombardment much of the target material was converted to the oxide due to the heat generated in the front foils and in the backing plate. Due to the refractory nature of plutonium oxide[110] and neptunium oxide[111] special care was taken in these cases to be sure that complete dissolution was effected. The target was first treated with nitric and hydrochloric acids until the aluminum was in solution. This solution was then heated at about 80°C for an hour with 6M nitric acid. The uranium targets dissolved readily upon heating with nitric and hydrochloric acids. After the targets were dissolved the solution was diluted to a known volume and radiometric assays were taken for alpha counting to check the amount of target material bombarded.

The separation procedures will be outlined briefly and the spallation product purifications described. The individual chemical purifications for the fission products are modifications of standard procedures[112,113] and have been outlined in detail by others;[87,94,98] hence, these procedures will not be repeated here.

3. Chemical separations for plutonium and neptunium bombardments

In the plutonium and neptunium bombardments the separation procedures were very similar and will be discussed together. The separation scheme is illustrated in Fig. 1. When ruthenium carrier was

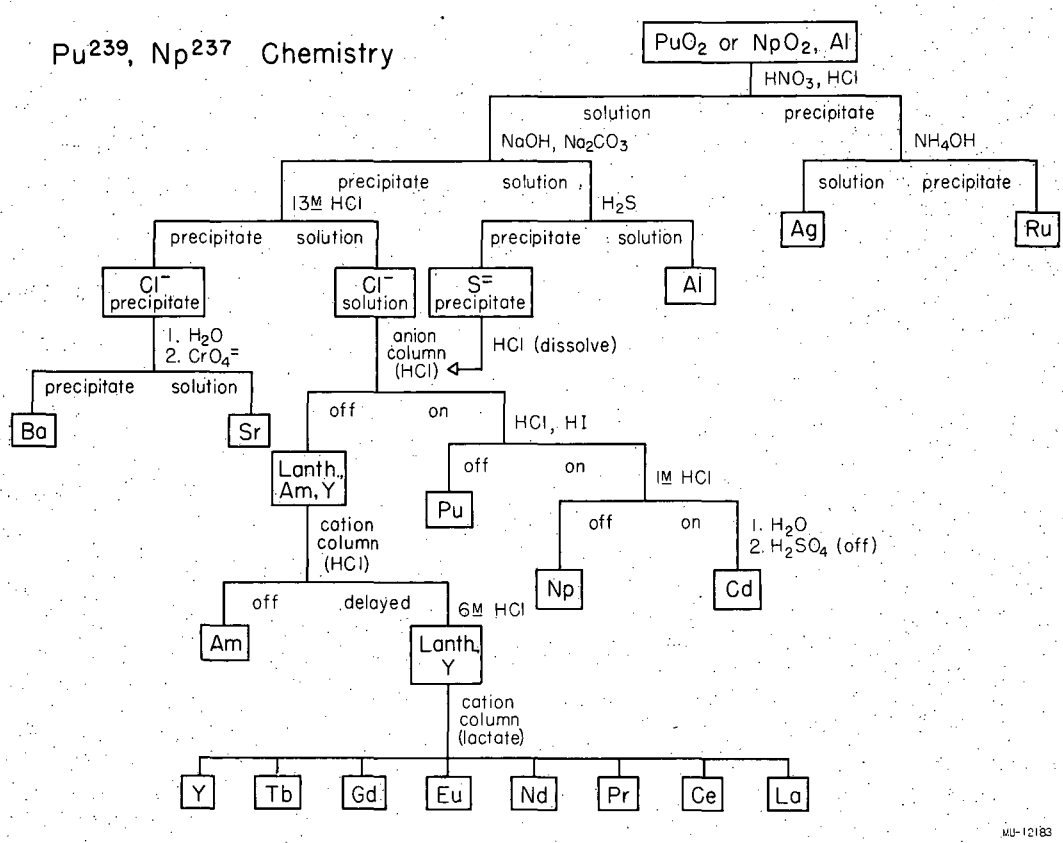

Fig. 1 The chemical separation scheme used in the plutonium and neptunium bombardments.

Ruthenium and Silver

present initially it was reduced to ruthenium metal by the aluminum during the dissolution. Also, when silver carrier was present, silver chloride was precipitated at this stage. The solution was centrifuged and the precipitate washed with dilute hydrochloric acid. The precipitate was then removed from the glove box and the silver and ruthenium were separated from each other by dissolving the silver chloride in 6N ammonium hydroxide. Standard procedures[112] were then used to further purify the ruthenium and silver.

Separation from Aluminum

The supernate from the target solution was then treated with sodium hydroxide and sodium carbonate to precipitate barium, strontium, yttrium, the rare earth elements and part of the cadmium. Americium, plutonium, and neptunium were carried on the precipitate. Aluminum and part of the cadmium remained in the supernate. It was found that in the neptunium bombardments only about 25 percent of the neptunium was carried on the precipitate in the presence of excess carbonate. It was often desirable to have as much of the neptunium carry on the precipitate as possible, so in these cases iron carrier was added and the hydroxide was precipitated by the addition of carbonate-free sodium hydroxide. This was centrifuged and sodium carbonate was added to the supernate to precipitate barium and strontium. The hydroxide and carbonate precipitates were combined and dissolved in hydrochloric acid. The resulting solution

Barium and Strontium

was saturated with hydrogen chloride gas to precipitate barium and strontium chloride. The precipitate was twice dissolved in water and re-precipitated with hydrogen chloride gas in order to reduce the alpha activity of this fraction to a low enough level to remove from the glove box. The barium and strontium were separated from each other by precipitating barium chromate from a neutral buffered solution leaving strontium in the supernate. Standard procedures[112] were used to further purify barium and strontium.

Cadmium sulfide was precipitated from the original hydroxide solution with hydrogen sulfide gas, dissolved in hydrochloric acid and added to the chloride supernate at this point. The chloride supernate was passed through a glass column (3 mm x 2.5 cm) packed with Dowex

A-1[114] anion exchange resin. The americium, yttrium, and rare-earth elements passed through the resin in the concentrated hydrochloric acid fraction. The plutonium, neptunium, and cadmium were adsorbed on the resin. The plutonium was desorbed with concentrated hydrochloric acid plus 0.1 M hydroiodic acid and the neptunium was desorbed with 4 M hydrochloric acid. After washing the column with a small amount of water the cadmium was desorbed with 0.75 M sulfuric acid and further purified using standard procedures.[112]

Plutonium and Neptunium

Americium and Rare Earth Separations

Hydrogen fluoride was added to the americium, yttrium, rare-earth fraction to precipitate the rare-earth and yttrium fluorides. The precipitate was dissolved in nitric and boric acids and the rare-earth and yttrium hydroxides precipitated by the addition of excess ammonium hydroxide. Americium was carried on both of these precipitates. In the cases that the rare-earth elements or yttrium were not taken out as fission products, about 5 mg of lanthanum was added to carry the americium. The hydroxide precipitate was dissolved in a minimum of concentrated hydrochloric acid and the americium was separated from the rare earths and yttrium by passing them through a glass column packed with 4 percent cross-linked Dowex-50 cation exchange resin.[114] The eluant was 20 percent absolute ethanol saturated with hydrogen chloride gas.[94] The americium was eluted in about 8 column volumes and the heavy rare-earth elements began to elute after about 12 column volumes of eluant had been used. The americium fraction was reduced to a low volumn and vaporized from a tantalum filament (see Sec. D) onto a platinum disc for counting. The rare earth and yttrium fraction were desorbed from the resin with 15 ml of 6 M hydrochloric acid, precipitated as a hydroxide with ammonium hydroxide and dissolved in a minimum of 6 M hydrochloric acid (3 - 4 drops). This solution was diluted to 15 ml with water and equilibrated with one ml of Dowex-50 cation exchange resin. The yttrium and each of the rare-earth elements were then separated from each other in a long (9 mm x 70 cm) glass column packed with Dowex-50 cation exchange resin. The eluant used was ammonium lactate of continuously varying pH over the pH range 3.5 to 5.0.[115]

Rare Earth and Yttrium Separation

Plutonium Purification

The plutonium fraction from the neptunium bombardments was carried on a lanthanum fluoride precipitate, dissolved in hydrochloric and boric acids, carried on a lanthanum hydroxide precipitate, and dissolved in concentrated hydrochloric acid. The plutonium was adsorbed on a small anion column and desorbed with concentrated hydrochloric, 0.1 M hydroiodic acid. The plutonium was then plated for counting.

After a month had elapsed (to allow the 22-hr Np^{236} to decay) plutonium tracer (Pu^{242}) was added to the neptunium fraction from the neptunium bombardments and the plutonium was again removed with two cycles of the plutonium procedure given in the previous paragraph. The plutonium tracer used in the original separation was Pu^{239}.

The neptunium fraction from the plutonium bombardments was purified according to the scheme outlined in the following section.

4. Chemical separations for uranium bombardments

A special problem was present in the series of deuteron bombardments on U^{233}. Extremely fast neptunium separations were required in order to characterize the (d,2n) and (d,3n) products (35-min Np^{233} and 13-min Np^{232} respectively). Because of this limitation, time consuming column separations had to be avoided and fission products which would tend to slow down the separation and purification of neptunium had to be left out. Hence, such fission products as ruthenium and silver which precipitated when the target was dissolved were only taken out in the bombardments at low energy (less than 15 Mev) where the 13-min neptunium activity could not be made in sufficient quantities to observe. The general separation scheme is illustrated in Fig. 2.

Neptunium

The chemistry used for the separation and purification of neptunium was essentially a modification of that proposed by Magnusson et al.[116] and is described in detail by Ritsema.[87] The neptunium was reduced to the plus-four state with ferrous ion and hydrazine then carried on zirconium phosphate by the addition of phosphoric acid (zirconium carrier was present initially). Protactinium was also carried on the precipitate. The zirconium phosphate was dissolved in hydrofluoric and nitric acids and

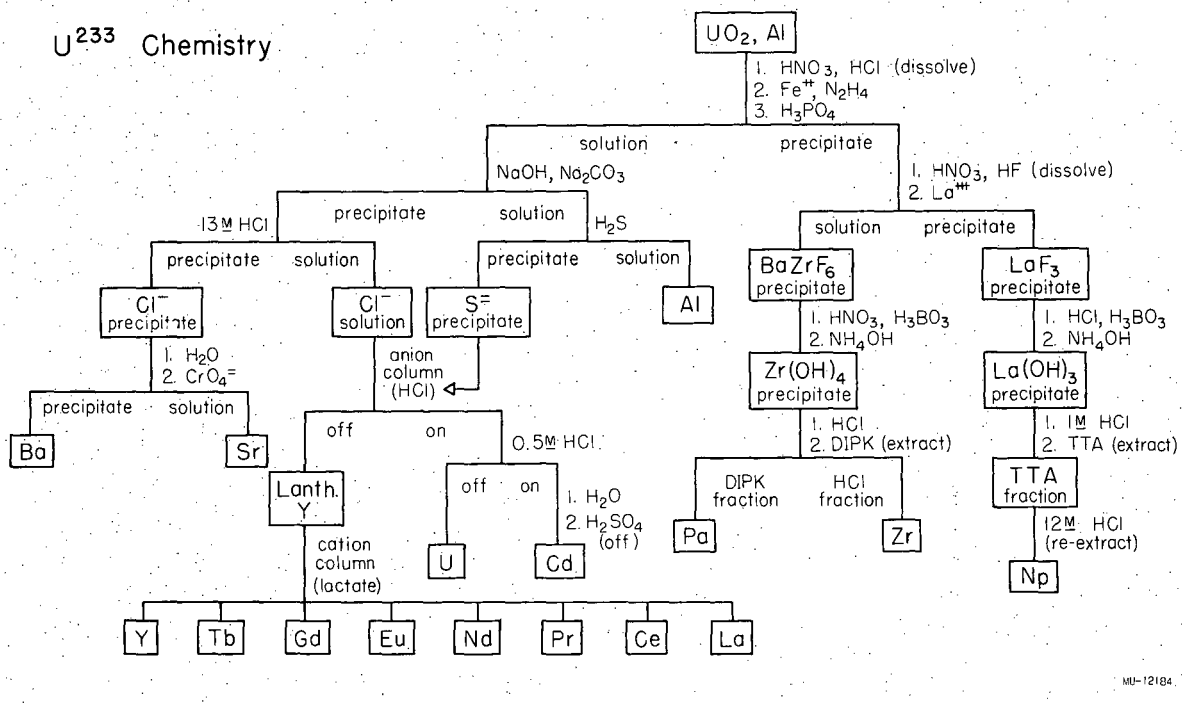

Fig. 2 The chemical separation scheme used in the uranium bombardments

lanthanum fluoride was precipitated by the addition of lanthanum carrier. Neptunium was carried on the precipitate, zirconium and protactinium remained in the supernate. The lanthanum fluoride was dissolved in boric and nitric acids and lanthanum hydroxide was precipitated by the addition of ammonium hydroxide. The neptunium was carried on the precipitate. The hydroxide precipitate was dissolved in 1 M hydrochloric acid, the neptunium was extracted into TTA (thenoyltrifluoroacetone) then re-extracted with 12 M hydrochloric acid. The 12 M hydrochloric acid was stirred once with benzene to remove dissolved TTA. The benzene fraction was discarded. The neptunium was then evaporated onto a platinum disc for counting. This neptunium procedure, including the dissolving step, was completed in times as short as 25 min, giving radiochemically pure neptunium in about 30 percent yield.

Zirconium and Protactinium Separation

The fluoride supernate containing the zirconium and protactinium was treated with excess barium nitrate solution, precipitating barium fluozirconate which carried the protactinium. The precipitate was dissolved in nitric and boric acids and barium sulfate was precipitated by addition of sulfuric acid. Zirconium hydroxide was precipitated with ammonium hydroxide carrying the protactinium and was dissolved in 7 M hydrochloric acid. The protactinium was then extracted into DIPK (di-isoproplketone). After being washed with 7 M hydrochloric acid the DIPK was evaporated to a low volume, transferred to a tantalum filament and the protactinium was vaporized onto a platinum disc. (See section on mounting samples.) The zirconium was purified by extraction into TTA from 2 M hydrochloric acid. After being washed with 6 M hydrochloric acid the TTA was evaporated to dryness in a porcelain crucible and the zirconium was ignited to the oxide for mounting and counting.

The uranium, barium, strontium, cadmium, yttrium, and rare-earth elements remaining in the supernate from the zirconium phosphate precipitation were then separated according to the scheme outlined for the plutonium and neptunium bombardments. The uranium adsorbed on the anion resin in concentrated hydrochloric acid and was desorbed with 0.5 M hydrochloric acid.

D. Mounting Samples

1. Spallation Products

The spallation product activities were mounted on 2-mil platinum discs one inch in diameter. The actinide samples from the series of plutonium bombardments and from most of the neptunium bombardments were volatilized onto the platinum disc from a hot (~2000°C) tantalum filament in an evacuated system. The advantage of this method is that very thin plates can be obtained so that the resolution of different alpha groups on the alpha pulse analyzer is improved, and the absorption of low-energy radiations from electron-capture isotopes is reduced to a minimum. The disadvantages of the method are the expenditure of time necessary to prepare the filament and evacuate the system (30 - 45 min on the apparatus used) and the erratic and often low (< 50%) yields obtained. Occasionally a coating of tantalum oxide was deposited on top of the sample which introduced the same thick sample errors that the method was designed to eliminate. Due to the time expenditure involved in the volatilization of samples this method could not be utilized for the neptunium fraction from the uranium bombardments. Because of the short-lived activities present these samples were merely evaporated to dryness on a platinum disc and ignited to a red heat in a bunsen burner.

A new method of plating tracer quantities of actinide (or lanthanide) elements in an extremely thin layer in high yields has recently been developed in this laboratory.[117] The method consists of electroplating the activity from a 2 - 4 M ammonium chloride solution which has been adjusted to the methyl red end point with ammonium hydroxide and hydrochloric acid. The activity is plated onto a platinum disc which acts as the cathode; the anode is a stationary platinum disc or rod. It was found that greater than 70 percent of the activity could be plated in a 3-min period when the current was maintained at 2 - 3 amperes per square centimeter and the electrode spacing was set to keep the potential drop across the cell at 6 - 8 volts. An excess of ammonium hydroxide was added to the plating cell before the current was shut off in order to quench the reaction and prevent the activity from redissolving. This plating method was used for the americium samples on

a few of the high-energy neptunium bombardments and for all of the plutonium milking samples from the same series. The plates obtained have been determined (by observing the energy resolution of alpha particles) to be thinner than the plates obtained by the volatilization method.

It might be expected that different efficiencies for counting electron capture isotopes would result from using the three plating methods. This problem is discussed in the appendix.

2. Fission Products

The fission products were slurried with ethyl alcohol or acetone into tared 2-mil aluminum "hats." These were then dried under a heat lamp and weighed. Sample loss was prevented by coating the samples with a thin coat of zapon lacquer (Atlas Powder Co., North Chicago, Ill.) which had been diluted with ethyl acetate.

E. Counting Techniques and Treatment of Data

The disintegration rate, hence the number of atoms, of a given product nuclide was determined by resolution of decay curves or when possible by resolving radiations of a given unique energy. Four types of counters were used, the first three being used to determine the disintegration rates or the yields for the spallation products, the latter being used for fission product determinations.

1. Spallation Products

Alpha counter. To determine the absolute disintegration rate of alpha emitting products or the chemical yield of alpha-emitting tracers, an argon filled ionization chamber attached to a standard scaling circuit was used. The efficiency of this counter for alpha particles is 52 percent.[118]

Alpha pulse analyzer. The alpha-active samples were counted in a 48-channel differential alpha particle pulse-height analyzer.[119] It is possible with this instrument to determine the relative amounts of alpha-particle emitting isotopes which have alpha particles differing in energy by about 200 kev or more. The instrument amplifies and electronically sorts pulses of different energy produced by alpha particles in a methane-filled ionization chamber. These are then recorded as a

function of energy on 48 separate registers. The energy range measured can be controlled and is determined roughly by counting electronically produced pulses of a given approximate energy, or an accurate determination can be made by counting isotopes having accurately known alpha particle energies. The "peak" corresponding to an alpha particle of a given energy is spread over 3 - 5 registers. The number of counts in the total peak in a given time is proportional to the number of alpha disintegrations per minute of that particular energy. It is essential, for adequate energy resolution, to use extremely thin samples. Otherwise the energy of the alpha particles is altered by collisions within the sample and prohibitive "tailing" on the low-energy side of the peak results. It was found that volatilized or electroplated samples gave adequate resolution with electroplating being the superior of the two methods.

All samples to which alpha-emitting tracers had been added were counted on the alpha-pulse analyzer. This was to establish the portion of the total alpha activity which was due to the tracer. For example, the Np^{237} used as target material for the helium ion bombardments contained a small amount of Pu^{238}. The presence of this Pu^{238} in the plutonium fraction from the bombardment would result in an erroneous yield had it not been counted on the pulse analyzer. (It was established that no Pu^{239} contaminant was present in the Np^{237}.)

The cross section for the $(d,\alpha n)$ reaction on U^{233} was determined by observing the growth and decay of U^{230} in the protactinium fraction. The theoretical growth and decay curve, based on an 8 percent beta-branching for Pa^{230}, [120] is shown in Fig. 3. Fission product (probably zirconium) contamination of the protactinium fraction prevented determination of Pa^{230} directly.

The $(\alpha,\alpha n)$ cross section for Np^{237} was determined by allowing the 22-hr Np^{236} to decay completely, chemically removing the plutonium from the neptunium and counting the Pu^{236} alpha particles on the alpha pulse analyzer. A value of 57 percent was used for the beta-branching of Np^{236}. [121] Plutonium (242) tracer was added to give the chemical yield.

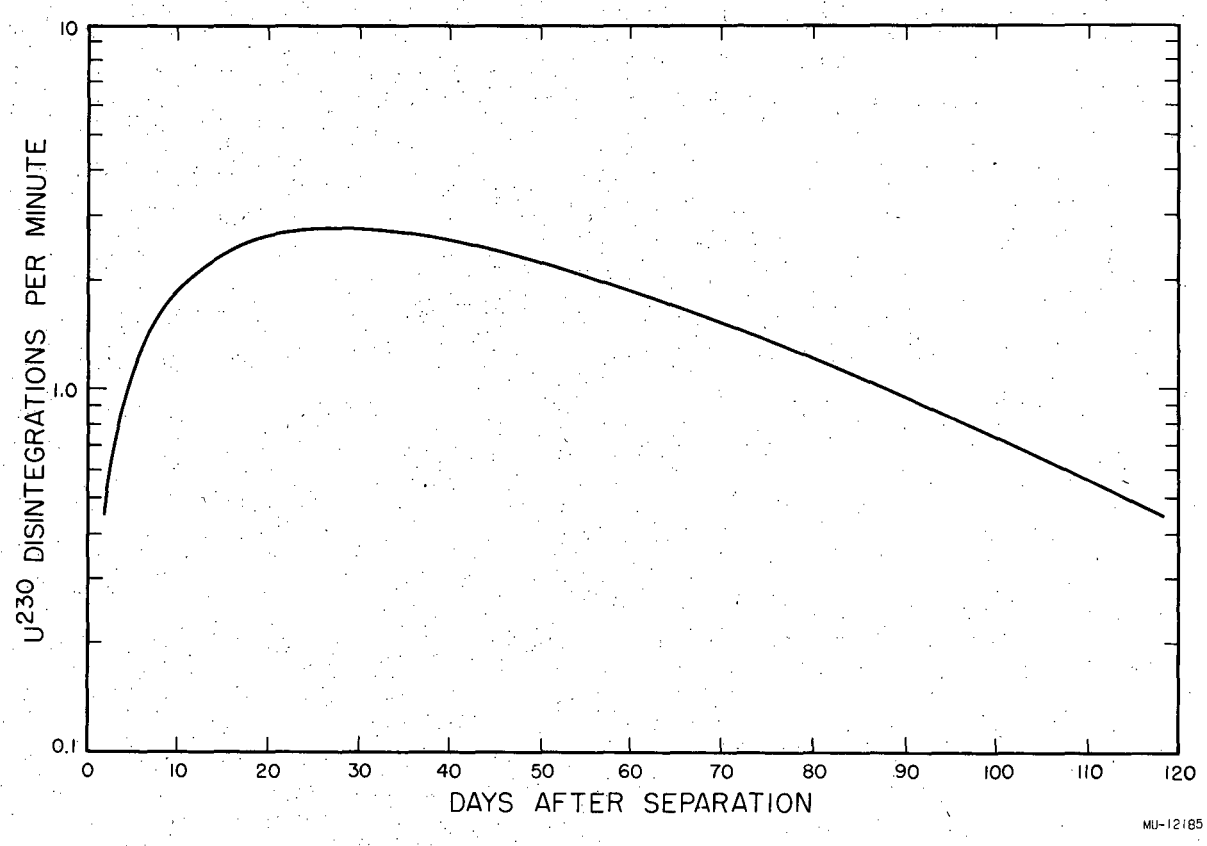

Fig. 3 Growth and decay (theoretical) of U^{230} in a sample containing 100 disintegrations per minute of Pa^{230} initially. Based on an 8 percent beta-branching of Pa^{230}.

Windowless Proportional Counter (Nucleometer). Isotopes decaying by electron capture were counted in a nucleometer.[122] The high efficiency of this instrument makes it especially favorable for counting electron-capture isotopes since it can detect auger electrons. The nucleometer is a methane flow windowless proportional counter. There aretwo plateaus on this instrument separated by the proportional region. The operating plateau has been determined for a number of electron-capture isotopes.[123] and was checked for each of the isotopes investigated in this study. On the basis of these determinations, an operating voltage of 3900 volts was chosen. The plateau was redetermined periodically to detect any change in the operating characteristics of the instrument. An efficiency factor (or "K" factor) for the counting system used must be applied in order to convert the number of counts per minute of a given activity to disintegrations per minute. The determination of counting efficiencies for the electron-capture isotopes constituted a major problem in the present study. The counting efficiencies of Am^{239}, Am^{240} and Np^{234} were determined by counting the alpha-particle emitting daughters in each case. The details of these determinations along with a discussion and summary of nucleometer counting efficiencies of electron-capture isotopes are given in the appendix. Table II gives a tabulation of the counting efficiencies used in the cross-section calculations. In the cases where the nuclide decayed by both electron capture and by beta-emission, the efficiency for beta-particles was extrapolated from the data given by Ritsema.[87] A value of 60 percent was assumed for the counting efficiency of all unmeasured electron-capture isotopes. (See appendix)

The alpha branching associated with the decay of Np^{233} and Am^{239} [120] and the positron emission associated with the decay of Np^{234} [124] are present in such small amounts as to not affect the counting efficiency.

Table II. Nucleometer Counting Efficiencies Used in the Present Study

Nuclide	Mode of Decay	Counting Efficiency (Percent)
Np^{232}	E.C.	60[a]
Np^{233}	E.C.	60[a]
Np^{234}	E.C.	63[b]
Np^{236}	E.C. 43% β^- 57%[c]	70[a,d]
Np^{238}	β^-	80[d]
Am^{238}	E.C.	60[a]
Am^{239}	E.C.	60[b]
Am^{240}	E.C.	91[b]

a. Assumed
b. Determined, this study
c. Ref. 35, p. 36
d. Ref. 15, p. 17

2. Fission Products

Geiger-Müller counter. The fission products, all of which were beta minus emitters, were counted on a standard Geiger-Müeller counter. The counting tube was an end-window Amperex 100c tube with a mixture of chlorine and argon. This was attached to a standard scaler. The tube and sample holder was surrounded by a thick-walled lead case to reduce background counts. The sample could be placed in any one of five positions (shelfs) relative to the counting tube. Whenever possible (i.e.; if the counting rate was not too high) the same position was always used (shelf 2). This was approximately 2 cm from the counting tube.

The conversion of counts per minute on the Geiger-Müller counter to disintegrations per minute is complicated by several factors, some of which cannot be determined very accurately. The general problem of absolute beta counting has been investigated by many workers and is the subject of many papers[125-128] and at least one symposium.[126] In spite of the efforts expended in this field the determination of absolute disintegration rates is frequently uncertain to greater than 20 percent although in some cases where the energy of the emitted beta particle is

high, the decay scheme is uncomplicated, and the daughter is stable or long-lived the disintegration rate can be determined to 5 percent. The factors entering into the conversion are given in the following equation:

$$d/m = (c/m + cc)\ \frac{(AW)\ \ 100}{(BS)\ \ (SSSA)\ \ (G)},$$

where d/m is the disintegration rate, c/m the counting rate and the other factors are discussed below.

cc-coincidence correction. Each time a beta particle is received and counted in the ionization chamber (G-M tube) there is a time delay before another beta particle can be counted. This is known as the "dead time" of the instrument. Since beta particles entering the counting tube during this "dead time" are not counted, a suitable correction must be made. The correction is proportional to the counting rate (since the dead time is constant) and has been determined to be 0.45 percent per thousand counts per minute.[129]

AW - air-window correction. In passing from the sample to the inside of the counting tube some of the beta particles are absorbed or scattered by the air or by the mica window in the tube. The air thickness was 2.4 mg/cm^2 and the window thickness was 3.5 mg/cm^2. The mass absorption coefficient is proportional to Z/A of the absorber[130] so for light elements where Z/A is approximately constant, this quantity is nearly independent of the absorber. Therefore the air-window correction can be determined by extrapolating aluminum absorber curves back 5.9 mg/cm^2 from the counting rate obtained with zero absorber. This has been done for beta particles of various energies by Ritsema, (Ref. 87, p. 19) and the values used in this work were taken from that tabulation. This correction was usually less than 10 percent but in some cases was greater than 100 percent (Ex. for Ru^{103} AW = 2.25).

B.S. - backscattering correction. The backscattering correction was determined from the curves of Burtt[131] for beta particles scattered from a saturation aluminum backing material. For high-energy beta minus particles (> 0.8 Mev) this factor is 1.28.

SSSA - self-scattering self-absorption correction. Whenever possible the empirical curves of Hicks and Gilbert[132] and Hicks, Stevenson, Gilbert, and Hutchin[133] were used. In other cases the correction factor was estimated from the curves of Nervik and Stevenson.[127]

The interpolation was made on the basis of summed atomic numbers as described by Ritsema.[87] For low-energy beta particles for which specific correction curves have not been measured errors due to uncertainties in the SSSA correction may be as high as 20 percent. In most other cases, especially where the curves of Hicks, et al. are applicable the errors due to this factor are certainly less than 10 percent.

G - geometry correction. The geometry factor is essentially the ratio of the solid angle subtended by the window of the Geiger tube and the total solid angle about the sample (this assumes that all of the beta particles entering the Geiger tube will be counted, this is not exactly but almost true). This factor can be determined from geometric considerations or can be measured indirectly. The geometry of shelf 2 of the counter used was determined to be 3.16 percent by counting a weightless sample of known disintegration rate mounted on a "weightless" backing material (zapon film). The geometry is simply the fraction of the total number of emitted beta particles which get into the counting tube after the air-window absorption factor has been applied.

Except for the cases noted for the SSSA correction, the above correction factors are straightforward and errors arising from un certainties in these values are estimated to be less than 10 percent.

Corrections for activity due to daughters. For fission products decaying to stable or long-lived daughters, application of the above correction factors gives directly the number of disintegrations per minute. In many cases, however, the nuclide of interest decays to a daughter which is also radioactive and has a lifetime of the same order of magnitude or shorter than the parent. Therefore, that part of the observed activity due to the daughter must be subtracted from the total activity in order to obtain the yield of the parent. Obviously each nuclide must be considered separately but there are a few general considerations in making this correction. The number of atoms of a radioactive daughter can be calculated from the formula:

$$N_2 = \frac{\lambda_1}{\lambda_2 - \lambda_1} \quad N_1^{\,o} \quad (e^{-\lambda_1 t} - e^{-\lambda_2 t})$$

where N_2 is the number of atoms of the daughter present at the time, t, after the separation of the parent from the daughter, N_1^o is the number of atoms of the parent nuclide present at the separation time and λ_1 and λ_2 are the decay constants of the parent and daughter respectively. The total measured activity A is:

$$A = C_1A_1 + C_2A_2 = C_1N_1\lambda_1 + C_2N_2\lambda_2$$

where C_1 and C_2 are the counting efficiencies (detection coefficients) of the parent and daughter respectively. The counting efficiencies C_1 and C_2 are by no means necessarily the same and often are very different in magnitude. It is in the determination or estimation of the relative counting efficiencies that the largest uncertainty is often introduced. The problem is further complicated by the fact that along with beta minus particles emitted by the daughter nucleus one must often consider conversion electrons emitted when the decay of the parent or daughter proceeds through a short-lived meta-stable state and subsequent de-excitation gamma radiation is converted. This requires a detailed knowledge of the decay scheme of both parent and daughter including gamma-ray intensities and conversion coefficients. The information required is often lacking. In order to estimate the relative counting efficiencies it has been assumed in this study that except for one case,[134] conversion electrons have the same backscattering and self-scattering self-absorption characteristics as beta particles having a maximum energy three times as high. For example a 0.50-Mev conversion electron was treated the same as a beta particle of 1.5 Mev maximum energy. This assumption is based on the fact that the most probable energy for a beta particle is about one third of its maximum energy.[135] The relative counting efficiencies can then be estimated by comparing the relative air-window, back-scattering, and self-scattering self-absorption factors. Since the last of these is strongly dependent on the mass of precipitate, the correction must be determined separately for each sample. The decay data required was taken from the compilation of Hollander, Perlman, and Seaborg.[120] The errors introduced by this treatment are difficult to assess, but probably range from about 5 percent for the best cases to as high as 30 percent for the worst cases.

3. Resolution of decay curves

The spallation product and fission product activities were obtained by resolution of decay curves. In most cases the number of counts per minute of a given nuclide could be determined by subtraction of longer-lived components. Occasionally, however, the half lives of two components did not differ sufficiently to give a straightforward subtraction[136] or the relative amount of two components was very different causing a large uncertainty in the resolution of the nuclide present in smaller abundance.[137] In these cases the well-known "Biller plot" method was employed. For two activities decaying independently with the decay constants λ_1 and λ_2 respectively:

$$A = C_1A_1 + kC_2A_2 = C_1\lambda_1N_1^{\circ}\ e^{-\lambda_1 t} + C_2\lambda_2N_2^{\circ}\ e^{-\lambda_2 t}$$

where A is the observed activity at the time t after the bombardment and N_1° and N_2° are the number of atoms of 1 and 2 at the end of the bombardment. Multiplying the above expression by $e^{\lambda_2 t}$ we get:

$$Ae^{\lambda_2 t} = C_1\lambda_1N_1^{\circ}\ e^{(\lambda_2 - \lambda_1)t} + C_2\lambda_2N_2^{\circ}$$

if we then plot $Ae^{\lambda_2 t}$ vs $e^{(\lambda_2 - \lambda_1)t}$ a straight line is obtained the slope of which equals $C_1\lambda_1N_1^{\circ}$ and the intercept of which equals $C_2\lambda_2N_2^{\circ}$.

The samples were counted at least four times during each half-life period of the shortest lived isotope.

F. Cross Section Calculations

The activity of each isotope was extrapolated to the end of the bombardment and the number of atoms present at the end of the bombardment was calculated from the formula:

$$N = \frac{(d/m)\ (t_{1/2})}{(0.693)\ (\text{chemical yield})}$$

where d/m is the number of disintegrations per minute at the end of the bombardment and $t_{1/2}$ is the half-life of the isotope in minutes. The cross section in millibarns was then calculated from,

$$\sigma\ (mb) = \frac{N}{(n/cm^2)\ (It)}\ (10^{27})$$

N is the number of atoms at the end of the bombardment, n/cm^2 is the number of target atoms per square centimeter and (It) is the number of particles striking the target. When the half-life of any isotope was so short that appreciable decay took place during the course of the bombardment the following expression was used:

$$\sigma\ (mb) = \frac{(0.693)\ (N)\ (10^{27})}{(t_{1/2})\ (m/cm^2)\ (I)\ (1-e^{-\lambda t})}$$

N is the number of atoms at the end of the bombardment, $t_{1/2}$ is the half life of the isotope in minutes, I is the beam intensity (particles per minute), λ is the decay constant of the isotope, and t is the length of the bombardment. This expression assumes a constant beam intensity (I). The cyclotron was tuned prior to each bombardment and an attempt was made to keep the beam intensity constant during the bombardment. For those cases in which large variations in the beam intensity was noted during the bombardment the recorder trace was used to make stepwise integrations over periods in which the beam intensity was essentially constant.

III. RESULTS

A. Spallation Cross Section

The minimum projectile energy at which a given spallation reaction is energetically possible is called the threshold energy. This energy can be calculated from the formula:

$$\text{Threshold energy} = Q \frac{M_c}{M_T}$$

where M_c is the mass of the compound nucleus formed and M_T is the mass of the target nucleus. Q is the nuclear reaction energy and can be obtained from the reaction;

$$Q = c^2(\Sigma M_R - \Sigma M_P)$$

where ΣM_R is the sum of the reactant masses and ΣM_P is the sum of the product masses. For example for the reaction $Pu^{239}(d,n)Am^{240}$; $Q = c^2(M_{Pu^{239}} + M_d - M_{Am^{240}} - M_n)$. The masses used in the threshold calculations were taken from the compilation of Glass, Thompson, and Seaborg.[59]

1. Pu^{239} plus deuterons.

The cross sections for the Pu^{239}(d,spallation) reactions are given in Table III. The excitation functions are shown in Fig. 4 and 16. The limits of error are estimated.

2. Np^{237} plus helium ions.

The spallation cross sections are given in Table IV and the corresponding excitation functions are shown in Fig. 5 and 25. A value of 57%[121] was used for the beta-branching of Np^{236} in order to calculate the cross section for the $Np^{237}(\alpha,\alpha n)Np^{236}$ relation.

3. U^{233} plus deuterons.

The spallation produce cross sections are tabulated in Table V and the excitation functions are in Fig. 6 and 29. The cross sections for the $U^{233}(d,\alpha n)Pa^{230}$ reaction are based on a value of 8%[120] for the beta minus branching of Pa^{230}. This cross section was determined by observing the U^{230} grow and decay in the protactinium fraction.

The quoted limits of error on the spallation cross sections do not include uncertainties in the counting efficiencies used. These are discussed in the appendix.

Table III

Pu^{239} plus Deuterons; Spallation Cross Sections (millibarns)

Reaction	d,n	d,2n	d,3n	d,dp	d,αn	d,α3n
Product	Am^{240}	Am^{239}	Am^{238}	Np^{238}	Np^{236}	Np^{234}
Threshold(Mev)	-1.87	3.84	11.04	6.20	-7.62	4.99
Deuteron Energy (Mev)[a]						
9.2	1.20±0.11	3.0±0.3				
12.3	10.4±0.9	25.9±2.8				
15.0	14.2±1.3	27.5±3.0	<4	0.054±0.01	<0.05	
16.1	12.7±1.1	27.3±3.0	<7			
17.9	13.3±1.2	20.8±2.3	10.0±1.7			
20.2	13.3±1.2	22.9±2.5	18.1±3.0			
20.6	13.0±1.2	20.4±2.2		0.81±0.11	0.35±0.04	<0.1
23.4	12.8±1.1	19.2±2.2	22.6±3.8			

[a] ±0.5 Mev

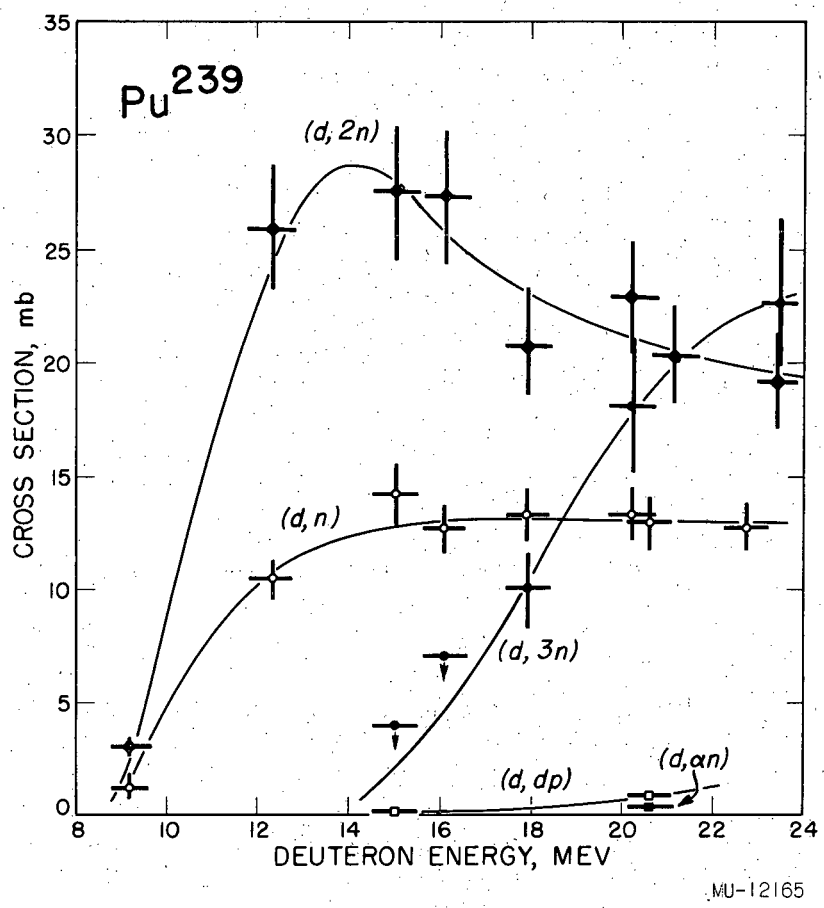

Fig. 4 Spallation excitation functions for deuteron-induced reactions of Pu^{239}.

Table IV

Np^{237} plus Helium Ions Spallation Cross Sections (millibarns)

Reaction	(α, n)	(α, 2n)	(α, 3n)	(α, αn)
Product	Am^{240}	Am^{239}	Am^{238}	Np^{236}
Threshold(Mev)	12.8	18.6	25.9	6.9
Helium Ion Energy(Mev)[a]				
19.8		1.88±0.11		
22.7	0.85±0.11	8.02±0.48		0.107±0.004
24.2	0.82±0.11	11.8±0.71		
28.1	2.31±0.30	15.5±0.9	<3	0.426±0.017
31.5	3.50±0.46	15.4±0.9	6.1±1.2	4.39±0.17
31.6	3.00±0.39	14.2±0.8	4.8±1.0	
35.0	2.30±0.30	13.0±0.8	8.7±1.4	5.76±2.3
38.1	2.67±0.35	14.2±0.8	13.4±2.2	11.75±0.47
40.7	2.78±0.36	10.2±0.6	9.8±1.6	16.9±0.7
44.9	1.96±0.26	9.58±0.57	5.4±0.7	
45.7	2.78±0.36	11.2±0.7		21.7±0.9

[a] ±0.5 Mev

Table V

U^{233} plus Deuterons Spallation Cross Sections (millibarns)

Reaction	(d, n)	(d, 2n)	(d, 3n)	(d, αn)
Product	Np^{234}	Np^{233}	Np^{232}	Pa^{230}
Threshold(Mev)	-1.88	4.14	11.73	-7.19
Deuteron Energy(Mev)[a]				
9.0	<1.2	0.56±0.08		
12.1	10.5±1.6	16.2±2.2		
14.0	10.7±1.6	13.4±1.8		0.08±0.03
15.4	13.2±2.0	11.6±1.6	<3	0.10±0.04
19.6	11.0±1.7	4.93±0.67	12.9±2.7	0.91±0.36
21.5	13.8±2.1	5.82±0.79	14.5±3.0	
23.4	12.6±1.9	7.67±1.04	10.9±2.3	1.86±0.74

[a] ±0.5 Mev

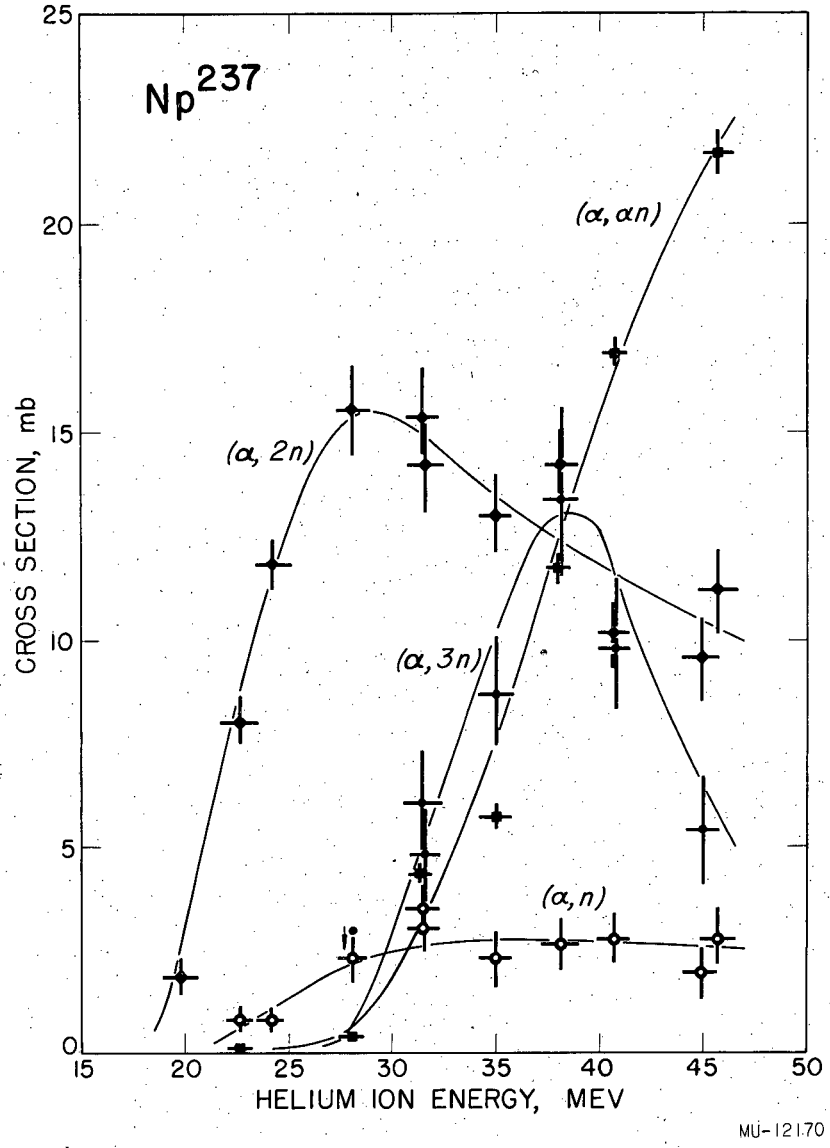

Fig. 5 Spallation excitation functions for helium ion-induced reactions of Np^{237}.

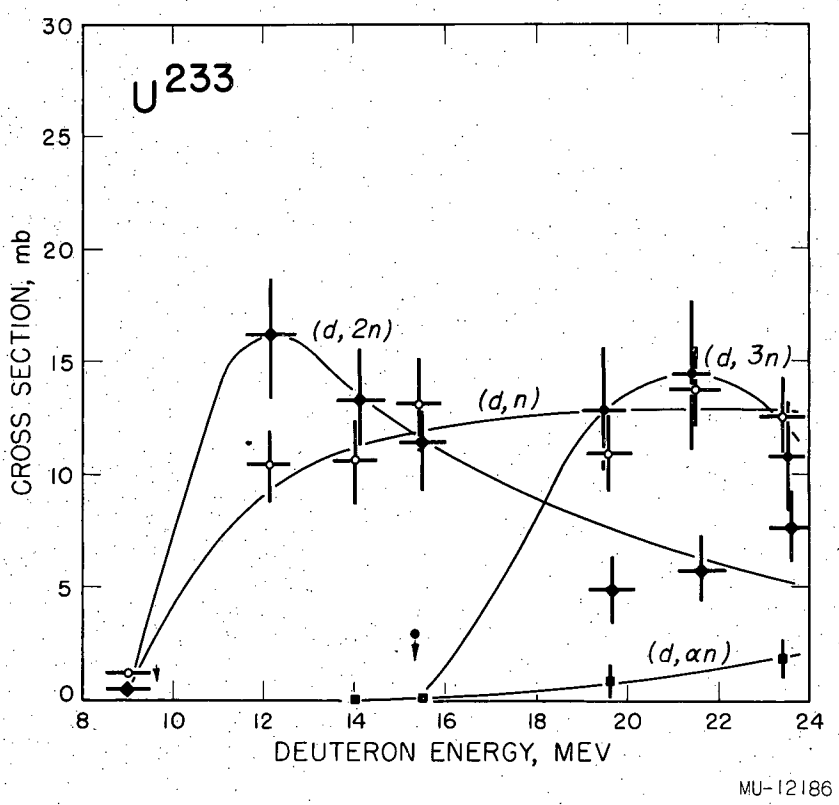

Fig. 6 Spallation excitation functions for deuteron-induced reactions of U^{233}.

B. Fission Cross Sections

In the determination of a total fission cross section by the radio-chemical method, the yield of a sufficient number of selected mass chains must be determined to define the fission yield curve. The fission yield curve (yield vs. mass number) can then be summed over the masses in order to obtain the total fission yield for incident particles of a given energy.

1. Primary fission yields.

For low energy neutron induced fission of U^{233}, U^{235} and Pu^{239}, the primary fission products have considerable neutron excess and beta decay toward stability with a general increase in half-life of the members of the decay sequence. For any mass number there is a distribution of "primary" fission products with respect to the nuclear charge but those near stability appear in low yield. Consequently, the yield of a beta emitting nuclide one or two removed from stability represents essentially the total yield for that particular mass number, providing sufficient time has elapsed to allow shorter-lived predessors to decay. The yields of selected fission products can then be used to define the fission yield curve.[138] It has been postulated that for low energy fission the most probable primary fission products for different mass chains are displaced on equal distance (3.5 to 4.1 nuclides) from the beta stability line independent of mass number.[66]

For fission induced by high energy particles (> 100 Mev) the yield of a given beta decaying fission product no longer represents the total yield of the mass chain. The most probable fission product is often stable or even neutron deficient.[2,139] For 190 Mev deuterons on bismuth it has been suggested that the most probable primary fission product for a given mass chain has the same neutron to proton ratio as the fissioning nucleus.[2]

The energy range under consideration in the present work is intermediate to the very low and very high energy cases for which information is available on primary fission yields. The behavior in this energy region cannot, therefore, be predicted with any certainty.

It is not possible to measure by radiochemical methods the independent yields of each member of even one beta decay chain. In fact, it is only possible to measure the primary yields of scattered individual nuclides which are shielded by stable or long-lived isotopes. For example, if nuclide Z of mass number A is radioactive but nuclide Z-1 with the same mass number is stable, any of Z observed in fission must be produced directly since it cannot be produced by decay of Z-1.

It is from these scattered individual primary yields that we must attempt to derive a coherent picture of the primary fission product distribution. The primary fission cross sections of several fission products have been determined and are tabulated in Table VI. The fraction of the total chain yield has been estimated in each case and is shown with the cross section. The limits of error are estimated. The large limits of error given for Pr^{143} are a result of uncertainty in the Ce^{143}-Pr^{143} separation time.

In order to put the fractions of total chain yield from Table VI into a form which will enable us to get total mass-chain cross sections from the measured fission product cross sections, we will have to anticipate some of the discussion and conclusions of the next section.

The fractions of total chain yield have first been plotted according to the chain positions predicted by the hypothesis of equal charge displacement which Glendenim and others have applied so successfully to low-energy neutron induced fission.[66,67,138] The modified treatment of Pappas,[67] which takes into account the effect of shell structure in the fission products, was used for the calculations. The result of this treatment is shown in Fig. 7.

The fractions of total chain yield were also plotted according to the chain positions predicted on the basis of the assumption that the most probable primary fission products have the same neutron to proton ratio as the fissioning nucleus. This is shown in Fig. 8. In both figures, the chain position $Z-Z_p = 0$ refers to the most probable primary fission product for each mass chain as predicted by each treatment. Fig. 8 was used for the correction of measured fission yields to obtain the total mass chain yields.

The assumptions on which Fig. 7 and 8 are based and other aspects of the problem are discussed in section IV. It should be mentioned here that the apparent fissioning nucleus was estimated from the best values for the center of symmetry of the fission yield curves. The mass at the center of symmetry was doubled to give the mass of the apparent fissioning nucleus. This is essential in the calculations leading to Fig. 7 and 8 and in the application of Fig. 8 to the fission yield corrections. The center of symmetry was first obtained from the uncorrected fission product cross sections. This value was used to calculate a preliminary version of Fig. 8 which was used in turn to correct the fission cross sections. New fission yield curves were then plotted and the new, slightly different value for the center of symmetry was used to construct a more refined version of Fig. 8. This procedure was repeated until the changes in the fission yield curves and in Fig. 8 became negligibly small. In general, two or three such cycles were required.

Table VI

Primary Fission Product Cross Sections and Fractions of Total Chain Yield

Target Material	Helium Ion or Deuteron Energy	Product	Independent Cross Section (mb)	Estimated Fraction of Total Chain Yield (percent)
Pu^{239}	20.6 Mev deuterons	Y^{90}	0.46±0.08	2.1±0.5
		La^{140}	7.6±1.5	21.1±6.0
		Pr^{143}	6.3±2.6	19.0±9.1
Np^{237}	31.5 Mev helium ions	Ag^{112}	1.6±0.4	7.1±1.6
		La^{140}	6.3±1.3	23.0±5.3
		Pr^{142}	0.84±0.21	5.4±1.6
Np^{237}	45.7 Mev helium ions	Ag^{112}	9.24±1.79	15.0±3.2
		La^{140}	12.6±3.0	40.2±10.3
		Pr^{142}	1.86±0.44	12.1±3.2
		Pr^{143}	8.3±3.2	33.2±14.0
U^{233}	23.4 Mev deuterons	La^{140}	8.8±1.6	22.0±4.2

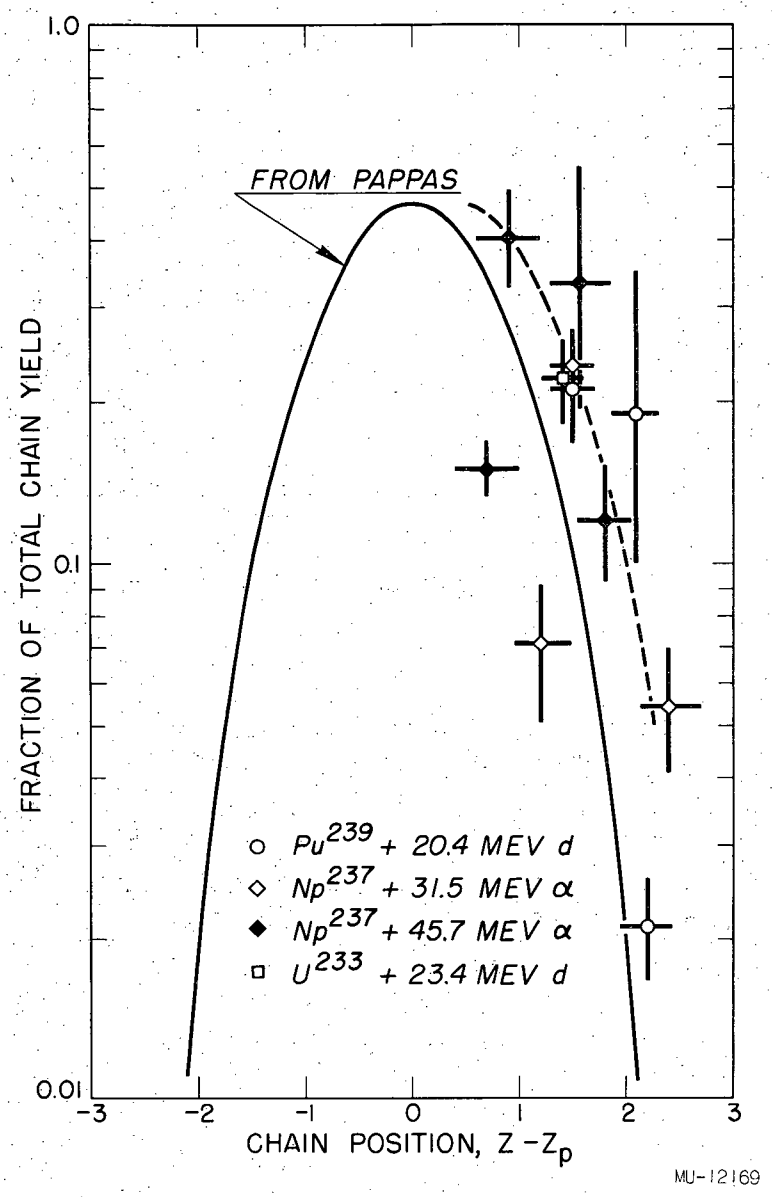

Fig. 7. Fractions of total chain yield vs the chain positions predicted by the equal charge displacement hypothesis. The solid curve is from Pappas (Ref. 67).

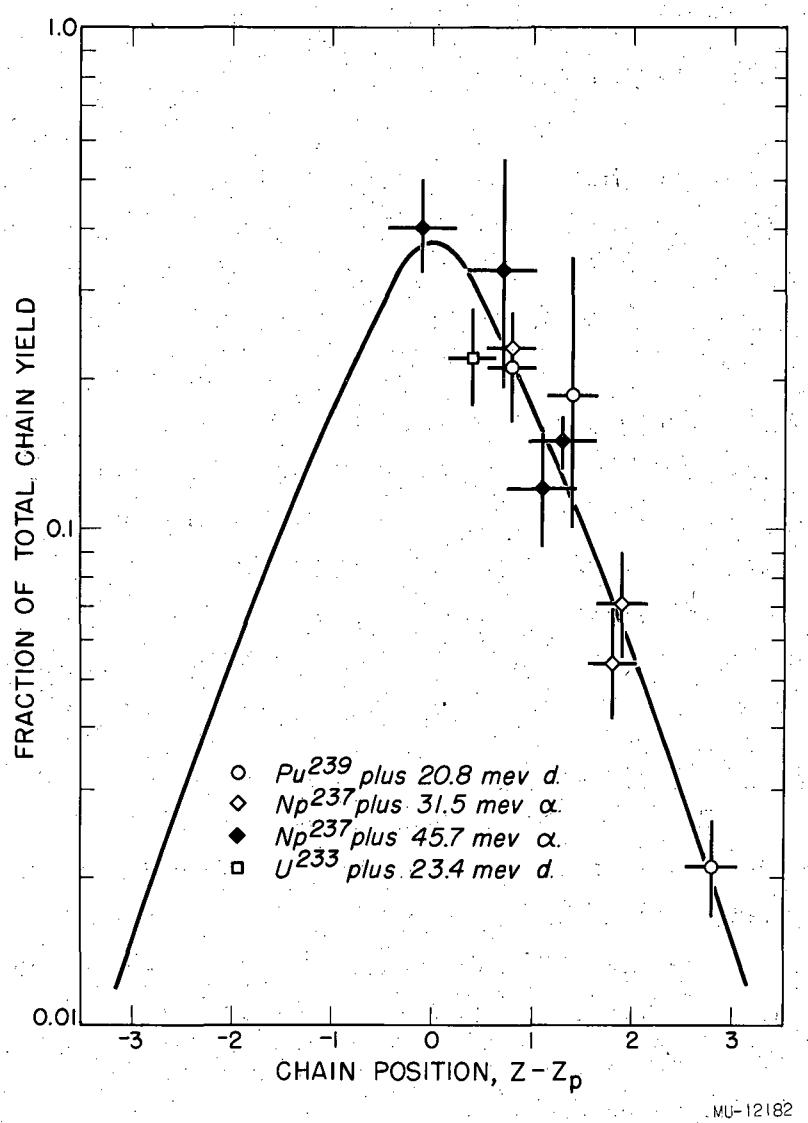

Fig. 8 Fractions of total chain yield vs the chain positions predicted by assuming the same neutron to proton ratio for the most probable primary fission products as for the apparent fissioning nucleus.

2. Pu^{239} plus deuterons.

The fission product cross sections for the reaction of deuterons on Pu^{239} are given in Table VII. Both the measured cross sections for a given fission product and the corrected cross section for the total mass chain are listed. The Cd^{115m} cross sections should be regarded as upper limits because low counting rates often prevented characterization of this isotope by decay analysis. In these cases any residual activity after decay of the Cd^{115} was treated as Cd^{115m}. The fission yield curves for deuterons of different energies are shown in Fig. 9-14. Total chain yields are plotted and the limits of error are estimated to be about 10-20%. The cross sections for 20.2 and 20.6 Mev deuterons have been averaged and plotted for 20.4 Mev deuterons since these two bombardments fall within the limits of error of the energy determination of being at the same energy. The variation in the magnitude and shape of the fission yield curves with increasing deuteron energy are shown in Fig. 15. The total fission yields, obtained by summing the individual fission yield curves over the mass numbers from A = 70 to A = 170, are compared to the spallation cross sections in Fig. 16.

3. Np^{237} plus helium ions.

The measured fission product cross sections and the corrected total mass chain cross sections for the reaction of helium ions are tabulated in Table VIII. The fission yield curves for helium ions of different energies are illustrated in Fig. 17-23. The variation of the fission yield curves with increasing helium ion energy is shown in Fig. 24. The total fission cross sections are compared to the spallation cross sections in Fig. 25.

4. U^{233} plus deuterons.

The fission product cross sections and the corrected total mass chain cross sections for the reaction of deuterons on U^{233} are listed in Table IX. Very fast chemical procedures were required to separate and characterize the short-lived neptunium isotopes produced in the bombardments, particularly at the highest energies. Consequently some of the fission product decay chains were broken before sufficient time had elapsed for all of the short-lived predecessors of some of the fission products to decay. The correction for this effect was made when possible, but because of it the probable error of some of the fission product cross sections are increased. The limits of error are estimated to be about 20-30%. The fission yield curves for deuterons of increasing energy are shown in Fig. 26 and 27. The variation of the fission yield curves with different energy deuterons in shown in Fig. 28. The total fission cross sections are compared to the spallation cross sections in Fig. 29.

Table VII

Pu^{239} plus deuterons; fission cross sections (millibarns)[a]

Deuteron Energy(Mev)[b]	9.2		12.3		15.0		16.1		17.9		20.2		20.6		23.4	
	σ[c]	corr.σ[d]	σ	corr.σ	σ	corr.σ	σ	corr.σ	σ	corr.σ	σ	corr.σ	σ	corr.σ	σ	corr.σ
Isotope																
Sr^{89}	0.96	0.96			8.19	8.22			23.7	24.0	28.2	28.5	27.2	27.5	34.5	35.0
Sr^{91}	1.08	1.08			10.0	10.1			22.9	23.4	28.7	29.3	33.8	34.5	34.4	36.0
Y^{91}													32.1	32.8		
Y^{93}													34.7	35.8		
Zr^{95}					21.3	21.7							42.6	43.4		
Zr^{97}					21.3	22.4							40.1	42.2		
Ru^{103} [e]					19.2	19.3							44.3	44.5		
Ru^{105}					18.0	18.3							35.8	36.6		
Ag^{111}					17.0	17.1							44.3	44.7		
Ag^{113}					16.7	17.1							45.5	46.8		
Cd^{115}	0.39	0.39	6.55	6.64	18.4	18.7	20.8	21.2	26.3	26.9	39.2	40.0	42.3	43.2	53.5	55.0
Cd^{115m} [f]			1.12	1.14	1.57	1.60	2.23	2.27	5.89	6.02	5.54	5.65	4.64	4.74	7.18	7.40
$Cd^{115}+Cd^{115m}$	0.43	0.44	7.67	7.78	20.0	20.3	23.0	23.5	32.2	32.9	44.7	45.7	46.9	47.9	60.7	62.4
Cd^{117} [g]	0.43	0.45	7.31	7.60			27.1	28.5	34.7	36.8	41.3	43.8			44.1	48.0
Ba^{139}	2.31	2.54	16.7	18.3			25.4	29.0	36.4	43.3	42.2	50.2				
Ba^{140}	2.45	2.92	13.5	16.1	17.7	21.8	25.2	31.0	32.6	41.2	35.9	45.4	32.9	41.6	39.3	49.7
Ce^{143}	2.07	2.19											37.5	46.3	39.2	56.7
Nd^{147}	1.02	1.05					16.1	16.9			26.6	28.4	27.9	33.4		
Eu^{156}							1.93	2.14			2.88	3.42				
Eu^{157}							1.62	1.92			2.62	3.32	2.17	2.75		

-55-

Table VII (cont'd)

Deuteron Energy(Mev)[b]	9.2 σ[c]	9.2 corr.σ[d]	12.3 σ	12.3 corr.σ	15.0 σ	15.0 corr.σ	16.1 σ	16.1 corr.σ	17.9 σ	17.9 corr.σ	20.2 σ	20.2 corr.σ	20.6 σ	20.6 corr.σ	23.4 σ	23.4 corr.σ
Gd^{159}													1.31	1.57		
Tb^{161}							0.43	0.48			0.84	0.95				
Total Fission Cross Section	53 ± 11		390 ± 78		588 ± 117		817 ± 163		1205 ± 240		from curve plotted from average cross sections 1410 ± 280				1780 ± 360	

[a] ± 10-20%

[b] ± 0.5 Mev

[c] The measured cross section for the isotope given

[d] The corrected cross section for the corresponding mass chain

[e] ± ~30% due to uncertainties in counting low energy beta particle

[f] Upper limit (see text)

[g] ± ~30% due to uncertainty in correcting for daughter

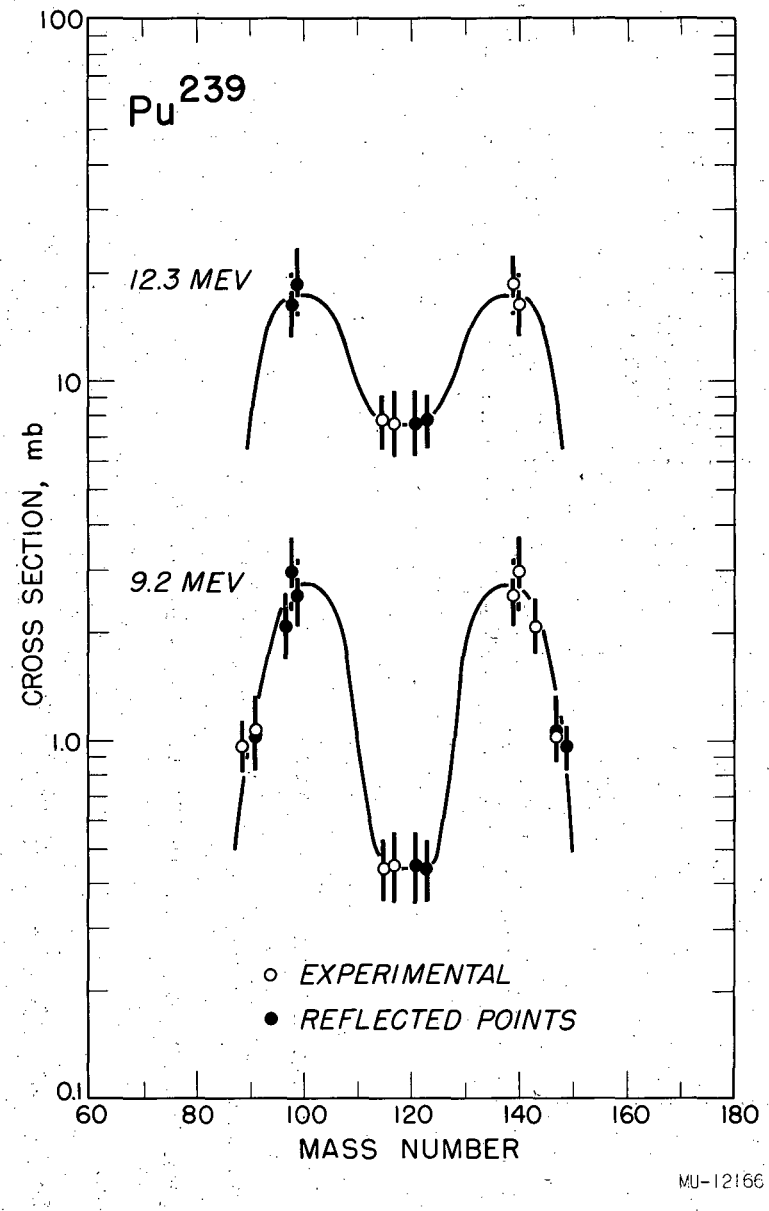

Fig. 9 Fission yield curves for 9.2- and 12.3-Mev deuteron-induced fission of Pu^{239}.

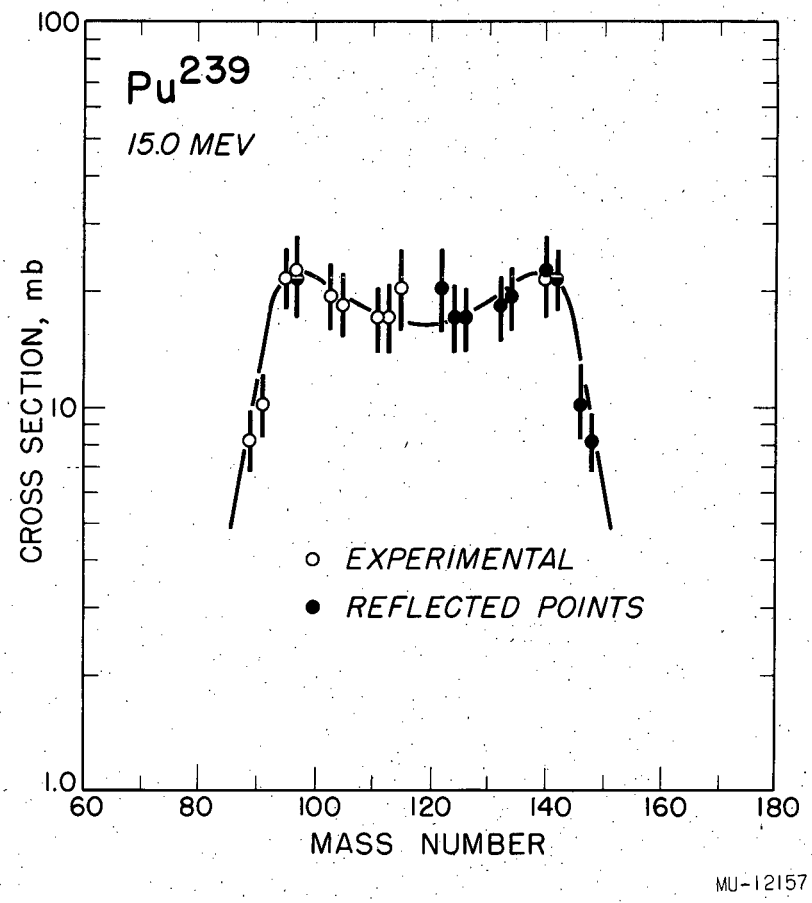

Fig. 10 Fission yield curve for 15.0-Mev deuteron-induced fission of Pu^{239}.

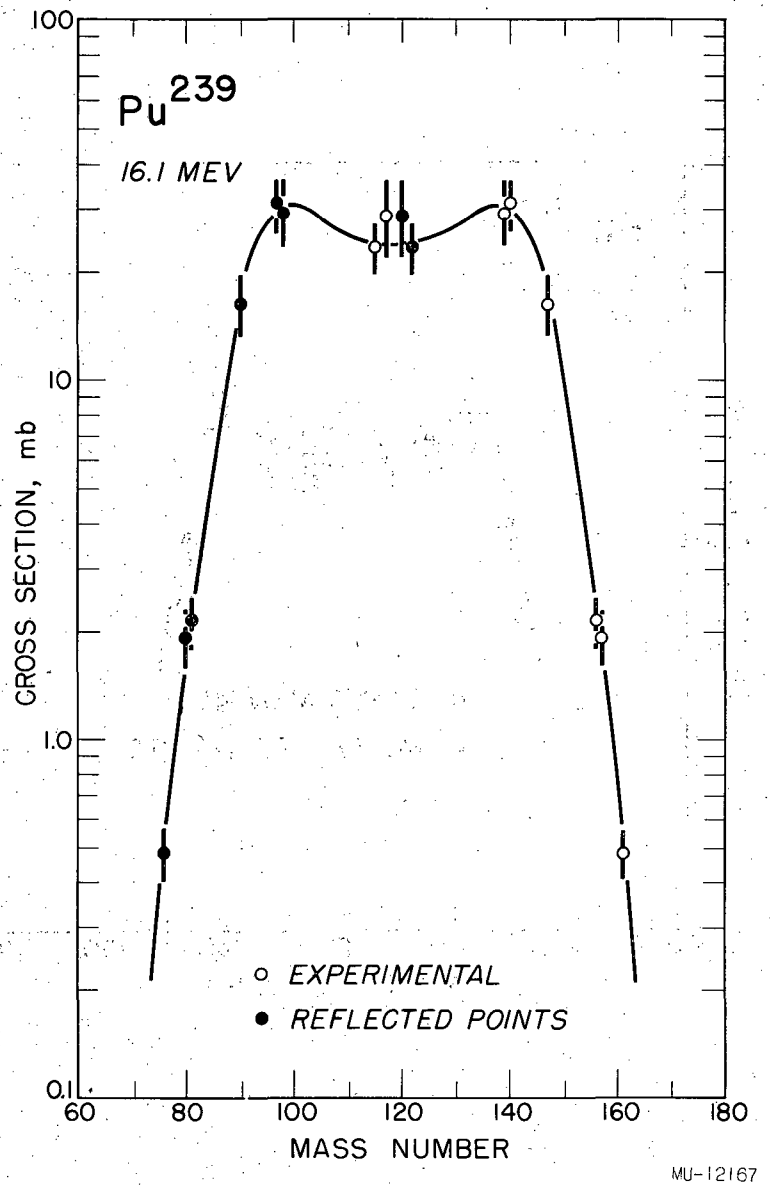

Fig. 11 Fission yield curve for 16.1-Mev deuteron-induced fission of Pu^{239}.

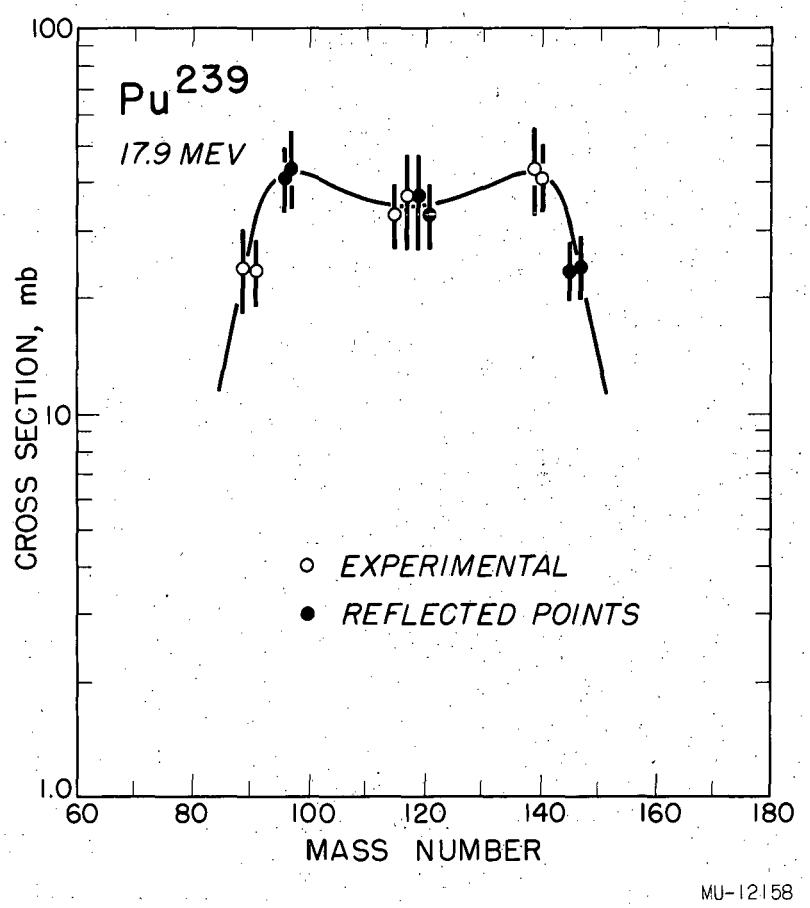

Fig. 12 Fission yield curve for 17.9-Mev deuteron-induced fission of Pu^{239}.

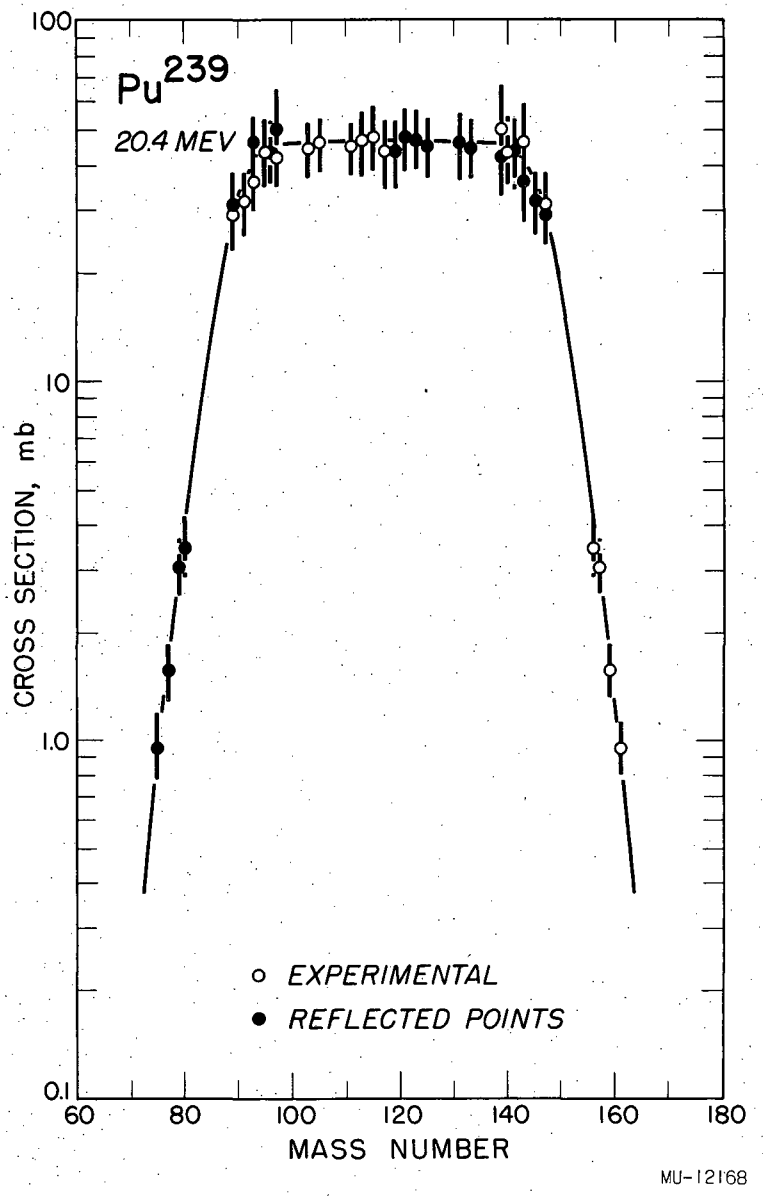

Fig. 13 Fission yield curve for 20.4-Mev deuteron-induced fission of Pu^{239}. Constructed from average of 20.2- and 20.6-Mev deuteron fission cross sections.

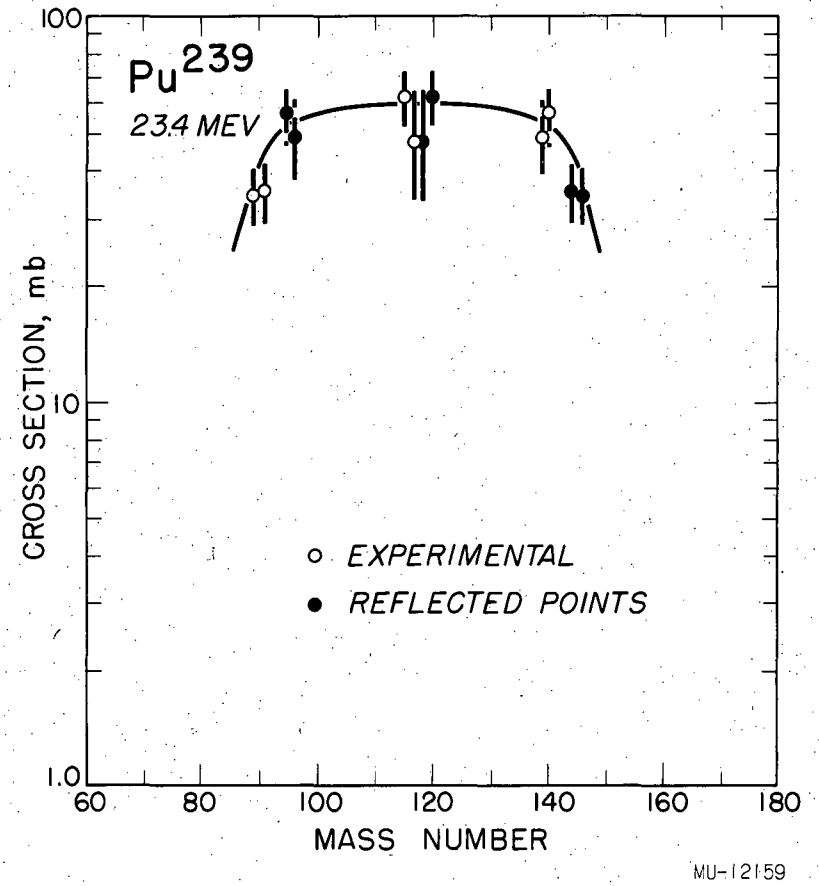

Fig. 14 Fission yield curve for 23.4-Mev deuteron-induced fission of Pu^{239}.

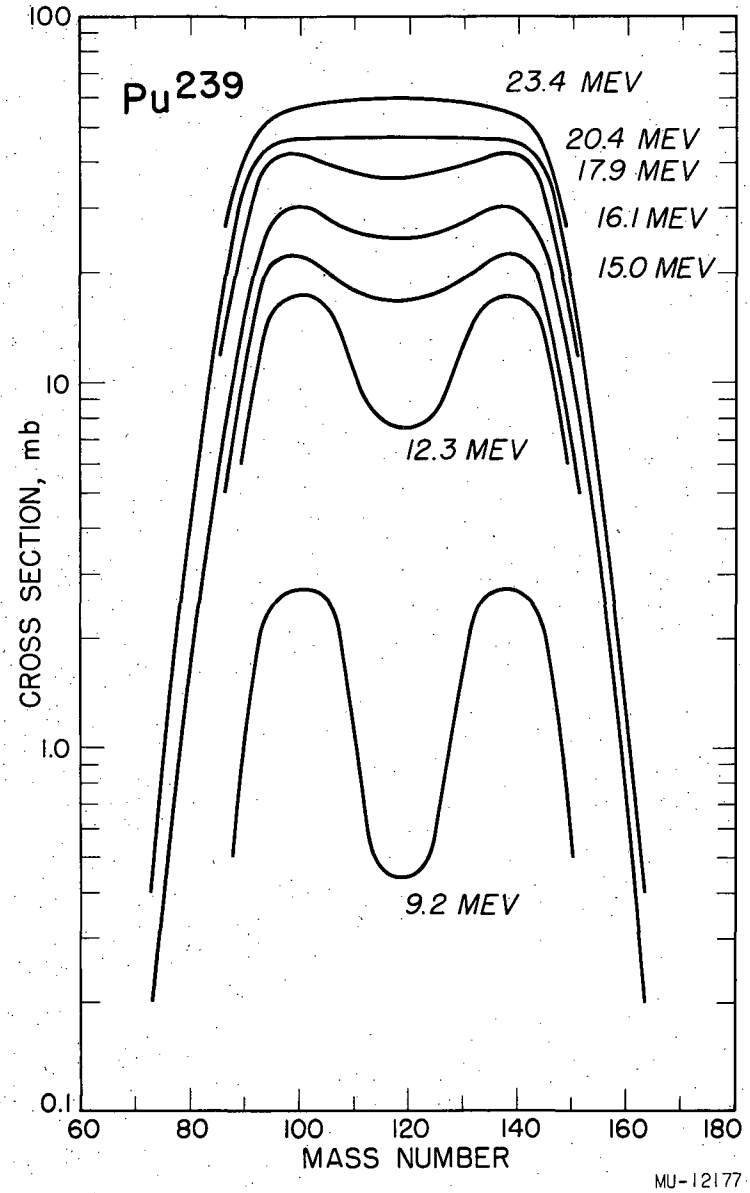

Fig. 15. Variation of fission yield curves with energy for deuteron-induced fission of Pu^{239}.

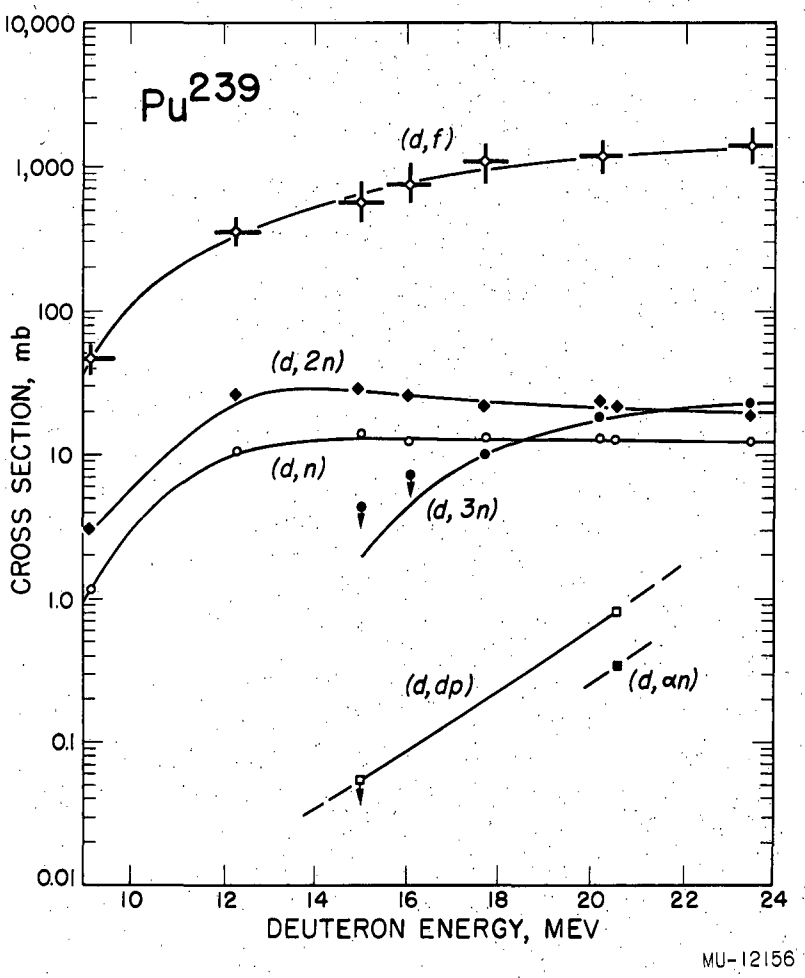

Fig. 16. Comparison of total fission excitation function with spallation excitation functions for deuteron-induced reactions of Pu^{239}.

Table VIII

Np^{237} plus helium ions; fission cross sections (millibarns)[a]

Helium ion Energy(Mev)[b]	19.8		22.7		24.2		28.1		31.5		35.0		38.1		44.9		45.7	
	σ[c]	corr. σ[d]	σ	corr. σ	σ	corr. σ	σ	corr. σ	σ	corr. σ	σ	corr. σ	σ	corr. σ	σ	corr. σ	σ	corr. σ
Isotope																		
Sr^{89}			2.88	2.90			13.9	14.0	17.0	17.2	14.4	14.6	16.1	16.4	20.2	20.5	20.8	21.2
Sr^{91}	0.31	0.31	3.27	3.34			12.7	13.1	14.6	15.1	14.4	14.9	18.4	19.2	18.3	19.4	21.4	22.7
Zr^{97}									21.3	22.4							39.2	43.2
Ru^{103}[e]									21.2	21.3								
Ru^{105}	0.45	0.45	4.10	4.16	4.80	4.88			19.9	20.3			29.7	30.4			40.9	50.7
Pd^{109}															37.9	38.9	48.1	49.3
Pd^{112}															45.2	50.4	46.0	51.2
Ag^{111}									24.0	24.3							46.3	47.2
Ag^{113}									21.0	21.6							34.9	36.7
Cd^{115}	0.14	0.15	2.55	2.59	3.21	3.27	19.0	19.3	19.8	20.2	22.4	22.9	39.2	40.3	37.6	39.4	49.7	51.9
Cd^{115m}[f]							2.08	2.12	2.71	2.77	5.10	5.23	3.35	3.46	8.17	8.60	8.5	8.9
$Cd^{115}+Cd^{115m}$	0.16	0.16	2.78	2.82	3.50	3.56	21.1	21.4	22.5	22.9	27.4	28.1	42.6	43.8	45.8	48.0	58.2	60.8
Cd^{117}[g]	0.16	0.16	2.44	2.54			18.8	19.8	21.3	22.6	23.0	24.4	33.6	36.4			46.2	53.0
Ba^{139}	0.54	0.59	3.80	4.18	5.87	6.71	18.9	21.6	22.8	27.3	22.4	26.7	22.0	27.9	26.1	38.9	13.8	24.2
Ba^{140}	0.61	0.73	4.45	5.30	5.94	7.33	16.7	20.6	17.5	22.2	18.0	22.7	17.3	25.0	19.4	38.1	18.8	37.0
Ce^{141}																	22.1	24.0
Ce^{143}									17.4	21.4							14.8	19.3
Ce^{144}																	13.2	20.3

-65-

Table VIII (cont'd)

Helium ion Energy(Mev)[b]	19.8 σ[c]	19.8 corr. σ[d]	22.7 σ	22.7 corr. σ	24.2 σ	24.2 corr. σ	28.1 σ	28.1 corr. σ	31.5 σ	31.5 corr. σ	35.0 σ	35.0 corr. σ	38.1 σ	38.1 corr. σ	44.9 σ	44.9 corr. σ	45.7 σ	45.7 corr. σ
Nd^{147}			3.34	3.45					15.2	16.2								
Eu^{157}									1.72	2.18							2.76	4.52
Gd^{159}			0.28	0.31					0.80	0.96							1.65	2.62
Total Fission Cross Section	12.8 ± 2.6		131 ± 37		183 ± 37		647 ± 132		720 ± 147		783 ± 160		1040 ± 210		1319 ± 269		1357 ± 277	

[a] ± 10-20%

[b] ± 0.5 Mev

[c] Measured cross section for isotope

[d] Corrected cross section for mass chain

[e] ~ ± 30% due to uncertainty in A.W. and SSSA corrections for low energy beta particles

[f] Upper limit

[g] ~ ± 30% due to uncertainty in daughter correction

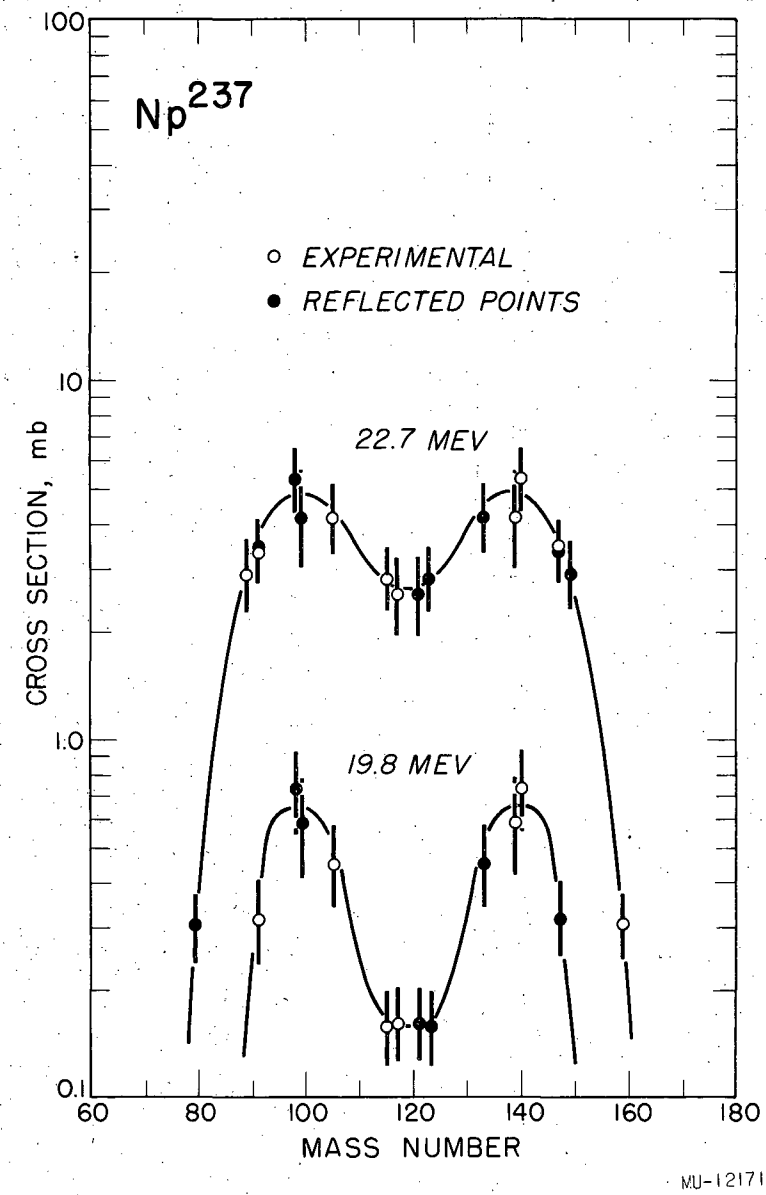

Fig. 17 Fission yield curves for 19.8- and 22.7-Mev helium ion-induced fission of Np^{237}.

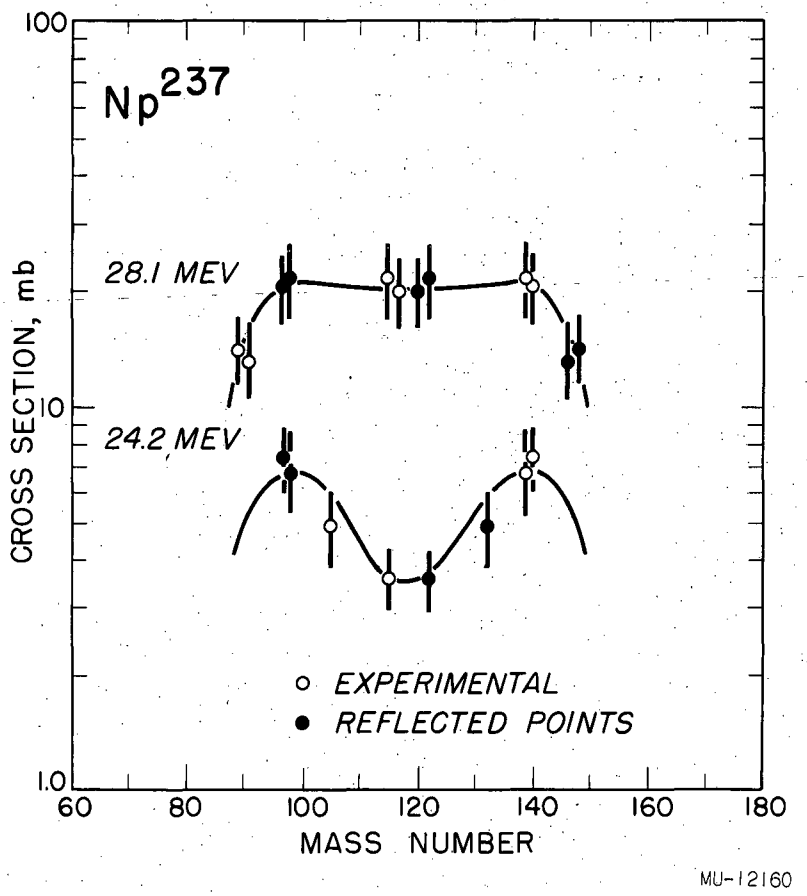

Fig. 18 Fission yield curves for 24.2- and 28.1-Mev helium ion-induced fission of Np^{237}.

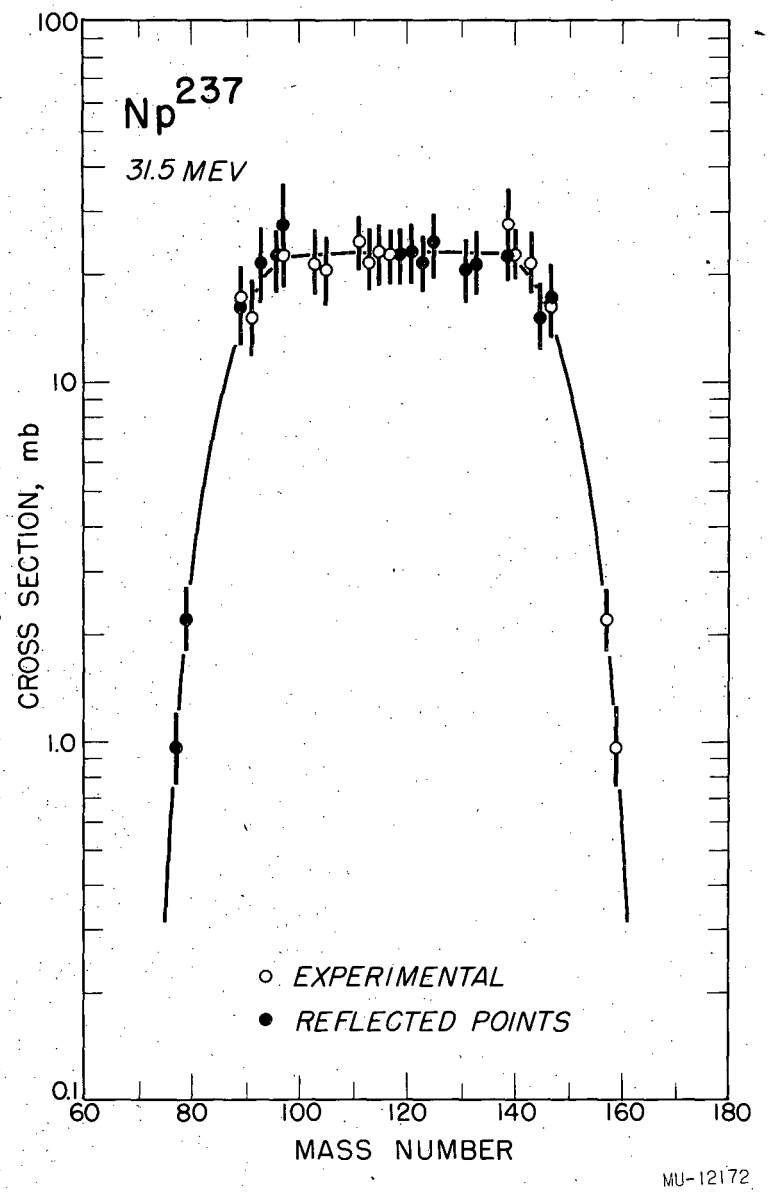

Fig. 19 Fission yield curve for 31.5 Mev helium ion-induced fission of Np^{237}.

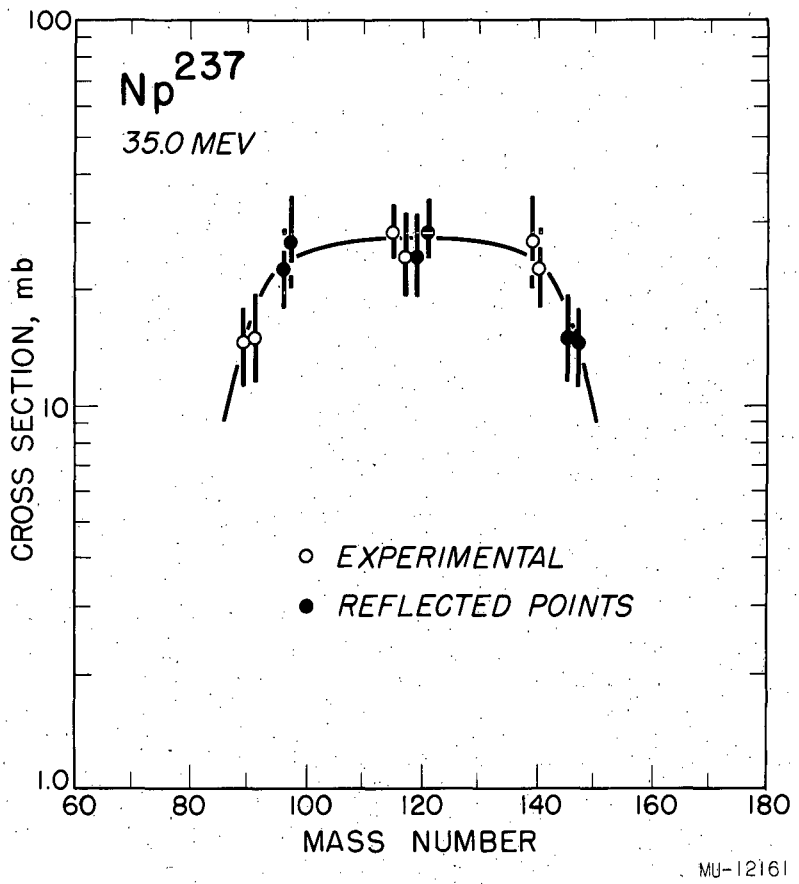

Fig. 20 Fission yield curve for 35.0-Mev helium ion-induced fission of Np^{237}.

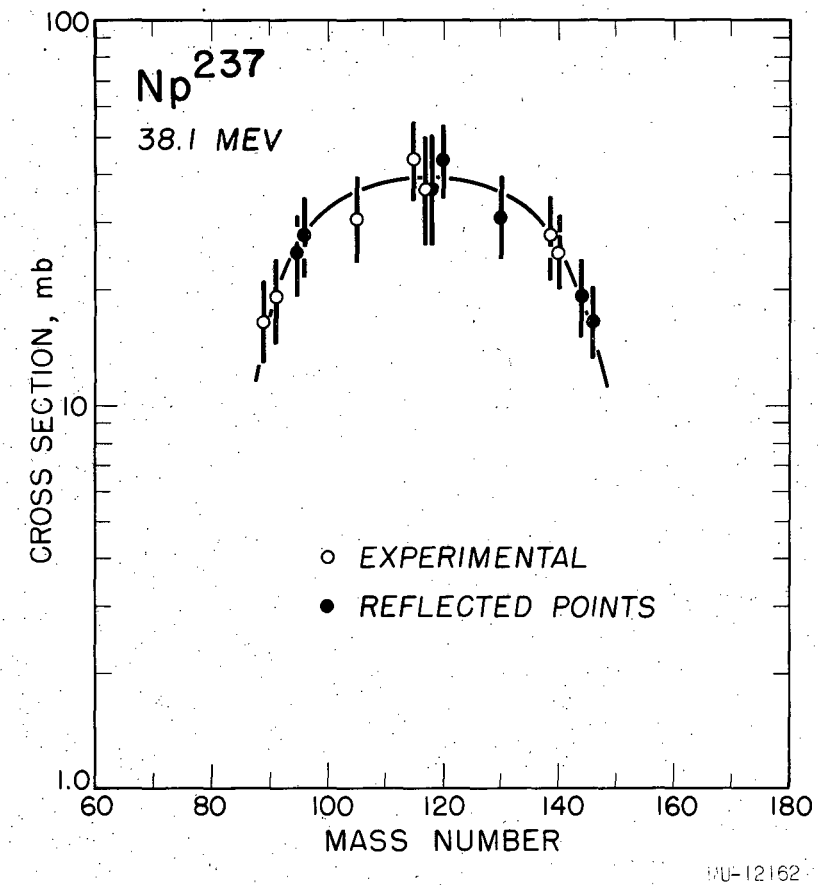

Fig. 21 Fission yield curve for 38.1-Mev helium ion-induced fission of Np^{237}.

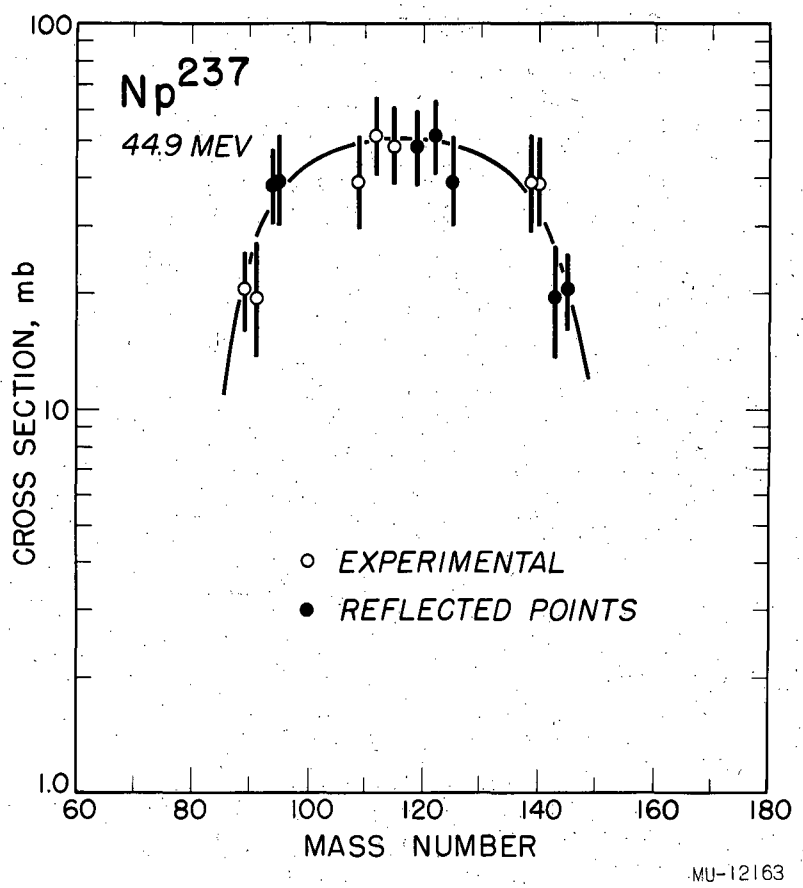

Fig. 22. Fission yield curve for 44.9-Mev helium ion-induced fission of Np^{237}.

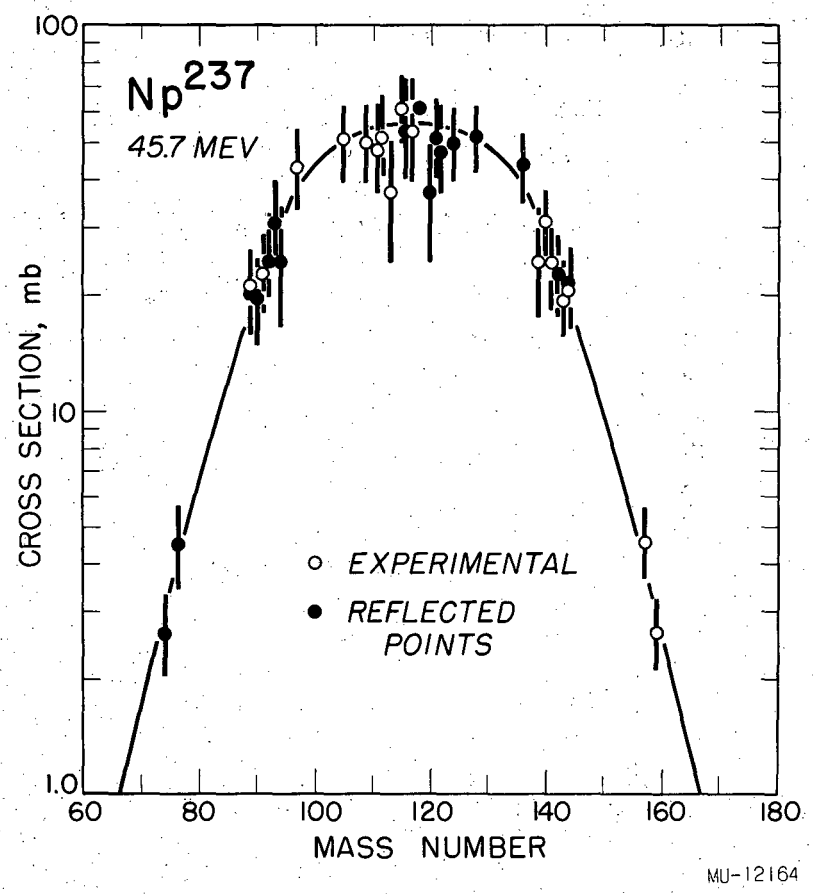

Fig. 23 Fission yield curve for 45.7-Mev helium ion-induced fission of Np^{237}.

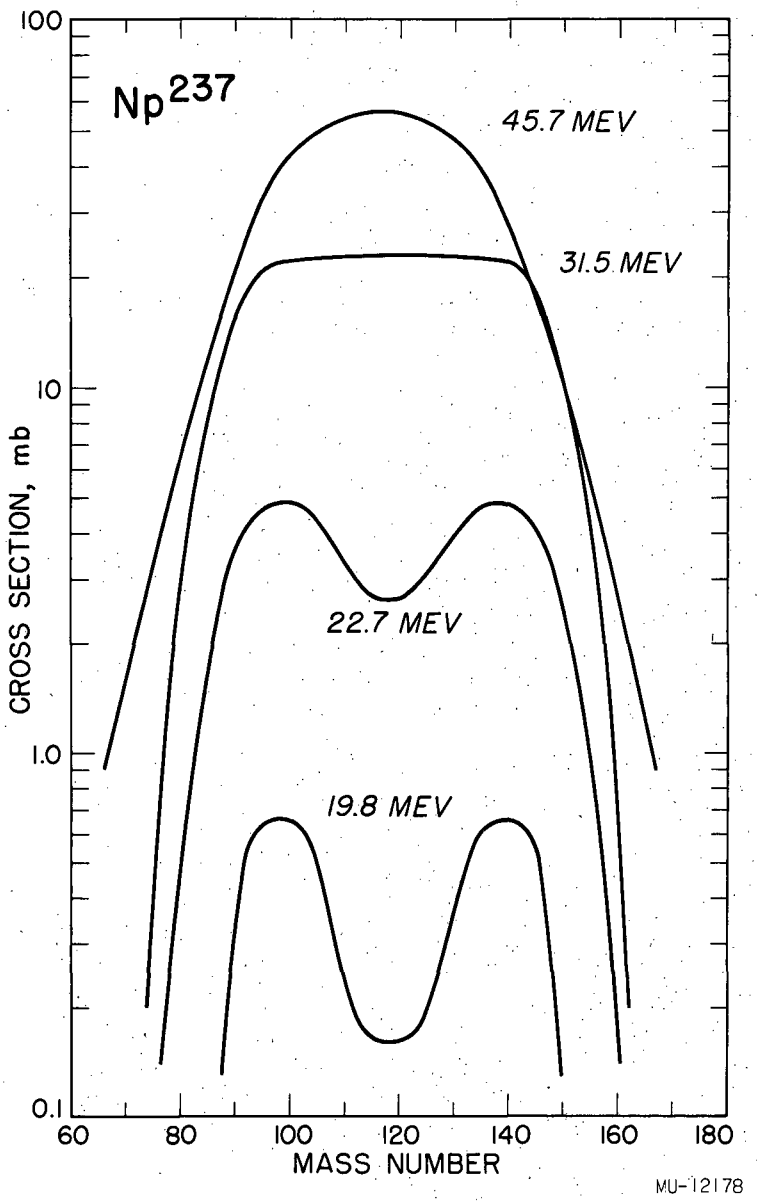

Fig. 24 Variation of fission yield curves with energy for helium ion-induced fission of Np^{237}.

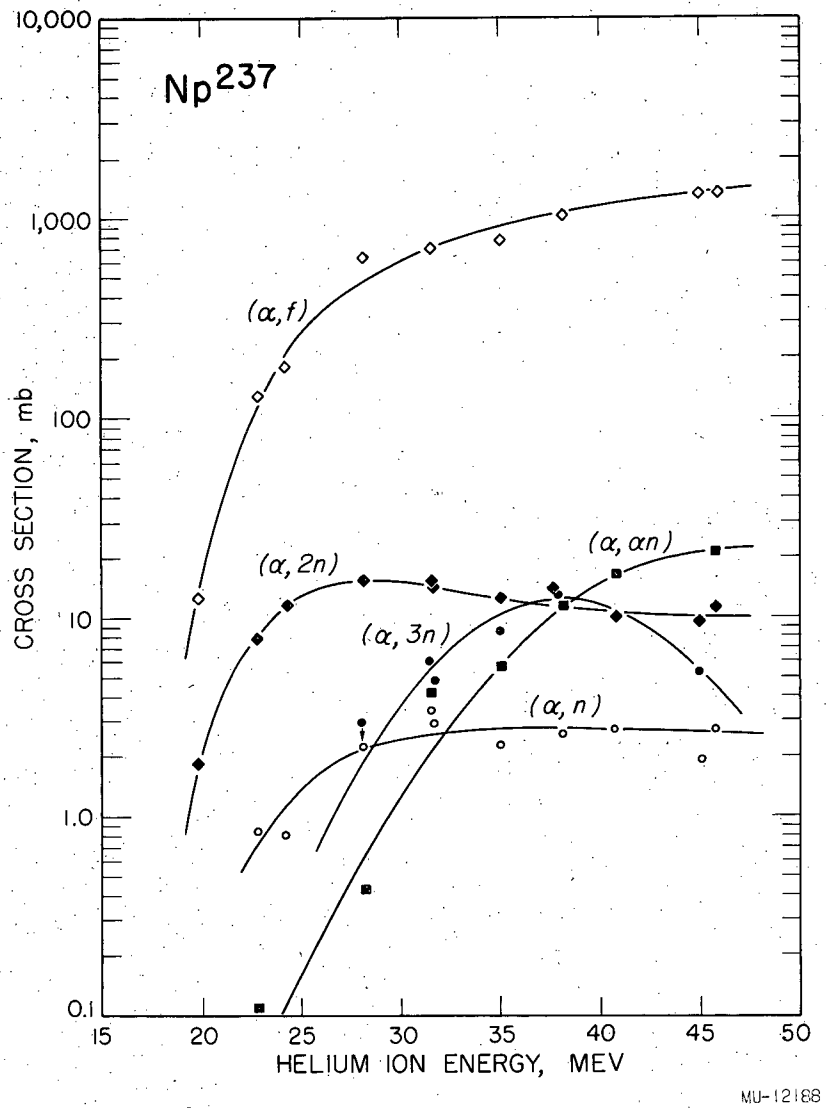

Fig. 25 Comparison of total fission excitation function with spallation excitation functions for helium ion-induced reactions of Np^{237}.

Table IX

U^{233} plus deuterons; fission cross sections (millibarns)[a]

Deuteron Energy(Mev)[b]	9.0		12.1		14.0		15.4		19.6		21.5		23.4	
	σ[c]	corr.σ[d]	σ	corr.σ	σ	corr.σ	σ	corr.σ	σ	corr.σ	σ	corr.σ	σ	corr.σ
Isotope														
Sr^{89}	4.59	4.64	14.4	14.6	18.9	19.1	26.4	26.7	46.5	48.2	34.6	35.1	42.7	43.3
Sr^{91}	3.90	4.01	23.1	23.8	18.7	19.2	31.0	32.0	36.9	38.0	52.5	54.6	44.3	46.2
Zr^{95}	6.45	6.55			44.8	45.6			58.5	59.7	61.6	63.0	54.2	55.5
Zr^{97}	4.59	4.80	25.6	26.8	39.3	41.1			49.8	52.4	61.8	66.0	53.5	57.2
Ru^{105}	5.03	5.11												
Pd^{109}											46.7	47.5		
Pd^{112}											52.9	56.9		
Cd^{115}	1.22	1.24	8.43	8.57	14.7	15.0	22.9	23.4	44.0	45.0	47.3	48.6	63.9	65.7
Cd^{115m}[e]			1.55	1.58	1.97	2.0	3.92	4.00	5.58	5.70	8.5	8.7	4.8	4.9
$Cd^{115}+Cd^{115m}$	1.34	1.36	9.98	10.2	16.1	17.0	26.8	27.4	49.6	50.7	55.8	57.3	68.7	70.6
Cd^{117}	1.70	1.78	12.1	12.5	19.5	20.4	21.9	23.2	41.8	44.2	50.0	53.8	59.0	63.5
Ba^{139}	4.26	4.82	20.4	23.1			39.3	46.2	49.2	57.9	46.5	58.1	34.0	45.3
Ba^{140}	3.50	4.27	17.1	20.9	21.8	26.6	29.2	41.7	37.5	53.6	35.5	53.0	31.5	47.0
Nd^{147}													12.2	13.3
Eu^{157}													0.76	1.03
Gd^{159}													0.54	0.70
Total Fission Cross Section	125 ± 34		605 ± 163		857 ± 231		1093 ± 295		1502 ± 406		1687 ± 456		1861 ± 503	

[a] ± 20-30%

[b] ± 0.5 Mev

[c] Measured cross section for isotope

[d] Corrected cross section for mass chain

[e] Upper limit

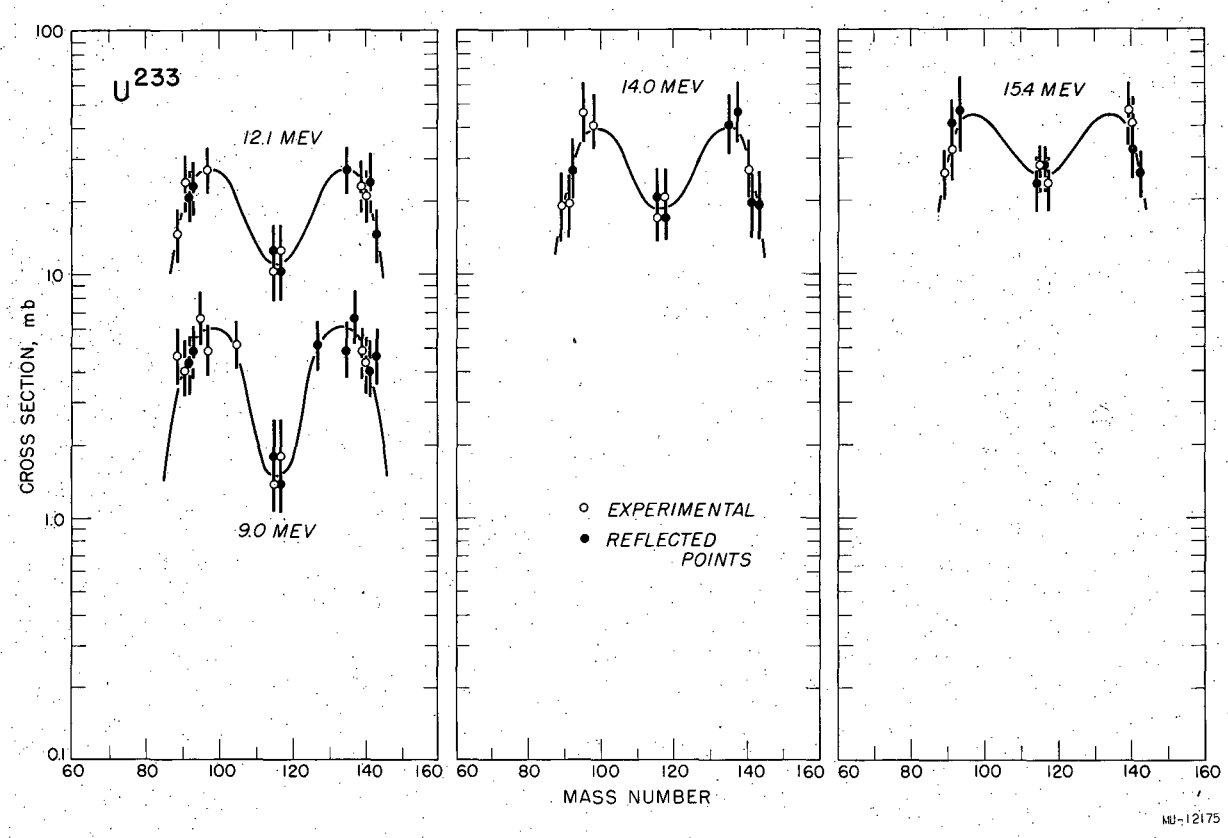

Fig. 26 Fission yield curves for deuteron-induced fission of U^{233}.

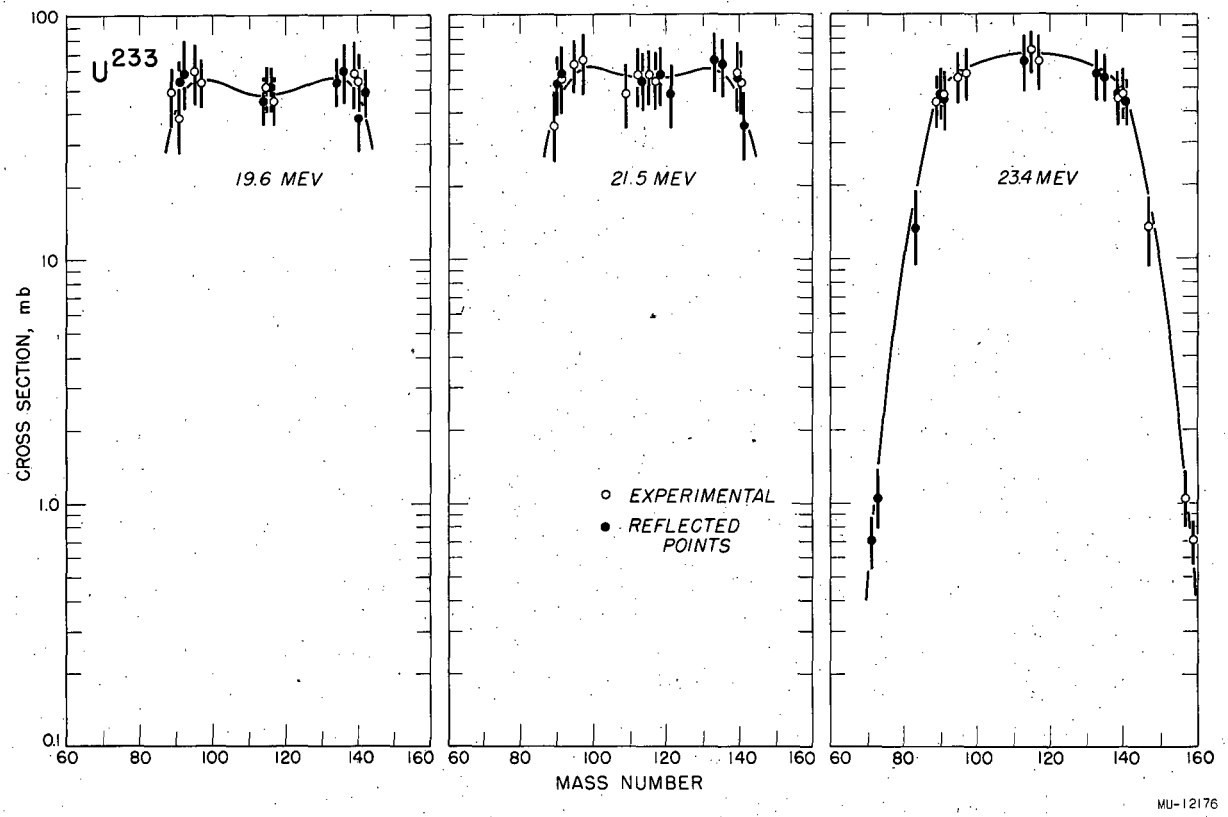

Fig. 27 Fission yield curves for deuteron-induced fission of U^{233}.

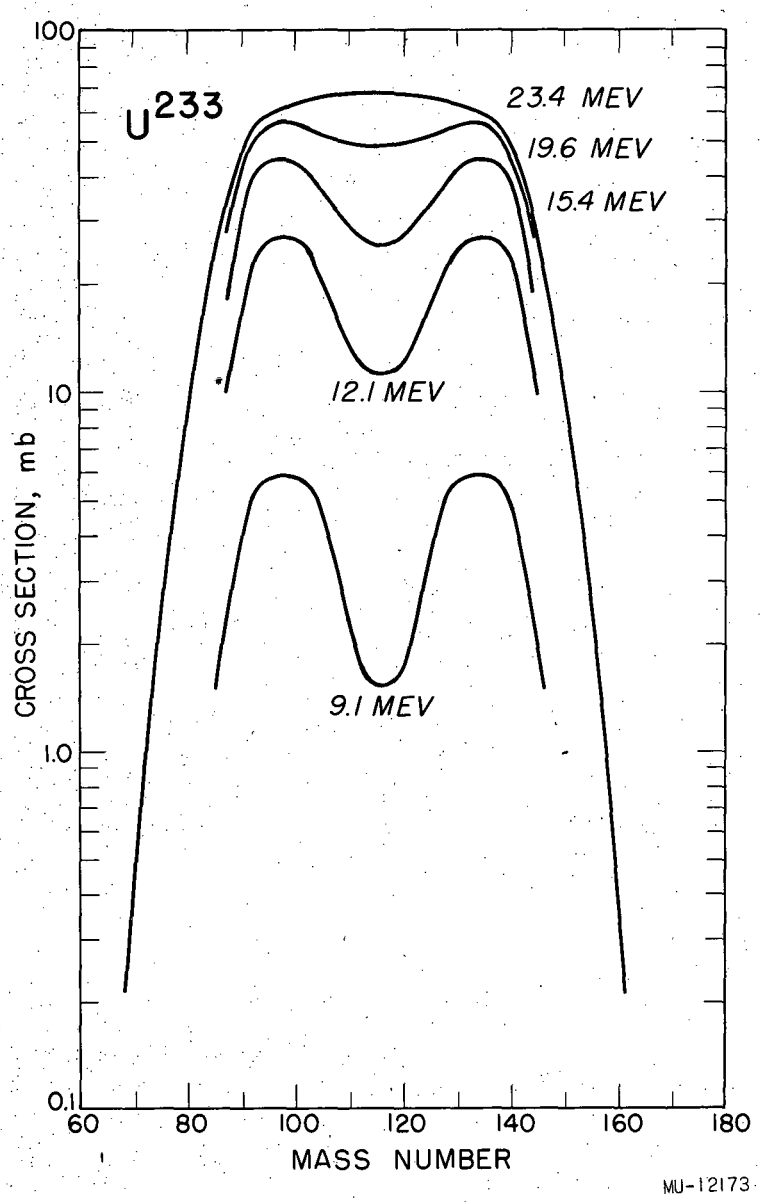

Fig. 28 Variation of fission yield curves with energy for deuteron-induced fission of U^{233}.

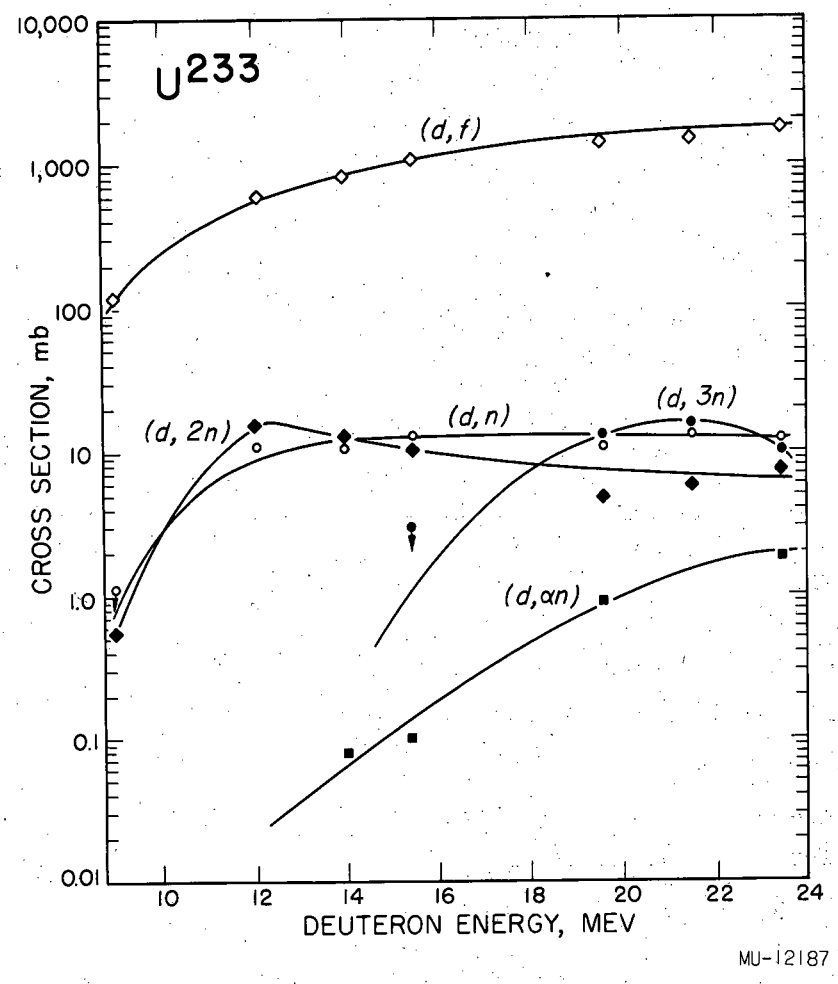

Fig. 29 Comparison of total fission excitation function with spallation excitation functions for deuteron-induced reactions of U^{233}.

IV. DISCUSSION

Fission is the most predominant single reaction observed in the heavy element region ($Z > 90$) for excitation energies above about 5 Mev. This can be seen from Figs. 16, 25, and 29 where the fission cross section is more than ten times the sum of the observed spallation cross sections. The competition between this large fission reaction and each of the reactions leading to spallation products is unique in this region of the periodic table. This study was designed to investigate the effect of this competition in an effort to obtain further information about the nature of the nuclear reactions involved. The energy range used ($E < 50$ Mev) is such that the number of possible reactions is low enough for convenient study, and the statistical model [3,9] of nuclear reactions can be used as a starting point for the interpretation of the results.

A. Fission Yields

Since the total fission cross section can be determined without a detailed study of the exact shape of the fission yield curve, the large expenditure of time and effort in these determinations prompted a limitation on the number of fission products measured at most energies. However, the information about the fission process that can be gained by a more detailed investigation of the fission yield curves has led to the careful determination of the fission product distribution at selected helium ion and deuteron energies (Figs. 10, 13, 19, 23, and 27). The fission process will be discussed first because it is the largest single reaction and because it will be of interest to have well in mind the importance and magnitude of this process in discussing the spallation reactions.

1. Charge distribution in fission.

The primary fission yields in Table VI were determined to allow correction of the measured fission product cross sections for chain yield losses. In order to obtain the total chain yield a correction must be made for direct production of fission products of higher Z than the observed product in any given mass chain. Before this correction can be made one must estimate the charge distribution in fission from the primary yield data. The nature of the data is such that it is not possible to uniquely determine the charge distribution for a given mass chain. Only a very approximate picture of the actual charge distribution is obtained.

The following assumptions are present in our estimate of the charge distribution in fission and in the correction applied to the fission yields.

(a) The charge distribution for a given mass chain is a smoothly varying function of the nuclear charge (Z) and is symmetric about the charge (Z_p) of the most probable fission product for that mass chain.

(b) The shape of the charge distribution is the same for all mass chains.

(c) The apparent fissioning nucleus can be estimated from the center of symmetry of the mass yield curve. Actually this assumption is very poor. The bulk of the prompt neutrons accompanying fission probably come from the excited fission fragments (this point will be discussed in detail later). Since we see only the end products of the fission process we must regard the "primary" fission fragments to be those remaining after the prompt neutron emission and before beta decay takes place. These are the beginnings of the respective beta decay chains. Therefore the assumption we are actually making in even presuming to reflect the fission yield curves about a center of symmetry is that the ratio of the prompt neutrons from each of the fission fragments is the same as the ratio of their masses. There are indications that, for low energy fission, neutron emission from the light fragment is on the average about 30% greater than for the heavy fragment.[85] In spite of the approximate nature of the method, a reasonable value for the number of emitted neutrons is obtained (from ~4 to ~8 for the helium ion bombardments on Np^{237}).

(d) The charge distribution was assumed to be independent of excitation energy in the range of energies studied.

(e) Along with the above assumptions, an additional assumption must be made about the charge of the most probable fission product for a given mass. For low energy fission Glendenin[66] has postulated that the most probable charge (Z_p) is displaced a constant amount from the beta stability line. The estimated chain yields are plotted according to this postulate in Fig. 7. The Z_A used in the calculation was that of Coryell, Brighton and Pappas[140] and the solid curve is the distribution predicted by Pappas[67] according to the equal charge displacement postulate. The

dotted curve shows the fit of the data to the solid curve if we assume that two additional neutrons are emitted in each case. The emission of two more neutrons is just inside the estimated limits of error of the determination of neutron multiplicaties. Such an assumption, however causes the primary yield of Ag^{112} which appears below the solid curve in Fig. 7 to deviate even further. For very high energy (190 Mev) deuteron induced fission of bismuth it has been suggested that the most probable fission products have the same charge to mass ratio as the fissioning nucleus.[2] The primary chain yields are plotted on this basis in Fig. 8. A better correlation is obtained in this case. The Ag^{112} yields which were very low in Fig. 7 now have moved into line with the other primary yields. The solid curve is merely a best fit of the data and has been reflected about $Z-Z_p = 0$. The solid curve in Fig. 8 has been used to correct the measured fission yields for chain yield losses. Although a reasonably straightforward correlation is noted in Fig. 8 this does not give an unambiguous indication of the actual charge distribution. The first thing to be noted about Fig. 8 is the shape of the distribution. It has been suggested that the distribution for both low and high energy fission is gaussian.[66,2] A gaussian distribution would be parabolic on a semi logarithmic plot of this type. The second thing to note is that summing under the distribution curve gives a total probability of 0.90 whereas the total probability should be unity.

The actual charge distribution may be intermediate to the two cases considered. The assumed energy independence is obviously incorrect but these shortcomings do not invalidate the use of Fig. 8 in estimating the corrections to be applied to the fission yields. The primary yields in Fig. 8 were measured in all regions of the fission yield curve so the purely empirical correlation which Fig. 8 represents can still be used with some confidence.

Very recently, the primary fission yields of certain iodine and bromine isotopes have been measured with high accuracy on a mass spectrometer.[68] These studies indicate that the treatment of Glendenin and Pappas may not represent a true picture of charge distribution in low energy fission. Abnormally high values for the primary yields of I^{128} and I^{130} show the possible influence of the 50 proton closed shell. If the charge

distribution is assumed to be such that the energy release is maximized the iodine yield can be accounted for. According to preliminary estimates[68] this mechanism gives approximately the same distribution as predicted by the equal charge displacement postulate away from the closed shell of 50 protons. The observed trend of the charge distribution is best explained in terms of a statistical process. For low excitation energies of the fissioning nucleus the modes of fission leaving higher excitation energy in the fission fragments (consequently those in which the sum of the fragment masses is minimized) will be favored. Even more important is the fact that these modes of fission have many more levels that can be populated, than the modes giving lower energies. As the excitation energy of the fissioning nucleus becomes large these energy differences in the fission fragments become less important and the distribution approaches the random case which is the same charge to mass ratio as the fissioning nucleus.

A more detailed study of the variation of charge distribution as a function of fission asymmetry (i.e. excitation energy) for a given nucleus would be both instructive in the elucidation of the fission mechanism and useful for the determination of accurate mass chain yields.

2. Fission asymmetry.

Perhaps the most striking feature of the fission yield curves (summarized in Figs. 15, 24, and 28) is the variation of fission asymmetry with the energy of the bombarding particle. The shape of the mass yield curves is extremely dependent on the chain yield corrections. This is especially true at higher excitation energies where the correction is very large for some of the important mass chains. For example, for the 45 Mev helium ion bombardment of Np^{237} the Ba^{140} yield must be multiplied by 1.7 to give the total yield for mass 140, which is used as an indication of the asymmetric fission probability, and the Cd^{115} yield must be multiplied by only 1.04 to give the yield for mass 115, which is an indication of symmetric fission. Since the total probability of the estimated charge distribution adds up to less than unity (Fig. 8) it is believed that the corrections for chain yield losses may be too small. This means that the mass yield curves are probably more asymmetric than indicated, especially at the higher energies. The variation of fission asymmetry with excitation

energy is shown in Fig. 30. The ordinate is the ratio of the fission yield of mass 138 to mass 118 in the case of the Pu^{239} and Np^{227} bombardments and of mass 133 to mass 116 for the U^{233} bombardments. These mass yields correspond to the most probable asymmetric mode of fission and the most probable symmetric mode of fission respectively. The mass yields were determined from the smooth mass yield curves. The abscissa is the excitation energy of the compound nucleus as calculated from the masses and binding energies compiled by Glass et al.[59]

Before the features of Fig. 30 are discussed it is desirable to point out other characteristics of the fission yield curves which can be conveniently discussed at the same time. The first thing to note is that the positions of the asymmetric fission peaks do not appear to change appreciably with excitation energy. The peaks appear to shift to slightly lower mass because of the emission of more neutrons, but it is clear that the increase in symmetric fission is not a result of the two asymmetric peaks moving together. This evidence is supported by many other fission yield measurements.[86,141,142] Secondly, the mass yield distribution becomes wider as the excitation energy is increased. This can be seen from Fig. 24 where the relative yield of the products of very asymmetric fission ($150 < A < 80$) is increased at the highest helium ion energies.

From Fig. 30 note that the ratio of the asymmetric to symmetric modes of fission appear to approach unity as the excitation energy is increased. Because of the uncertainties in the chain yield corrections it is more realistic to say that these results are consistent with the statement that the above ratio approaches unity, but does not necessarily prove it or exclude other possibilities. Proton[132,142] and helium ion bombardments[87] of U^{238} indicate that the above conclusion is correct. Since U^{238} has a larger neutron to proton ratio than Np^{237}, Pu^{239} or U^{233}, the primary fission products are displaced farther from the beta stability line. Consequently the chain yield losses are much smaller and do not have as much effect on the fission yield curves. These three features of the fission yield curves, namely the consistency of the asymmetric peak positions with energy, the increasing relative yield of extremely asymmetric modes of fission as the energy is increased, and the possible limiting ratio of unity for asymmetric to symmetric fission, can be

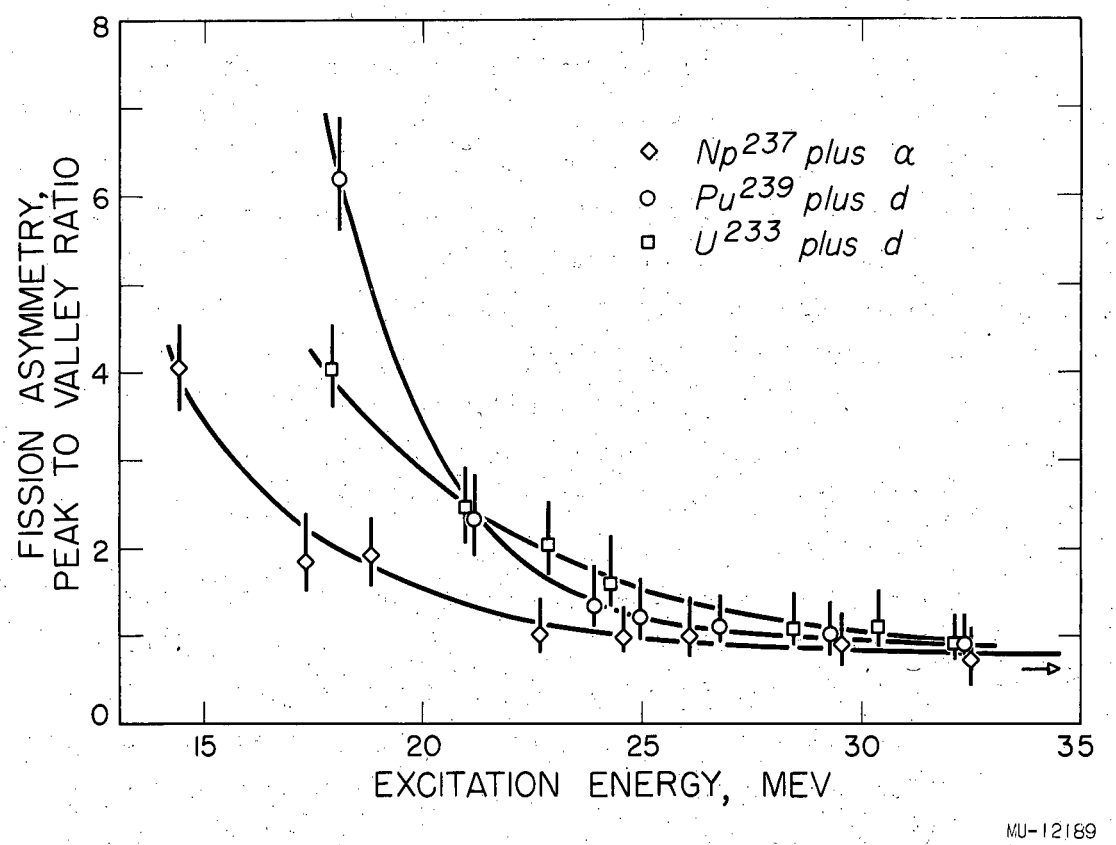

Fig. 30 Fission asymmetry (peak to valley ratio) vs excitation energy for deuteron bombardments of U^{233} and Pu^{239} and for helium ion bombardments of Np^{237}.

explained qualitatively by a statistical fission mechanism. The first requirement is that the asymmetric modes of fission (corresponding to the position of the double-humped peaks) be energetically favored over the symmetric modes by at least a few Mev, also the energy requirement for very asymmetric modes of fission should increase rapidly as the mass ratio of the large fission fragment to the small fragment increases. These general requirements are satisfied by simple mass considerations (see Fig. 8, curve a of reference 55). An admittedly naive but very reasonable picture of the fission process can then be deduced. At low excitation energies the most energetically (hence statistically) favored modes will predominate. As the excitation energy is increased, the probability of the fission proceeding through less favored modes will increase and the central minimum in the fission yield curves will become less pronounced. The increased production of the products of more asymmetric fission than the most probable mode will tend to widen the fission yield curve. The latter effect is smaller since the energy requirements are greater. It should be emphasized that the most probable modes of fission are still the same as for low excitation energies, hence the positions of the peaks should be changed very little (a slight shift to lower mass may be noted because of increased neutron emission). The limiting case is reached when the excitation energy is large compared to the difference in the energy release of the symmetric and asymmetric modes. The probability then becomes about the same for both. The fission yield curve becomes relatively flat and wider with increasing energy.

Exception to the above description may appear in the fission of nuclides of much higher or lower mass than those considered in this study. Swiatecki[143] has observed a striking relationship between the asymmetric peak positions and Z^2/A of the compound nucleus. In this treatment a regular decrease of $(M_2-M_1/A)^2$ is noted as Z^2/A is increased. M_2 and M_1 are the mass numbers at which the maximum of the heavy and the light peaks are observed. It is suggested that at a limited value of Z^2/A ($=40.2$) M_2-M_1 will be zero so the two peaks would then superimpose giving a single maximum even for very low energy fission. This systematic decrease of the spacing is not inconsistent with a statistical

mechanism of fission. As the mass of the fissioning nucleus is increased there is an increase in the number of neutrons in excess of those required to fill the 82 neutron closed shell in the heavy fragment and the 50 neutron closed shell in the light fragment. The 82 neutron closed shell in the lighter fragment might then begin to exercise an influence. When the number of neutrons in the fissioning nucleus exceeds 164 it may be possible to increase the energy release by putting 82 neutrons into each fission fragment. This would then give a single peaked distribution. Since we are really using the masses in the determination of the most probable mode at each step, the variation must necessarily be continuous so the peaks will shift toward each other in a regular fashion. It is interesting to note that an extrapolation of the beta stability line to higher masses by Glass[94] predicts that the first beta stable nuclide with 164 neutrons is element 104 of mass 256. Z^2/A for this nuclide is 40.3 as compared to the limiting value of 40.2 as predicted by Swiatecki.[143] A similar result is obtained at lower mass regions. For a fissioning nucleus containing fewer than 132 neutrons we can no longer satisfy the requirements of a closed shell of 50 neutrons in one fragment and 82 neutrons in the other. It is not unlikely, therefore, that the 50 neutron shells in each fragment would then tend to exert the larger influence and symmetric fission yield curves of somewhat reduced half-width would result. This may partially explain the abnormally narrow and peaked distribution found in the fission of Bi^{210} with 22 Mev deuterons by Fairhall.[144] The very speculative nature of the observations contained in this paragraph cannot be overemphasized. Throughout this discussion the effect of factors other than the neutron shells have been ignored. Such factors as the influence of proton shells, and the requirement that a reasonable neutron to proton ratio be considered in the fission fragments may exercise a profound influence on the respective masses. Only a careful treatment of the energy release of the various modes will show if the above speculations have any basis in fact.

According to Bohr[3] the decay of a compound nucleus should be independent of the way in which it is formed. A comparison of the asymmetry of fission in the decay of the compound state Am^{241*} gives an apparent dependence on the mode of formation. The same compound nucleus

was made by Pu^{239} plus deuterons and Np^{237} plus helium ions. From Fig. 30 it can be seen that for an excitation energy of 18 Mev, the asymmetry (peak to valley ratio) of the fission yield curve is 3.3 times higher in deuteron bombardment of Pu^{239} than in the helium ion bombardment of Np^{237}. This surprising result is not so serious as one might first suppose and does not necessarily invalidate either the statistical model or the independent formation and decay postulate.

The observed fission distribution is the final result of two quite different processes. The first involves the formation of a compound nucleus by amalgamation of the bombarding particle into the target nucleus and subsequent fission or particle evaporation followed by fission. It is immaterial to the independent decay postulate whether fission is first or follows particle evaporation so long as the kinetic and binding energy of the bombarding particle is completely distributed among the nucleons before decay takes place. The first process (compound nucleus formation) makes up most of the fissions observed in the bombardment of Np^{237} with helium ions in the energy range studied. This is not true of the bombardment of Pu^{239} with deuterons. One of the most prominent reactions of deuterons with heavy nuclei is stripping. The loosely bound deuteron can give up part of its energy to the nucleus by having either its neutron or its proton captured by the nucleus while the other nucleon is not stopped. Because of the coulomb barrier, which tends to repel the proton, the neutron is most likely to be captured at low deuteron energies. This (d,p) or Oppenheimer-Phillips reaction can take place without the proton penetrating the coulomb barrier. For compound nucleus formation to take place the entire deuteron must penetrate the barrier hence this process is reduced much more than the stripping reaction at lower energies by the coulomb barrier. The ratio $\sigma_{(d,p)}/\sigma_c$, where $\sigma_{(d,p)}$ is the cross section for stripping a neutron from the deuteron and σ_c is the cross section for compound nucleus formation by capture of the deuteron, is very large ($\gg 1$) at energies below the barrier and decreases to a small value (<1) at higher energies. The energy dependence of this ratio can be seen by comparing the (d,p) excitation function on Bi^{210} to the (d,2n) excitation function as measured by Kelley.[31] The (d,2n) reaction is principly due to compound nucleus formation and the initial portion of the

curve is determined by the effect of the barrier on the incoming deuteron.[31] The fission of Pu^{239} with low energy deuterons therefore may contain relatively large contributions due to fission of Pu^{240} nuclei resulting from the stripping process. Since these excited Pu^{240} nuclei are excited to a lower level than the Am^{241} nuclei produced by capture of the deuteron, the fission is more asymmetric. The relative contribution due to the stripping process should decrease as the energy is increased and as noted in Fig. 30 the fission asymmetry for the Pu^{239} bombardments approaches that for the Np^{237} bombardments as the excitation energy is increased.

The intermediate position of the fission asymmetry in the deuteron bombardment of U^{233} is probably due to a lower barrier and possibly a charge or mass effect.

The valley to peak ratios of the mass yield curves determined in this study as well as other recently reported results are plotted vs $(E_x - 5)^{-1/2}$ in Fig. 31 as suggested by Fowler, Jones and Phaehler.[64] The values reported by Jones, et al.[142] are also included for completeness. It should be noted that the ordinate of figure 31 (fission asymmetry) is the reciprocal of the ordinate of figure 30. The abscissa is proportional to the reciprocal temperature of the distorted nucleus. The proportionality constant can be determined if the level density of these highly excited and strongly deformed nuclei is assumed to be of the form $w(E) = C \exp [2(E/a)\ 1/2]$ as predicted by Weisskopf.[9,65] Jones, Timmick, Phaeler and Handley[142] have used this approach to derive the relation $Y\ min/Y\ max = 2.8 \exp [-2.9/T]$ which corresponds to the diagonal straight line in Fig. 31. Since the relative probability of two states differing in energy by an amount ΔE is $\exp [-\Delta E/T]$, it is thus suggested that 2.9 Mev is the additional energy required to produce symmetrical in preference to asymmetrical fission. The relatively large deviations of the recent data from the predicted behavior is considered to be well outside the limits of error of the experimental measurements. This may indicate that the simple energy dependence assumed for the level density is not applicable to the high energy fission process. It is not surprising that the above simplifications are not completely valid although a definite trend is indicated so that qualitative conclusions based on a treatment of this type are not invalidated.

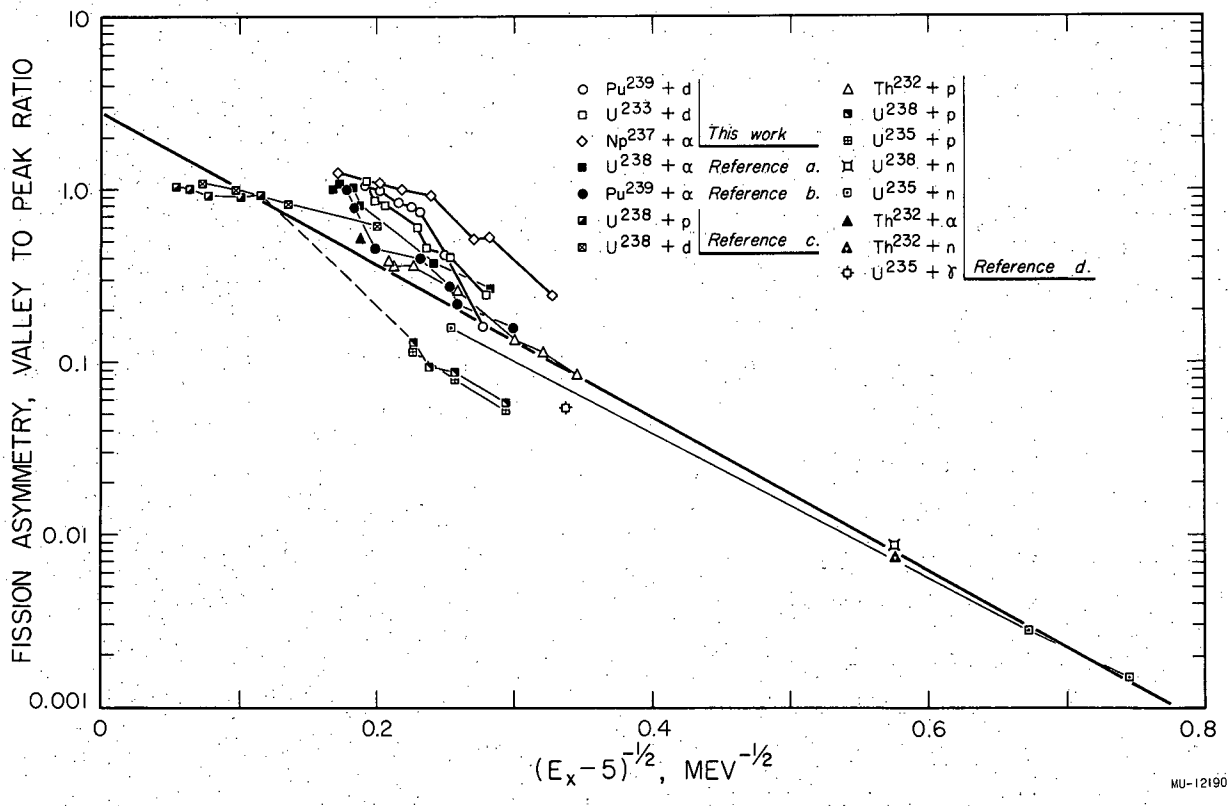

Fig. 31 Fission asymmetry (valley to peak) vs $(E_x-5)^{-1/2}$ for the fission of various heavy element nuclides excited by charged particles, neutrons and photons.

The references indicated are: (a) S. E. Ritsema (M.S. Thesis) UCRL-3266, University of California Radiation Laboratory (1956); (b) R. A. Glass, Ph.D. Thesis, University of California Radiation Laboratory Unclassified Report UCRL-2560 (1954); (c) H. S. Hicks and R. S. Gilbert, Phys. Rev. 100, 1286 (1955); and (d) W. J. Jones, A. Timnick, J. H. Phaeler and T. H. Handley, Phys. Rev. 99, 184 (1955). The heavy solid line is from reference (d).

3. Total fission cross sections.

The total fission cross sections obtained by summing under the mass yield curves are shown in Figs. 32, 33, and 34. The fission cross sections are represented as open diamonds. The estimated limits of error are indicated. The dotted lines above each of the diamonds represent the total fission cross section plus the sum of the observed spallation cross sections.

The large preponderance of the fission reaction as compared to the spallation reactions is clearly shown by these figures. Since U^{233} and Pu^{239} have different barrier heights, a comparison of the absolute fission yields may not be too instructive. It is of interest however to note that at the highest energies where barrier effects are not so prominent the total fission cross section is the same in both cases. It is evident, therefore, that no strong Z^2/A dependence is operating at these energies (Z^2/A = 36.8 and 37.5 for the compound nuclei Np^{235} and Am^{241} respectively). A more sensitive measure of the fissionability will be noted in the effect of the fission reaction on certain spallation yields.

The solid curves in Figs. 32, 33, and 34 are theoretical cross sections for compound nucleus formation with different assumed nuclear radii. The nuclear radius is given by the relation $R = r_o A^{1/3}$ where the assumed r_o values are indicated in each case. The theoretical curves for the deuteron-induced reactions on Pu^{239} and U^{233} were taken from the data of Shapiro[32] while those for the helium ion-induced reactions on Np^{237} were taken from Blatt and Weisskopf.[9] The r_o value indicated by these studies is about $r_o = 1.5 \times 10^{-13}$ cm in each case.

In summary, the qualitative features of the fission yields obtained are best explained in terms of a statistical model of fission. This type of mechanism was one of the first proposed after the discovery of fission by Hahn and Strassman in 1939.

However a quantitative theoretical treatment applicable to a wide variety of energies and fissioning species has not as yet been developed. The work of Bohr and Wheeler[33] and of Fong[55] are notable steps in this direction. The latter treatment is especially complete and instructive in describing essential features of the fission process.

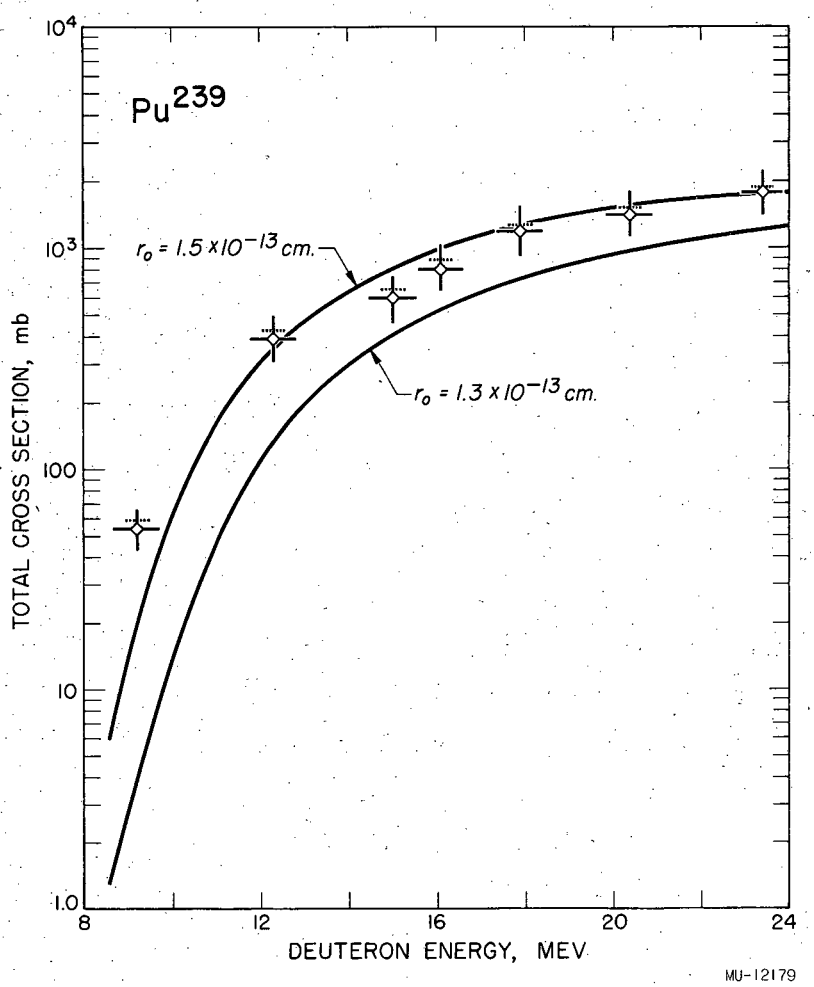

Fig. 32 The total fission yields (open diamonds) and the total fission yields plus the observed spallation yields (dashed lines) for deuteron bombardments of Pu^{239}. The solid curves are the theoretical total compound nucleus formation cross sections for the nuclear radius parameters indicated. The solid curves are from reference 32.

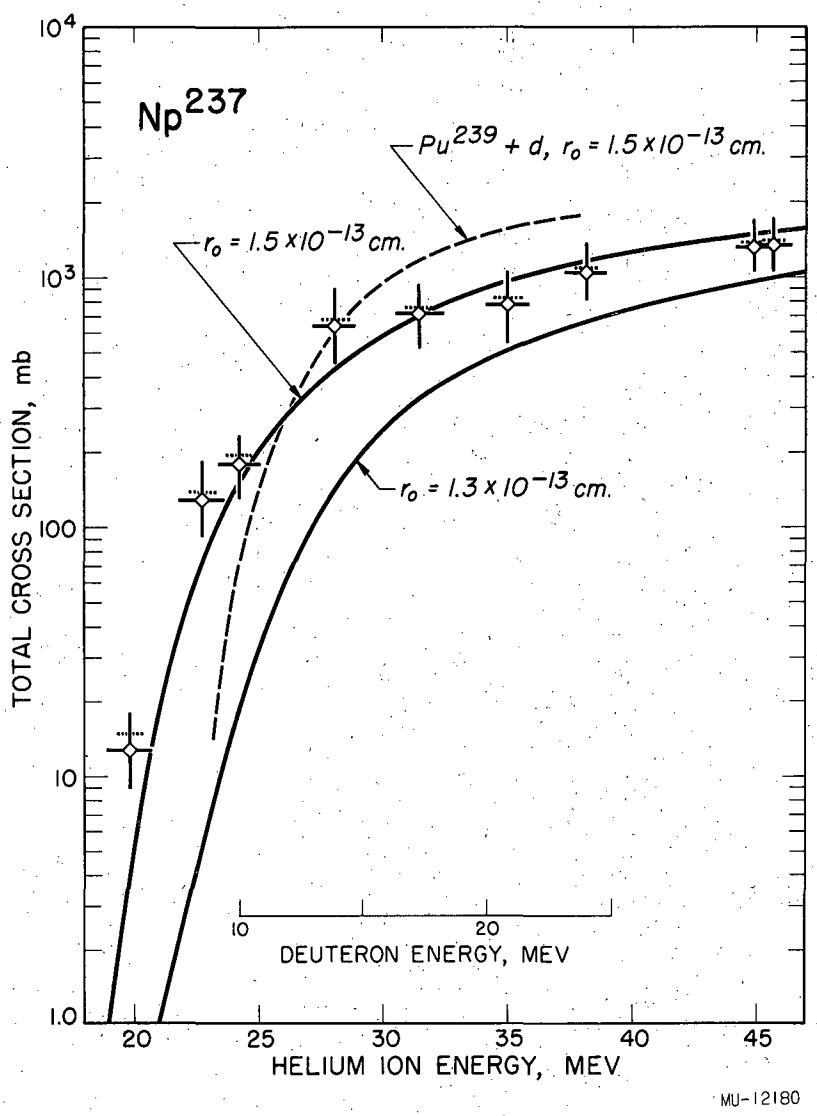

Fig. 33 The total fission yields (open diamonds) and the total fission yields plus the observed spallation yields (dashed lines) for helium-ion bombardments of Np^{237}. The solid curves are the theoretical total compound nucleus cross sections which are taken from reference 9.

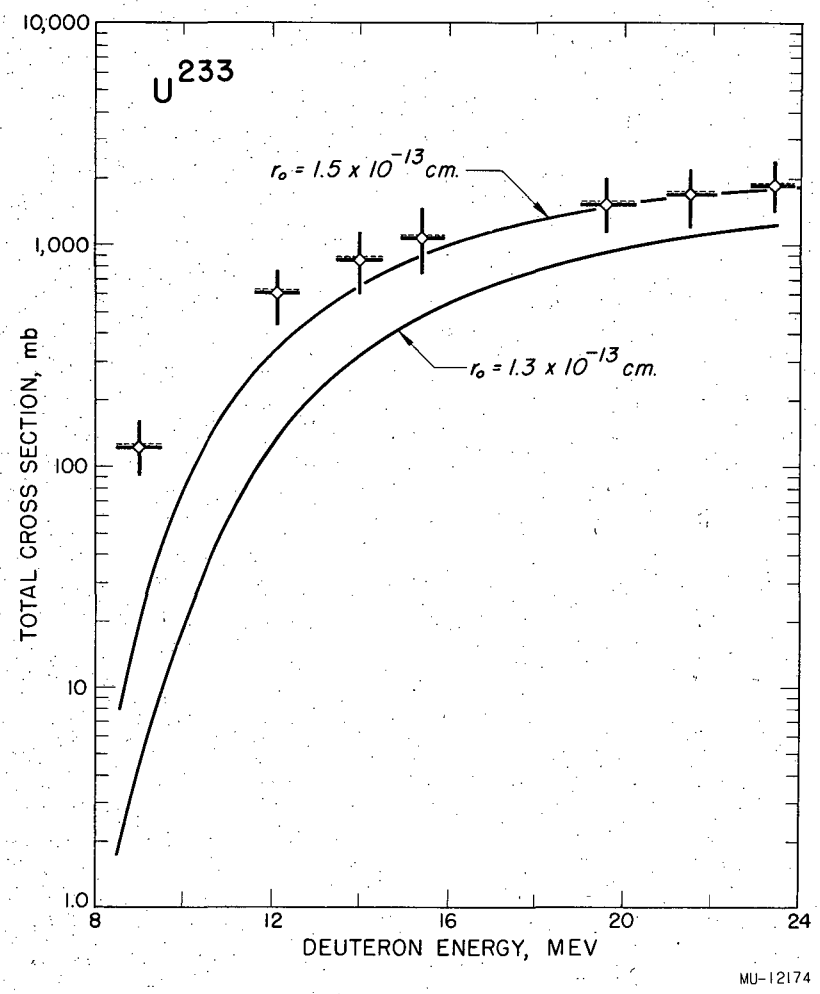

Fig. 34. The total fission yields (open diamonds) and the total observed reaction cross sections (dashed lines) for deuteron bombardments of U^{233}. The solid curves are the theoretical total compound nucleus formation cross sections and were taken from reference 32.

B. Spallation Yields

Throughout this discussion the spallation reactions will be described in terms of two general mechanisms or categories. The compound nucleus mechanism (or statistical mechanism) refers to the process in which the projectile is amalgamated with the target nucleus. The energy is distributed among all of the nucleons and when the statistical distribution of energy is such that a given particle has energy greater than its binding energy it can escape. The emission process is called "evaporation" in analogy to the evaporation of a wter molecule from a liquid drop. The lifetime of the compound state is long compared to the initial excitation or the final de-excitation process. Consequently, the emitted particles are not directly affected by the nature of the projectile, only by the energy of the compound state.

Reactions proceeding by other than the above process will be generally classed as direct interactions. Since this includes all reactions not proceeding specifically by compound nucleus processes they will also be referred to as non-compound nucleus reactions. In reality this category includes a wide variety of different and quite distinct types of reactions. Among these are "knock-on", "pickup", "stripping" or "hot spot" reactions. A "knock-on" reaction is one in which the projectile collides with individual nucleons, transferring sizable amounts of energy directly to one or to a small group of particles, allowing them to escape. It would perhaps be more exact even though less classical to say that the two particles interact instead of collide since the features of the mechanism need not be confined to those expected for a classical collision process. The bombarding particle may or may not be captured by the nucleus. "Pickup" reactions and "stripping" reactions are another closely allied pair of direct interaction processes. In a pickup reaction the projectile combines with a nucleon in the nucleus and the combination escapes. For example, a proton projectile may combine with a neutron from the nucleus to form a deuteron which carries off most of the energy of the incident proton. The stripping process is the reverse case where the nucleus removes or "strips" a nucleon from the projectile. Another type of reaction which shall be included in this direct interaction category is local excitation or "hot spot" reactions. In this case

a portion of the nucleus is excited by the incoming particle and the emission phase of the reaction or "evaporation" takes place before the excitation energy is distributed throughout the nucleus.

There are a number of important features which these non-compound nucleus reactions have in common that make it convenient to place them into the same category. First, the length of time necessary for the reaction to go to completion is usually very short compared to the formation and decay of a compound nucleus. Hence the nature of the incident particle can profoundly effect the nature of the reaction products. Secondly the energy of the initially emitted particles tends to be much higher than the energy of "evaporated" particles. Reactions proceeding by a non-compound nucleus mechanism are much less effected by the preponderant fission reaction, which appears in the heavy element region, than those reactions which are a result of a compound nucleus process. This is actually a direct consequence of the first two features listed but we have given it special notice because of its importance in interpretating spallation reactions in the heavy element region.

In general, little can be deduced from the present study about the relative contribution of individual direct interaction processes. Occasional suggestions may be made as to the probable contributing factors but the unambiguous resolution of this problem awaits other, more detailed experiments involving the measurement of energy and angular distribution of the reaction products.

1. Test of the predictions of Bohr's compound nucleus theory.

The same compound nucleus was produced by two separate mechanisms. Helium ion bombardment of Np^{237} and deuteron bombardments of Pu^{239} were used to produce the compound nucleus Am^{241*}. According to Bohr's compound nucleus theory, at the same excitation energy for the compound state the following relations should hold.

$$\text{(I)} \quad \frac{\sigma\,(d,2n)}{\sigma\,(d,3n)} = \frac{\sigma\,(\alpha,2n)}{\sigma\,(\alpha,3n)}$$

or alternatively

$$\text{(II)} \quad \frac{\sigma\,(d,2n)}{\sigma\,(\alpha,2n)} = \frac{\sigma_c(d)}{\sigma_c(\alpha)} = \frac{\sigma\,(d,3n)}{\sigma\,(\alpha,3n)}$$

Relation (I) has been tested for the compound nuclei Zn^{63}, Zn^{62} and Cu^{62} by Ghoshal[10] and for Po^{210} by John.[11] In these cases the prediction of relation (I) was clearly verified. It is interesting to note that in the proton bombardments of Bi^{209} and helium ion bombardment of Pb^{206} John was able to get almost perfect superposition of the (p,xn) excitation functions and the (α,xn) excitation functions merely by shifting the proton energy scale by 11.9 Mev. This result is very surprising in view of (II) since the relation $\sigma_c(p)/\sigma_c(\alpha)$ as predicted by Blatt and Weisskopf[9] is very energy dependent over the energy range used. The energy dependence of the ratio of the compound nucleus formation cross sections by protons and helium ions stems from the larger effect the coulomb barrier has on the helium ion. A condition analogous to that shown in Fig. 33 exists. The dotted line represents the theoretical cross section for Pu^{239} plus deuterons. The deuteron scale has been shifted by 14.2 Mev. The consequences of this superposition of excitation functions was not discussed by John but it may indicate that the theoretical treatment is not valid at low energies.

A comparison of the (α,2n) and (α,3n) excitation functions of Np^{237} and the (d,2n) and (d,3n) excitation functions of Pu^{239} is shown in Fig. 35. The energy scales have been shifted to make the (α,3n) and (d,3n) curves match. The cross sections have been normalized at the peaks of the (α,2n) and (d,2n) excitation functions. Compound nucleus theory predicts that the energy shift should be such that the compound nucleus produced by the corresponding deuteron and helium ion energy should have the same excitation energy. In the center of mass system this corresponds to:

$$E_d^{c.m.} = E_\alpha^{c.m.} - \Delta Mc^2$$

where $\Delta Mc^2 = (M_{Pu^{239}} + M_d - M_{Np^{237}} - M_\alpha)$ 931.2 Mev.

In the laboratory system

$$239/241 \; E_d = 237/241 \; E_\alpha - \Delta Mc^2$$

$$\text{or} \quad E_d = 237/239 \; E_\alpha - 241/239 \; \Delta Mc^2.$$

The value of $241/239 \; \Delta Mc^2$ found by matching the experimental curves at E_α = 34 Mev was 13.9 ± 1.0 Mev. Calculated from the masses of

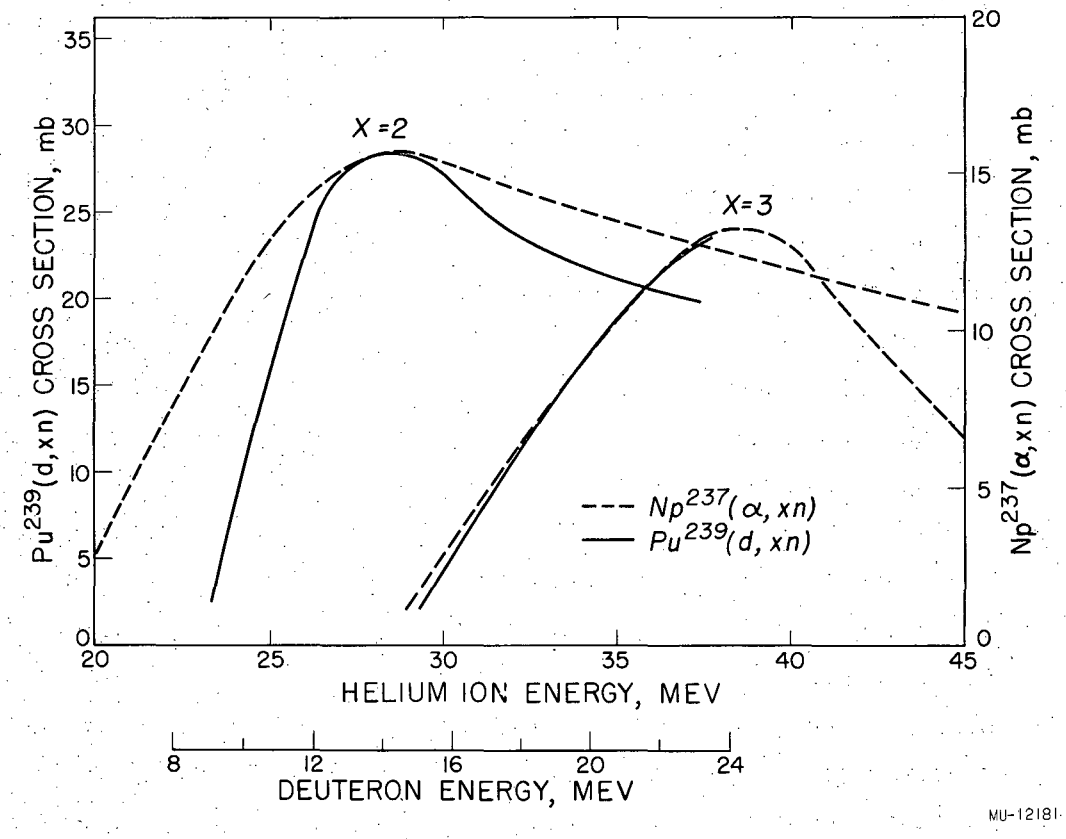

Fig. 35 Comparison of the excitation functions for Np^{237} + α and Pu^{239} + d.

Glass et al.[59] $241/239\ \Delta Mc^2 = 14.6$ Mev. The observed energy shift is the same as the calculated shift within the limits of error of the experimental determination.

The cross section ratios corresponding to (I) and (II) are shown graphically in Fig. 36. A reasonable agreement with the predictions of the Bohr postulate is obtained at all but the very lowest energies. The disagreement between the observed $\sigma(d,2n)/\sigma(\alpha,2n)$ ratio and the theoretical $\sigma_c(d)/\sigma_c(\alpha)$ ratio is not completely understood but may also be due to the failure of the theoretical treatment at low energies. The cross sections for compound nucleus formation were taken from Fig. 33. The curves for $r_o = 1.5 \times 10^{-13}$ cm^2 were used in each case. In view of the fact that these spallation reactions have survived the huge fission reaction, the agreement with the predictions of the compound nucleus model is remarkable. These $(\alpha,2n)$, $(\alpha,3n)$, $(d,2n)$ and $(d,3n)$ cross sections are less than five percent of the yield of similar reactions in the lead-bismuth region[11] where fission competition is not present. Yet these reactions still appear to take place principally by a compound nucleus mechanism. This is true at least in the region of the peak of the excitation function. Since both the fission reaction and the reactions leading to the emission of two or more neutrons are best explained by a statistical mechanism it is not surprising that the magnitudes of these particular spallation yields are very sensitive to the magnitude of the fission yield.

The independent treatments of Glass, Carr, Cobble, and Seaborg[86] and Batzel[145] indicate that fission is competing at each stage of any compound nucleus reaction. For example, in competing with the $(\alpha,3n)$ reaction on Np^{237}, fission takes place in the Am^{241} excited nucleus, in the Am^{240} excited nucleus and in the Am^{238} excited nucleus. It would also be very difficult to explain many features of the fission process if fission from the highly excited compound nuclei were not allowed. The explanation of fission asymmetry and the variation of charge distribution as given in the previous section depends on the fission of the highly excited compound states as well as those in lower states of excitation. One effect of this stepwise fission competition is to lower the maximum yield of each successive (α,xn) product. Another result is

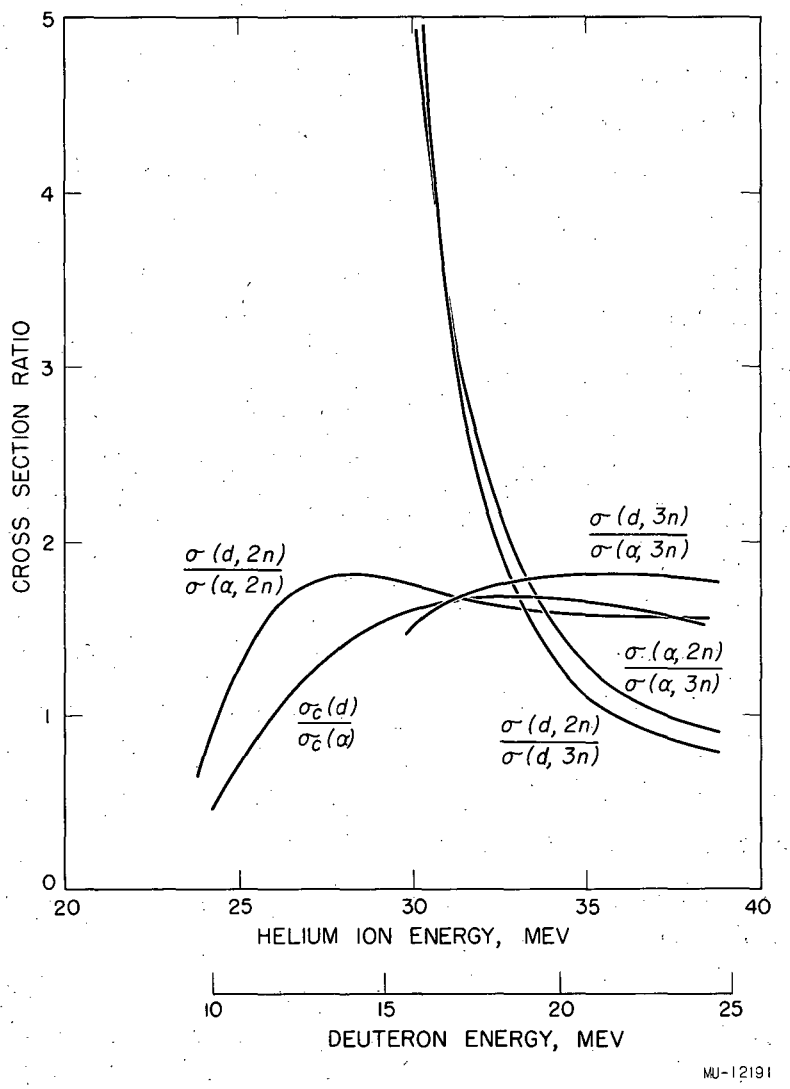

Fig. 36 Cross section ratios for Np^{237} + α and Pu^{239} + d. The theoretical compound nucleus cross sections are from reference 9 (Np^{237} + α) and reference 32 (Pu^{239} + d).

that fission can compete effectively with the evaporation of charged particles from the excited nuclei. It is generally assumed that evaporation of charged particles takes place from the initial highly excited compound states since the emitted particle must have sufficient energy to overcome the coulomb barrier as well as the binding energies.

An important consequence of these considerations is that the sensitivity of any given spallation reaction to the effects of fission competition may be used as an indication of the importance of compound nucleus processes in that reaction.

2. General features of the spallation excitation functions.

The general features of the spallation cross sections are very similar to those of other nuclides in this mass region.[86,87] The (α,n) excitation function on Np^{237} is low and flat, leveling off at about 2.5 mb. This reaction undoubtedly takes place by a direct interaction mechanism since compound nucleus theory predicts that the probability of evaporating such a high energy neutron is vanishingly small and very energy dependent.

The $(\alpha,2n)$ and $(\alpha,3n)$ excitation functions have been shown in the previous section to be principally due to compound nucleus processes. The prominent "tail" on the $(\alpha,2n)$ excitation function is not predicted by compound nucleus considerations. The tail on the $(\alpha,2n)$ excitation function for the bombardment of Pb^{208} was observed to be about 100 mb at 45 Mev. This was less than ten percent of the magnitude of the $(\alpha,2n)$ function at its highest point. It is therefore clear that in the neptunium bombardments the fission reaction is reducing the magnitude of the "peak" of the $(\alpha,2n)$ excitation function relative to the "tail". Although the "tail" also seems to be somewhat reduced it becomes relatively more prominent. The obvious conclusion is that the "tail" is less due to compound nucleus processes than the peak. A likely explanation is that one neutron is emitted by a direct interaction mechanism of some kind leaving the nucleus with high enough excitation energy to evaporate another neutron or to fission. The fission thus can compete with this reaction at the last step only. For the evaporation of two neutrons fission can compete in the decay of both intermediate excited nuclei. These same considerations hold true for the $(d,2n)$ excitation function for U^{233} and

Pu^{239}. There is undoubtedly some contribution due to the emission of two direct interaction neutrons but this mechanism is thought to contribute less than the one described. The reduction of the tail as well as the peak by fission competition is seen clearly in comparing the Pu^{239} and U^{233} (d,2n) excitation functions.

The reduced compound nucleus spallation reactions (d,2n) and (d,3n) for U^{233} (relative to Pu^{239}) shows clearly the greater fissionability of the uranium isotope at these excitation energies. This result is exactly opposite to the Z^2/A dependence of fissionability noted for spontaneous fission and low energy neutron-induced fission[34] since Z^2/A is greater for Pu^{239} (= 37.0) than for U^{233} (= 36.3). It is suggested that the effect of the mass on the fissionability at these energies is greater than the charge effect. In support of this one can cite the much higher (α,2n) cross section (hence the reduced fissionability) for Pu^{242} as compared to Pu^{238} [86] and the higher (d,2n) cross section for U^{235} as compared to U^{233}.[146] For these comparisons the relative (x,2n) cross sections should give very sensitive measurements of the relative fissionability since both the charge and nuclear type are the same and the cross sections should be very similar if fission were not competing.[147]

The (α,αn) excitation function for Np^{237} is probably due to either a purely direct interaction mechanism (knock-on or hot spot) in which a neutron is emitted and the incident alpha particle also escapes or it may be due to an inelastic collision between the helium ion and the nucleus after which the neutron is evaporated from the residual excited nucleus with attendant fission competition. The fact that this cross section is much lower than the (α,αn) cross section for U^{238} as measured by Ritsema[87] may indicate a preference for the latter mechanism, although the difference may be due to nuclear type. There is some indication that the (α,αn) cross section reported by Ritsema may be too high.[148]

A number of interesting features of the deuteron induced reactions of Pu^{239} and U^{233} merit consideration. The (d,n) reaction is almost entirely due to a stripping process and as such is quite insensitive to the fission reaction. The shape and magnitude of this excitation function is very similar to that predicted by Peaslee[149] for a stripping reaction in which fission is not competing.

The (d,αn) cross sections, as measured at one energy in the Pu^{239} bombardments and at four energies in the U^{233} bombardments, present an interesting but puzzling problem. The magnitude of the cross section is in reasonable agreement with that predicted by compound nucleus theory if fission competition is ignored.[150] However, the very fact that this reaction survives the fission competition is a strong indication that a direct interaction process is taking place.

The low cross section for the (d,dp) reaction, which is actually the sum of the (d,dp) and (d,2pn) reactions, on Pu^{239} is interesting in view of the very large (d,t) cross sections for heavy elements as recently measured by workers in this laboratory.[151] The difference in the magnitude of these reactions at these low energies gives little information about the mechanism since the barrier can still exercise a strong influence on the relative cross sections.

C. Summary

The main conclusions of this study can be summarized as follows,

1. The fission mechanism is best explained by a statistical or compound nucleus model.

2. The (α,2n), (α,3n), (d,2n) and (d,3n) reactions appear to be principally due to compound nucleus processes. These reactions are very sensitive to the magnitude of the fission reaction and therefore are very sensitive indicators of the relative fissionability of different nuclides.

3. The reactions not affected appreciably by the fission competition are due to direct interaction or non-compound nucleus processes. The relative contribution of these reactions to the total spallation cross section is therefore greatly increased for fissionable nuclides.

V. ACKNOWLEDGMENTS

I wish to express my gratitude to Professor Glenn T. Seaborg under those guidance and encouragement these investigations were performed. The constant support and advice of Dr. Richard A. Glass is also gratefully acknowledged.

Helpful discussions with and the assistance of Bruce M. Foreman Jr., Robert Vandenbosch, Susanne R. Vandenbosch, E. Victor Luoma, T. Darrah Thomas, Paul Donovan and Jose Gonzalez-Vidal were in large measure responsible for the completion of this study and the efforts of these people are much appreciated. The author also gratefully acknowledges many helpful discussions with and the aid of Dr. William H. Wade who was especially helpful with many of the tedious cross section calculations.

Appreciation is expressed to Dr. Joseph G. Hamilton, W. Bart Jones, the late G. Bernard Rossi and the crew of the Crocker Laboratory 60-inch cyclotron for their cooperation and help in carrying out the bombardments. The aid of the health chemistry group headed by Nelson Garden, especially the help of Sue Hargis, Robert Delk and Marshall Lombardo, is appreciated. Thanks are due Theresa K. Pionteki who so conscientiously carried out the tedious but important task of counting the many samples. I would also like to acknowledge the efforts of Jean E. Samson and Mrs. Patricia Howard in typing the manuscript.

The financial support and encouragement of the Civilian Institutions Division of the United States Air Force Institute of Technology is gratefully acknowledged. Finally I would like to thank my wife Nancy for her help, encouragement and patience during the course of this work.

This work was performed under the auspices of the United States Atomic Energy Commission.

VI. APPENDIX

Nucleometer (Methane Flow Windowless Proportional Counter) Counting Efficiencies for Electron Capture Isotopes.

A. Introduction

The determination of the absolute yield of a reaction product which decays by orbital electron capture is complicated by the fact that little is known about the efficiency with which these isotopes are counted by the various counting instruments available. There is no *a priori* reason that all electron capture isotopes should be counted with the same efficiency or even approximately so. Also, the manner in which the sample is mounted, as well as the instrument on which it is counted, may profoundly influence the counting yield.

The counting instrument used in the present study for counting electron capture isotopes was a methane flow windowless proportional counter. This type of counter was chosen because of its high efficiency for low energy radiations and because of its high geometry (approximately 2π). It was hoped that if the counting system used was sufficiently sensitive to detect the very low energy conversion electrons and auger electrons that the counting efficiency for most of the isotopes studied would be very high and would not vary too much from one isotope to another. The decay of most of the electron capture isotopes in this region generally involves the emission of several conversion or auger electrons per disintegration.

The counting efficiency for a few electron capture isotopes on this type instrument have been measured previously. On the basis of the earlier work, Higgins[152] adopted an efficiency of 60 percent for electron capture isotopes. Using the same data plus a few other determinations, Hulet[153] arrived at a best value of 33 percent. These values plus an efficiency of 58 percent first reported for the counting efficiency of Cm^{241} by Glass[154] and later revised upward to 82 percent[155] indicate the status of electron capture counting efficiencies at the time of the present work.

In the present study a total of six isotopes which decay almost completely by orbital electron capture (Am^{238}, Am^{239}, Am^{240}, Np^{232}, Np^{233},

Np^{234}) plus one which decays approximately half by beta minus and half by electron capture (Np^{236}) plus one which decays completely by beta minus (Np^{238}) were measured on the nucleometer. In order to transfer the nucleometer counting rate into an absolute disintegration rate, the counting efficiencies of as many of the above nuclides as possible were determined by measuring the alpha particles of the respective daughter nuclide. These experiments are described below.

B. Experimental

1. Am^{239} and Am^{240}.

The determination of the nucleometer counting efficiencies of Am^{239} and Am^{240} by measuring the alpha particles from the daughters Pu^{239} and Pu^{240} is complicated by the long half life of the plutonium isotopes. Also, the fact that the main alpha groups of Pu^{239} and Pu^{240} are almost identical (5.15 and 5.16 Mev respectively) further complicates the measurement.

To determine the counting efficiencies for Am^{238}, Am^{239} and Am^{240}, about 15 mg of high purity Pu^{239} was bombarded with 24 Mev deuterons in the Crocker Laboratory 60-inch cyclotron. The plutonium, bombarded in the form of $NH_4PuO_2PO_4$, was dissolved after the bombardment in 6 M hydrochloric acid plus 0.05 M hydrofluoric acid. The americium was then separated by the scheme outlined in section II-C. After separation of the americium from the rare earth fission products on a cation column using alcoholic-HCl eluant, the americium fraction was diluted to 1.00 ml in a volumetric flask. Americium (243) tracer was then added, the solution was stirred and a small portion was removed and vaporized from a hot tantalum filament onto a platinum disc (as described in section II-D) for counting in the nucleometer. Plutonium tracer (Pu^{236}) was then added to the americium fraction and this solution was saturated with hydrogen chloride gas and passed through a short glass column packed with Dowex-A-1 anion exchange resin. The americium passed through the column in the concentrated hydrochloric acid fraction. After washing the resin with concentrated hydrochloric acid and adding the wash to the americium fraction, the plutonium was removed with 4 M hydrochloric acid and this fraction was then evaporated to a low volume and vaporized onto a

platinum disc from a tantalum filament for alpha pulse analysis. The plutonium was periodically "milked" from the americium fraction in this manner in order to measure the amount of Pu^{238} and Pu^{239} plus Pu^{240} that had been produced by decay of Am^{238}, Am^{239}, and Am^{240} respectively. Before each "milking" the americium solution was measured carefully in a volumetric flask and an assay was taken of this solution to determine the amount of the original americium still present at the time of the milking. Although the alpha particles from Pu^{239} and Pu^{240} cannot be differentiated separately on the alpha pulse analyzer the amount of Am^{240} present could be determined uniquely by milking the plutonium from the americium solution after the 12 hr Am^{239} had completely decayed and then again after the Am^{240} had decayed. The plutonium produced in this period should be only Pu^{240} which was used to find the amount of Am^{240} present in the solution at the time of the preceeding separation. With this known, the contribution of Pu^{240} in the previous plutonium fractions could then be subtracted and the Pu^{239} and hence the Am^{239} determined.

After the various plutonium samples had been examined by alpha pulse analysis it became apparent that the original separation had failed to adequately remove all of the target plutonium and that the first two "milking" steps had failed to remove all of the plutonium. This conclusion was reached when it was noted that Pu^{238} was present in the "milked" plutonium fractions long after the Am^{238} had decayed. For this reason excess plutonium appeared in the plutonium fractions from the earlier milkings and resulted in abnormally low counting efficiencies of ~8 percent for Am^{238} and 17 percent for Am^{239}. The Am^{240} determination was considered good, however, since in the last two milkings the plutonium was completely removed from the americium fraction. The counting efficiency obtained for Am^{240} was 91 percent.

This experiment was repeated in order to re-determine the Am^{238} and Am^{239} counting efficiencies and to check the Am^{240} counting efficiency. Additional precautions such as the use of longer milking columns packed with more carefully graded (0.25 - 0.5 cm per minute settling rate) Dowex A-1 resin as well as assaying the plutonium fraction after each milking, were observed in order to insure complete removal of the plutonium in each milking step. In this second experiment

the separation of the americium from the rare-earth fission product activity had to be carried out twice because of insufficient separation the first time. When this had been completed the Am^{238} had completely decayed so the counting efficiency for this isotope could not be determined. However, a good determination of the Am^{239} counting efficiency and two checks of the Am^{240} counting efficiency were obtained. The counting efficiency determined for Am^{239} was 60.2 ± 5 percent, and the counting efficiencies of Am^{240} based on two separate milkings were 67 percent and 109 percent the average giving 89 percent. The large deviations in the Am^{240} counting efficiency are due to very low counting rates of Pu^{240} in the milked plutonium samples.

Advantage was taken of the large amounts of Am^{239} and Am^{240} produced in these experiments to measure the half life, the alpha particle energy and the partial alpha half life for Am^{239} and the half life of Am^{240}. These quantities had been previously measured by Higgins[152] using much smaller levels of activity. The values obtained were: For Am^{239} $t_{1/2}$ = 12.1 ± 0.4 hrs, $E\alpha$ = 5.77 ± 0.05 Mev, partial alpha half life = 28 ± 1 yrs. For Am^{240} $t_{1/2}$ = 51.0 ± 0.5 hrs. These determinations are discussed in detail elsewhere.[156]

2. $\underline{Np^{234}}$.

The counting efficiency of Np^{234} was measured in the same fashion as the americium isotopes discussed above. A ten mil U^{235} foil weighing a total of 6.1 grams was bombarded with 24 Mev deuterons for eight hours in the Crocker Laboratory 60-inch cyclotron. The deuterons incident to the target corresponded to a total of 101.5 micro-ampere-hours of current as measured in the target integrators. The intensely radioactive uranium foil was allowed to "cool" for 12 hrs. after which the neptunium was removed according to the scheme outlined in section II-C. The purified neptunium was diluted to 10 cc in a volumetric flask, 0.100 cc (100λ) was removed and this was in turn diluted to 25 cc. Twenty-five lambda (0.025 cc) was then removed from this second dilution and mixed with 3 cc of 12 M hydrochloric acid which had been stirred with 0.5 M TTA (thenoyltrifluoroacetone) in benzene and then washed with benzene. This was done in order to reproduce as nearly as possible the conditions used in the cross section measurements. This solution was

then evaporated onto a platinum disc for counting in the nucleometer. This sample will be referred to as NpI in the discussion which follows.

In order to test the effect of changing the way in which the sample is mounted, three additional nucleometer samples were prepared as follows: (1) A second 25 λ portion of the 25 ml neptunium sub-dilution was mixed with three ml of concentrated hydrochloric acid which had been stirred with a 0.5 M TTA solution but had not been washed with benzene (NpII). (2) 25 λ was evaporated onto a tantalum filament and vaporized onto a platinum disc as described in section II-D (NpIII) and (3) 25 λ of the neptunium solution was electroplated onto a platinum disc from ammonium chloride solution as described in section II-D (NpIV). The decay of these four neptunium samples was was then followed on the nucleometer and the activity due to Np^{234} was resolved from the Np^{235}, Np^{236}, Np^{238} and Np^{239} present in the sample. The Np^{238} and Np^{239} came from deuteron reactions on the U^{238} impurity (~7%) in the target material.

After two months had elapsed U^{232} tracer was mixed with the main neptunium stock solution and the uranium was separated from this solution to permit measurement of the amount of U^{234} produced by decay of the Np^{234}. The neptunium solution at the time of this separation still contained large amounts of activity due to Np^{235} as well as Pu^{236} and Pu^{238} which were produced by decay of the Np^{236} and Np^{238}. A column technique suggested by T. D. Thomas[157] was used to separate the uranium, neptunium and plutonium. The neptunium solution was first evaporated to a low volume (1-2 ml) and heated for five minutes with 6 M hydrochloric, 0.5 M hydriodic acids and 0.005 M hydrazine hydrochloride. This solution was passed through a jacketed glass column packed with very carefully graded Dowex A-1 anion exchange resin (settling rate 0.25 to 0.5 cm per minute). The column was maintained at 87° C by refluxing trichloroethylene through the glass jacket surrounding the column. The column was 4 mm in diameter and 5 cm long and was operated at a flow rate of one minute per drop. The plutonium was removed with 1 ml of pre-heated 6 M hydrochloric acid, and 0.5 M hydriodic acid the neptunium was removed with 1 ml of pre-heated 3 M hydrochloric acid and the uranium was removed with 0.5 ml of pre-heated 0.5 M hydrochloric acid.

It is notable that this single column run gave almost complete decontamination from an estimated 1.5×10^6 dpm of Pu^{236} and from 1.2×10^7 dpm of Np^{235}. Less than 0.5 cpm of Pu^{236} and less than 5 cpm of Np^{235} was detected in the uranium fraction. The uranium was electroplated from a neutral ammonium chloride solution onto a platinum disc for alpha pulse analysis (section II-D). Along with the U^{232} tracer the alpha pulse analyses showed 37 counts per minute of U^{234}, < 0.1 cpm of U^{235} and < 0.1 cpm of U^{236}. The absence of U^{235} shows that the original decontamination from the target material was complete and that all of the U^{234} observed came from decay of Np^{234}. The counting efficiency of Np^{234} in the various nucleometer samples is shown below.

Sample	Counting Efficiency (percent)
NpI	63
NpII	47
NpIII	68
NpIV	65

NpI was evaporated onto a platinum disc in the same fashion as the neptunium samples in the cross section studies. That is from 12 M HCl which had been stirred with 0.5 M TTA in benzene and then washed with benzene.

NpII was the same as NpI except that the 12 M HCl was not washed with benzene. A thin film of TTA was visible.

NpIII was vaporized in vacuo from a tantalum filament at about 2000°C onto a platinum disc.

NpIV was electroplated from a neutral 3 M NH_4Cl solution at 6-8 volts and 3 amps onto a platinum disc.

The difference in the counting efficiencies obtained for samples NpI, NpIII and NpIV are not considered significant. Due to losses in mounting samples NpIII and NpIV, these samples were normalized to NpI by using the alpha counting rates in each of the samples due to Pu^{236} which was produced by decay of the Np^{236}.

An attempt was made to measure the counting efficiency of Np^{232} by bombarding 5 mg of U^{233} with 24 Mev deuterons, separating the neptunium and measuring the U^{232} which appeared in the neptunium fraction. No alpha activity due to U^{232} was detected even though the original neptunium separation was completed forty minutes after the end of the bombardment. The short half-life of the Np^{232} (13 min) and the long half life of U^{232} (70 y) make this determination very difficult.

C. DISCUSSION

The nucleometer counting efficiencies determined in the present study as well as those measured by other workers are summarized in Table X.

Table X

Summary of Nucleometer Counting Efficiencies for Electron-Capture Isotopes

Isotope	Counting Efficiency (%)	Method in which Mounted[a]	Method Determined	Reference
At^{211}	39	EV	α-daughter[b]	153
U^{231}	33	?	" "	159
Np^{234}	63	EV	" "	This work
	68	V	" "	" "
	65	EP	" "	" "
Np^{236}	89	V	α-daughter plus[c] β^- branching	158
	95	EP	" "	158
Am^{239}	60	V	α-daughter	This work
Am^{240}	90	V	" "	" "
Cm^{241}	82	V	" "	155
Bk^{243}	26	EV	" "	153
Bk^{245}	33	EV	X-rays[d]	153
Bk^{245}	~100	EP	" "	160
Cf^{247}	80-90	EP	" "	160

(a) The following symbols are used to indicate the respective method of mounting the sample.

EV; evaporated onto a plutonium disc with care being taken to prevent deposition of extraneous mass.

V; vaporized onto a platinum disc in vacuo from a tantalum filament heated for a very short time to about 2000°C.

EP; electroplated onto a platinum disc from neutral 3-5 M ammonium chloride solution at 6-8 volts and 2.3 amps/cm^2.

(b) Determined by observing the alpha radiations due to the daughter of the electron capture isotope.

(c) For Np^{236} the alpha radiations due to the beta minus daughter Pu^{236} were observed. A beta minus branching ratio of 57 percent was assumed (reference 121).

(d) Determined by comparing the counting rate of K and L rays to the nucleometer counting rate. An assumption must be made about the number of x-rays per disintegration (.95 to 1 for heavy nuclides, see reference 121).

The counting efficiencies reported by Hulet (references 153 and 159) are consistently lower than the other determinations. In one case the counting efficiency for a single isotope (Bk^{245}) was determined both by Hulet[153] and by Harvey and Chetham-Strode[160] with the value obtained by Hulet lower by a factor of three. The reason for this discrepancy is not understood since Hulet used the same type of counting equipment as used in the present study.

On the basis of the determinations made in the present study, a counting efficiency of 60 percent was chosen for the electron capture isotopes discussed in the major part of this thesis for which direct determinations of the counting efficiencies were not made. On the basis of later information, which is also included in Table X, it appears that 60 percent may be too low and that a counting efficiency of 70-80 percent would be more realistic. Such a change would not appreciably effect the general features or the interpretation of the spallation excitation functions presented in section III.

For at least one isotope decaying by orbital electron capture (Np^{234}) the method of mounting the sample appears to make little difference if care is taken to avoid visible amounts of foreign matter.

VII. REFERENCES

1. M. Lindner and I. Perlman, Phys. Rev. 78, 499 (1950).
2. R. H. Goeckermann and I. Perlman, Phys. Rev. 76, 628 (1949.
3. N. Bohr, Nature 137, 344 (1936).
4. R. Serber, Phys. Rev. 72, 1114 (1947).
5. M. K. Goldberger, Phys. Rev. 74, 1269 (1948).
6. G. Bernardini, G. T. Booth and S. J. Lindenbaum, Phys. Rev. 85, 826 (1952); and Phys. Rev. 88, 1017 (1952).
7. J. W. Meadows, Phys. Rev. 91, 1885 (1953); and Phys. Rev. 98, 774 (1955).
8. V. F. Weisskopf, Lecture Series in Nuclear Physics, MDDC-1175, U. S. Government Printing Office, 1947.
9. J. M. Blatt and V. F. Weisskopf, Theoretical Nuclear Physics (John Wiley and Sons, New York, 1952).
10. S. N. Ghoshal, Phys. Rev. 80, 939 (1950).
11. W. John, Jr., Phys. Rev. 103, 704 (1956).
12. H. Nabholz, P. Stoll and H. Waffler, Phys. Rev. 86, 1043 (1952).
13. M. E. Toms and W. E. Stephens, Phys. Rev. 95, 1209 (1954).
14. J. E. Brolley, Jr., J. L. Fowler and L. K. Schlacks, Phys. Rev. 88, 618 (1952).
15. G. A. Price, Phys. Rev. 93, 1279 (1954).
16. O. Hirzel and H. Waffler, Helv. Phys. Acta, 20, 373 (1947).
17. E. B. Paul and R. S. Clarke, Can. J. Phys. 31, 267 (1953).
18. B. L. Cohen, E. Newman, R. A. Charpie and T. H. Handley, Phys. Rev. 94, 620 (1954).
19. P. C. Gugelot, Phys. Rev. 93, 425 (1954).
20. R. M. Eisberg and G. Igo, Phys. Rev. 93, 1039 (1954).
21. B. L. Cohen, Phys. Rev. 98, 25 (1955).
22. P. C. Gugelot and H. A. Lauter, Phys. Rev. 91, 486 (1953).
23. E. R. Graves and L. Rosen, Phys. Rev. 89, 1343 (1953).
24. P. C. Gugelot, Phys. Rev. 81, 51 (1951).
25. H. McManus and W. T. Sharp, Phys. Rev. 87, 188 (1952).
26. N. Austern, S. T. Butler, H. McManus and W. T. Sharp, Phys. Rev. 91, 453 (1953).

27. Karl G. Porges, Phys. Rev. 101, 225 (1956).
28. B. L. Cohen, Phys. Rev. 92, 1245 (1953).
29. Brookhaven Conference on Statistical Aspects of the Nucleus BNL-331 (C-21) (1955).
30. P. Morrison, Experimental Nuclear Physics, Vol. II, E. Segre, editor, (John Wiley and Sons, New York, 1952).
31. E. L. Kelley (Thesis) University of California Radiation Laboratory Report UCRL-1044, Dec. 1950. E. L. Kelley and E. Segre, Phys. Rev. 75, 999 (1949).
32. M. M. Shapiro, Phys. Rev. 90, 171 (1953).
33. N. Bohr and J. A. Wheeler, Phys. Rev. 56, 426 (1939).
34. G. T. Seaborg, Phys. Rev. 85, 157 (1952).
35. W. J. Whitehouse and W. Galbraith, Nature 169, 494 (1952).
36. S. Frenkel and N. Metropolis, Phys. Rev. 72, 914 (1947).
37. G. T. Seaborg, Phys. Rev. 88, 1429 (1952).
38. E. Fermi, Nuclear Physics Notes as compiled by J. Orear, A. H. Rosenfeld and R. A. Schluter (University of Chicago Press, 1949) p. 6.
39. J. Frenkel, Phys. Rev. 55, 987 (1939).
40. W. J. Whitehouse, Progr. Nuclear Phys. 2, 120 (1952).
41. R. W. Spence and G. P Ford, Annual Reviews of Nuclear Science (Stanford University Press, Stanford, California, 1953). 2, p 399.
42. See reference 1 of P. Fong, Phys. Rev. 102, 434 (1953).
43. M. G. Mayer and J. Hans. D. Jensen, Elementary Theory of Nuclear Shell Structure (John Wiley and Sons, Inc., New York, 1955).
44. L. Meitner, Arkiv. Fysik 4, 383 (1952).
45. M. G. Mayer, Phys. Rev. 74, 235 (1948).
46. L. Meitner, Nature 165, 561 (1950).
47. G. C. Wick, Phys. Rev. 76, 181 (1949).
48. K. H. Kingdon, Phys. Rev. 76, 136 (1949).
49. R. D. Hill, Phys. Rev. 98, 1272 (1955).
50. J. Frenkel, J. Phys. (USSR) 10, 553 (1946).
51. D. L. Hill and J. A. Wheeler, Phys. Rev. 89, 1102 (1953).
52. R. D. Present and J. K. Knipp, Phys. Rev. 57, 751 (1940).
53. W. J. Swiatecki, Phys. Rev. 83, 178 (1951).

54. Th. A. J. Maris, Phys. Rev. 101, 502 (1956).
55. P. Fong, Phys. Rev. 102, 434 (1956).
56. A. H. Wapstra, Physica 21, 385 (1955).
57. H. E. Duckworth, C. L. Kegley, J. M. Olson and G. S. Stanford, Phys. R v. 83, 1114 (1951); H. E. Duckworth and R. S. Preston, Phys. Rev. 82, 468 (1951); H. E. Duckworth, Nature 170, 158 (1952).
58. J. R. Huizenga, Physica 21, 410 (1955).
59. R. A. Glass, S. G. Thompson, and G. T. Seaborg, Journal of Inorg. and Nucl. Chem. 1, 3, (1955).
60. C. D. Coryell, R. A. Brightson and A. C. Pappas, Phys. Rev. 85, 732 (1952).
61. P. Fong, Phys. Rev. 89, 332 (1953).
62. Th. A. J. Maris, Phys. Rev. 101, 147 (1956).
63. J. K. Perring and J. S. Story, Phys. Rev. 98, 1525 (1955).
64. J. L. Fowler, W. H. Jones and J. H. Phaeler, Phys. Rev. 88, 71 (1952).
65. V. F. Weisskopf (private communication to J. L. Fowler).
66. L. E. Glendenin, C. D. Coryell and R. A. Edwards, The Fission Products, (National Nuclear Energy Series, McGraw-Hill Book Co., New York, 1951) paper 52.
67. A. C. Pappas, Proceedings of the International Conference on the Peaceful Uses of Atomic Energy (United Nations Publications, New Uork, 1956). Vol. 7, p. 19.
68. T. J. Kennett and H. J. Thode, Phys. Rev. 103, 3236 (1956).
69. D. C. Brunton, Phys. Rev. 76, 1798 (1949).
70. D. C. Brunton and G. L. Hanna, Can. J. Res. A28, 190 (1950).
71. J. Jungerman and S. C. Wright, Phys. Rev. 76, 1112 (1949).
72. E. M. Douthett and D. H. Templeton, Phys. Rev. 94, 128 (1954).
73. L. Wolfenstein, Phys. Rev. 82, 690 (1951).
74. B. L. Cohen, Phys. Rev. 81, 632 (1951).
75. W. C. Dickinson and J. E. Brolley, Jr., Phys. Rev. 90, 388 (1953).
76. J. E. Brolley, Jr., W. C. Dickinson and R. L. Henkel, Phys. Rev. 99, 159 (1955).
77. B. L. Cohen, W. H. Jones, G. V. McCormick and B. L. Ferrell, Phys. Rev. 94, 625 (1954).

78. B. L. Cohen, B. L. Ferrell-Bryan, D. J. Coombe and M. K. Hullings, Phys. Rev. 98, 685 (1955).

79. D. A. Hicks, J. Ise, Jr., and R. V. Pyle, Phys. Rev. 101, 1016 (1956).

80. B. C. Diven, H. C. Martin, R. F. Taschek and J. Terrell, Phys. Rev. 101, 1012 (1956).

81. R. B. Leachman, Phys. Rev. 101, 1005 (1956).

82. J. S. Fraser and J. C. Milton, Phys. Rev. 93, 818 (1954).

83. B. E. Watt, Phys. Rev. 87, 1037 (1952).

84. T. I. Bonner, R. A. Ferrell and M. C. Rinehart, Phys. Rev. 87, 1032 (1952).

85. I. S. Fraser, Phys. Rev. 88, 536 (1952).

86. R. A. Glass, R. J. Carr, J. W. Cobble and G. T. Seaborg, Phys. Rev. (to be published).

87. S. E. Ritsema (M.S. Thesis) UCRL-3266. University of California Radiation Laboratory 1956, (unpublished).

88. E. V. Luoma, (M. S. Thesis) UCRL-3495. University of California Radiation Laboratory 1956, (unpublished).

89. D. S. Hufford and B. F. Scott, The Transuranium Elements; Research Papers (McGraw-Hill Book Company, Inc., New York, 1949). National Nuclear Energy Series, Plutonium Project Record, Vol. 14B, p 1149.

90. I. Strong, Procedures in Experimental Physics, (Prentice-Hall Inc., New York, 1938) p 159.

91. J. L. Moore and G. W. Smith, Nucleonics 13, 66 (1955).

92. K. M. Glover, P. Borrell, AERE c/r-1359 (British) (Jan. 9, 1954).

93. M. S. Freedman, R. P. Metcalf and N. Sugarman, Radiochemical Studies; The Fission Products, (McGraw-Hill Book Company, Inc., New York, 1951). National Nuclear Energy Series, Plutonium Project Record, Vol. 9, p. 459.

94. R. A. Glass, Ph.D. Thesis, University of California Radiation Laboratory Unclassified Report UCRL-2560 (1954).

95. T. D. Thomas, private communication (1955).

96. B. B. Cunningham, A. Ghiorso and J. C. Hindman, Metallurgical Project Report CN-124 (A-1818) (Jan. 5, 1944) p 1.

97. E. Potter, unpublished data (1955).

98. R. Carr, Ph.D. Thesis, University of California, (September 1956).

99. J. C. Wallmann, Ph.D. Thesis, University of California Radiation Laboratory Classified Report UCRL-1255 (April 1951).

100. L. B. Magnusson and T. J. LaChappelle, The Transuranium Elements; Research Papers (McGraw-Hill Book Co. Inc., New York, 1949). National Nuclear Energy Series Plutonium Project Record, Vol. 14B, p. 1595.

101. E. K. Hyde, National Nuclear Energy Series, Plutonium Project Record (McGraw-Hill Book Co., New York, 1952) Vol. 17B p. 46 (classified).

102. W. A. Aron, B. G. Hoffman and F. C. Williams, U. S. Atomic Energy Commission Unclassified Document AECU-663 (May 1951).

103. B. M. Foreman, Jr., Unpublished data (1955).

104. W. B. Jones, private communication (November 1955).

105. K. D. Jenkins, Crocker Laboratory, 60-inch cyclotron, Declassified Report (60-68)(April 3, 1950).

106. N Garden and associates (unpublished data).

107. c.f. the Pu^{239} (d,n) Am^{240} excitation function figure 4.

108. The Pu^{240} (d,n) Am^{241} and Pu^{238} (d,n) Am^{238} have been determined by E. V. Luoma (reference 88).

109. R. M. Lessler, Unpublished data on the U^{235} (d,n) Np^{236} excitation function.

110. B. B. Cunningham, The Actinide Elements, (McGraw-Hill Book Co. Inc., New York, 1951). National Nuclear Energy Series, Plutonium Project Record, Vol. 14A, p. 394.

111. B. B. Cunningham and J. C. Hindman, Ibid, p. 476.

112. W. Meinke, University of California Radiation Laboratory Declassified Report UCRL-432 and supplements (1949).

113. C. D. Coryell and N. Sugarman (editors) Radiochemical Studies: The Fission Products (McGraw-Hill Book Co. Inc. New York, 1951) The National Nuclear Energy Series, Plutonium Project Record, Vol. 9.

114. Dow Chemical Company, Midland, Michigan.

115. W. E. Nervick, J. Phys. Chem. 59, 690 (1955).

116. L. B. Magnusson, J. R. Huizenga, T. H. Siddall and M. H. Studier, Argonne National Laboratory Classified Report ANL-4667 (May 1951).

117. W. H. Wade and G. R. Choppin, unpublished data (1956).

118. H. P. Robinson, unpublished data (1953).

119. A. Ghiorso, A. H. Jaffey, H. P. Robinson and B. B. Weissbourd, The Transuranium Elements; Research Papers (McGraw-Hill Book Co., Inc., 1949) National Nuclear Energy Series, Plutonium Project Record, Vol. 14B, p. 1226.

120. J. M. Hollander, I. Perlman and G. T. Seaborg, Rev. of Mod. Phys. 25, (1953).

121. P. G. Grey, Ph.D. Thesis, University of California Radiation Laboratory Unclassified Report UCRL-3104 (1955) p. 36.

122. Radiation Counter Laboratories, Skokie, Illinois.

123. c.f. reference 94 page 59.

124. R. J. Prestwood, H. L. Smith, C. I. Browne and D. C. Hoffman, Phys. Rev. 98, 1324 (1955).

125. L. R. Zumwalt, U. S. Atomic Energy Commission Declassified Document, MDDC-1346 (September 18, 1947).

126. Conference on Absolute Beta Counting Preliminary Report No. 8. (National Research Council, Division of Mathematical and Physical Sciences, Committee on Nuclear Science) Nuclear Science Series, October, 1950.

127. W. E. Nervick and P. C. Stevenson, Nucleonics 10, 18 (1952).

128. R. S. Baker and L. Katz, Nucleonics 11, 14 (1953).

129. H. P. Robinson, unpublished data (1955).

130. G. Friedlander and J. W. Kennedy, Introduction to Radiochemistry (John Wiley and Sons, Inc., New York, 1949). p. 159.

131. B. P. Burtt, Nucleonics 8, 28 (1949).

132. H. S. Hicks and R. S. Gilbert, Phys. Rev. 100, 1286 (1955).

133. H. S. Hicks, P. C. Stevenson, R. S. Gilbert and W. H. Huchin, Phys. Rev. 100, 1284 (1955).

134. Ru^{103} decays through Rh^{103m} which has a 40 kev gamma ray which is ~ 80 percent converted in the L and M shells giving a conversion electron of ~ 35 kev. The contribution of this conversion electron was neglected because of its very low energy.

135. c.f. reference 130 page 132.

136. The following pairs of activities have half-lives close enough together to complicate the resolution of the decay curves, Np^{236}, Np^{238}; Pd^{109}, Pd^{112}; Ag^{112}, Ag^{113} and Ce^{141}, Ce^{144}.

137. This was especially evident in the resolution of Np^{232} from the uranium bombardments and Am^{238} from the plutonium and neptunium bombardments.

138. c.f. E. P. Steinberg and L. E. Slendenin, Proceedings of the International Conference on the Peaceful Uses of Atomic Energy (United Nations Publications, New York, 1956)., Vol. 7, p. 3.

139. R. L. Folger, P. C. Stevenson and G. T. Seaborg, Phys. Rev. 98, 107 (1955).

140. C. D. Coryell, R. A. Brightson and A. C. Pappas, see C. D. Coryell, Ann. Rev. of Nuc. Sci. 2, 305 (1953).

141. H. A. Tewes and R. A. James, Phys. Rev. 88, 860 (1952).

142. W. H. Jones, A. Timmick, J. H. Phaeler and T. H. Handley, Phys. Rev. 99, 184 (1955).

143. W. J. Swiatecki, Phys. Rev. 100, 936 (1955).

144. A. W. Fairhall, Phys. Rev. 102, 1335 (1956).

145. R. E. Batzel, University of California Radiation Laboratory Report UCRL-4303 (unpublished), Calculations made from the data of M. Lindner and R. N. Osborne, Phys. Rev. 102, 378 (1956).

146. R. M. Lessler, unpublished data (1956).

147. For the theoretical probabilities see reference 9, for experimental verification see reference 11.

148. P. Donavon, unpublished results (1956).

149. D. C. Peaslee, Phys. Rev. 74, 1001 (1948).

150. V. F. Weisskopf and D. H. Ewing, Phys. Rev. 57, 472 (1940).

151. W. H. Wade and Jose Gonzales-Vidal, unpublished data (1956).

152. G. H. Higgins, Ph.D. Thesis, University of California Radiation Laboratory Unclassified Report UCRL-1796 (June 1952).

153. E. K. Hulet, Ph.D. Thesis, University of California Radiation Laboratory Unclassified Report, UCRL-2283 (July 1953).

154. Reference 94, p. 60.

155. R. A. Glass, private communication (1955).

156. R. A. Glass, R. J. Carr, W. M. Gibsin and J. W. Cobble, "Radioactive Decay of Am^{238}, Am^{239}, Am^{240}, Cm^{240} and Cm^{241}," Phys. Rev. (to be published).

157. T. D. Thomas and R. A. Glass, unpublished data.

158. R. Vandenbosch (unpublished data).

159. W. W. T. Crane, reported by E. K. Hulet (reference 153).

160. B. G. Harvey and A. Chetham-Strode, Jr., unpublished data, (1956).